NASA TN D-1618

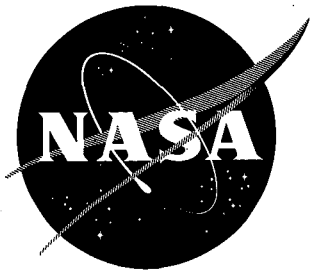

TECHNICAL NOTE

D-1618

PRESSURE DISTRIBUTIONS ON THREE RIGID WINGS SIMULATING PARAWINGS WITH VARIED CANOPY CURVATURE AND LEADING-EDGE SWEEP AT MACH NUMBERS FROM 2.29 TO 4.65

By Paul G. Fournier

Langley Research Center
Langley Station, Hampton, Va.

NATIONAL AERONAUTICS AND SPACE ADMINISTRATION
WASHINGTON
April 1963

NATIONAL AERONAUTICS AND SPACE ADMINISTRATION

TECHNICAL NOTE D-1618

PRESSURE DISTRIBUTIONS ON THREE RIGID WINGS SIMULATING PARAWINGS WITH VARIED CANOPY CURVATURE AND LEADING-EDGE SWEEP AT MACH NUMBERS FROM 2.29 TO 4.65

By Paul G. Fournier

SUMMARY

An investigation has been made at Mach numbers from 2.29 to 4.65 in the Langley Unitary Plan wind tunnel to determine the chordwise pressure distribution at supersonic speeds of three parawing models through an angle-of-attack range from 0° to 70°. Three rigid metal models simulated a parawing which had a basic flat planform with leading edges swept back 45°. These configurations were developed to have one-half-circle, one-third-circle, and one-quarter-circle curvature of the semispan trailing edges when viewed from downstream and resulting leading-edge sweeps of 61.5°, 52.5°, and 48.6°. The results of the investigation are presented as curves of chordwise pressure distributions at four spanwise locations for each model.

INTRODUCTION

The performance, stability, and control characteristics of parawings at subsonic, transonic, and supersonic speeds are being studied at the Langley Research Center. Some preliminary work on the paraglider and parawing concept is presented in references 1 to 7.

Widespread interest in the parawing for applications such as launch-vehicle recovery and terminal recovery of spacecraft has necessitated detailed load-distribution data over a range of Mach numbers. Observations of parawing models in previous investigations have shown that the shape the canopy assumes in flight can be closely represented by portions of a conical surface. With this assumption, rigid metal models of varying curvature were constructed (one-half-circle, one-third-circle, and one-quarter-circle curvature of the semispan trailing edges when viewed from downstream) to measure the chordwise pressure distribution over a Mach number range from low subsonic to high supersonic speeds.

Data on the pressure distributions for low subsonic and transonic speeds on three paraglider models are presented in references 8 and 9, respectively.

Although the term "paraglider" was used for this same configuration in references 8 and 9, the term "parawing" is used in the present paper since it is considered a more appropriate term for general use. Presented herein are results of an investigation at Mach numbers from 2.29 to 4.65 for an angle-of-attack range from 0° to 70° depending on the model and Mach number. Some discussion of the applicability and general characteristics of the data is included.

SYMBOLS

The coefficients and symbols used in the presentation of the data herein are as follows:

b span, in.

C_p pressure coefficient, $\frac{p_l - p}{q}$

c local projected chord, in.

M free-stream Mach number

p free-stream static pressure, lb/sq ft

p_l local pressure, lb/sq ft

q dynamic pressure, $\frac{1}{2}\rho V^2$, lb/sq ft

V free-stream velocity, ft/sec

x distance along local projected chord, in.

z distance above keel reference plane (horizontal plane through keel center line), in.

α nominal angle of attack relative to the keel center line, deg

ρ air density, slugs/cu ft

DESCRIPTION OF MODEL

Pressure distributions were obtained on three 1/10-inch-thick metal and plastic models constructed to simulate a range of conical shapes that the present type of parawing might assume in flight. These models are the same models that were used in the investigations of references 8 and 9. The models had a basic flat planform with leading edges swept back 45° (area of 1 square foot). These configurations were developed to have one-half-circle, one-third-circle, and one-quarter-circle curvature of the semispan trailing edges when viewed from

downstream and resulting leading-edge sweeps of 61.5°, 52.5°, and 48.6°. Photographs of the models are presented in figures 1 and 2.

The difference in curvature was accomplished by development of the panels of each model around a right circular cone. (See fig. 3.) The resulting models with panels forming one-half of a conical surface, one-third of a conical surface, and one-quarter of a conical surface are designated as models 1, 2, and 3, respectively. Geometric characteristics of all three models are presented in figure 4.

The right and left panels for each model were welded to a hollow center keel which carried small pressure tubes to the canopy. The right panel had the lower surface pressure orifices (including those on the leading edge and trailing edge), and the left panel had the upper surface pressure orifices. The locations of the orifices at each of the four spanwise stations, given in fraction of local projected chord, are presented in figure 5. In addition, these orifice locations are given in terms of vertical distance from the keel reference plane and longitudinal distance along the keel.

Plastic leading edges of approximately 3/8-inch diameter were cast to each model. An auxiliary strut extended below the reference plane of the models. (See figs. 1 and 2.) Wires were attached from the auxiliary strut to the leading edge of the model in order to reduce the flexure of the parawing panels. It is believed that the strut had some effect on the pressure data at these supersonic speeds, especially at the higher angles of attack; however, the effect of the strut was not determined.

APPARATUS, TESTS, AND CORRECTIONS

The sting-supported models were tested in the Langley Unitary Plan wind tunnel, which is a variable-pressure return-flow tunnel. The tunnel had a test section which was 4 feet square and approximately 7 feet in length. The nozzle leading to the test section is an asymmetric sliding-block-type nozzle, and the Mach number may be varied continuously through a range from 2.29 to 4.65. Further details of the wind tunnel may be found in reference 10.

The present parawing models were tested at Mach numbers of 2.29, 2.96, 3.95, and 4.65. The Reynolds number based on the model keel length varied from approximately 1.4×10^6 to 2.6×10^6 for the range of test Mach numbers.

The angles of attack have not been corrected for sting bending due to loads on the model; however, it was estimated that the maximum correction would be about 0.2° at maximum loads. The angles of attack indicated on the pressure plots are nominal angles of attack and should be corrected for flow angularity by adding the flow misalinement angle indicated in the following table to the nominal angle:

Mach number	Misalinement angle, deg
2.29	0.45
2.96	.25
3.95	.50
4.65	.90

The test angles of attack were not always the same for the different models at a particular Mach number (for example, see figs. 6(c), 7(c), and 8(b)), because in some cases vibration of the model and tunnel flow conditions prevented data points from being taken at these conditions.

PRESENTATION OF DATA

Data on the three parawing models through the Mach number range and angle-of-attack range are presented in figures 6 to 8 as plots of pressure coefficient C_p as a function of fraction of local chord projected to the plane of the leading edge and keel x/c. A short discussion of the applicability of the pressure data is presented as well as a few comments on the general characteristics of the data. It should be kept in mind that the effect of the auxiliary strut has not been determined in the presentation of these data.

DISCUSSION

Parawings now being considered for recovery of launch vehicles and spacecraft application have either large inflatable keel and leading edges or small metal-tube keel and leading edges. It is believed that the data on the three rigid parawings of the present paper will more closely simulate the loads expected on fixed-sweep configurations with rigid keels and leading edges of small diameter.

The pressure coefficients for supersonic speeds at low angles of attack (up to 10° or 15° depending on the particular wing) indicated that negative lift was carried on the entire wing surface. This characteristic at low angles of attack was noted in the data of references 8 and 9 (subsonic and transonic speeds) and is a result of the camber and twist (washout) shown in figure 5. This would be impossible for a flexible surface and indicates an angle-of-attack limitation for this type of fixed-sweep parawing. However, these data would be useful for rigid conical wings.

The pressure-distribution curves also indicate, in general, that the overall loads at the various spanwise stations decrease with increasing spanwise distance. The loss in spanwise loading increased with increasing amount of curvature of the canopy. This type of span loading would be expected from the considerations of the spanwise twist variations shown in figure 5. Because of the spanwise twist, angles of attack of 25° to 40° (depending on the wing configuration and Mach

number) were required to eliminate completely negative lift on the leading-edge portion of the wing surface at the tips.

In contrast to the pressure distributions of references 8 and 9, those of the present investigation indicate that the magnitude of the upper surface pressures diminishes whereas the magnitude of lower surface pressures increases with increasing supersonic Mach number, an indication that the lower surface distribution determines the lift characteristics of the wing, as would be expected for supersonic flow.

CONCLUDING REMARKS

An investigation has been made of the chordwise pressure distribution at Mach numbers from 2.29 to 4.65 of three rigid metal models simulating a parawing. In general the data indicated a loss of loading with increasing spanwise distance. This spanwise loss in loading increased with increasing amount of curvature of the canopy. Also, as expected for supersonic flow, the present data indicate that the lower surface carries an increasing amount of load with increasing Mach number.

Langley Research Center,
National Aeronautics and Space Administration,
Langley Station, Hampton, Va., December 14, 1962.

REFERENCES

1. Rogallo, F. M., and Lowry, J. G.: Flexible Reentry Gliders. Preprint No. 175C, Soc. Automotive Eng., Apr. 1960.

2. Rogallo, Francis M., Lowry, John G., Croom, Delwin R., and Taylor, Robert T.: Preliminary Investigation of a Paraglider. NASA TN D-443, 1960.

3. Naeseth, Rodger L.: An Exploratory Study of a Parawing as a High-Lift Device for Aircraft. NASA TN D-629, 1960.

4. Hewes, Donald E.: Free-Flight Investigation of Radio-Controlled Models With Parawings. NASA TN D-927, 1961.

5. Taylor, Robert T.: Wind-Tunnel Investigation of Paraglider Models at Supersonic Speeds. NASA TN D-985, 1961.

6. Penland, Jim A.: A Study of the Aerodynamic Characteristics of a Fixed Geometry Paraglider Configuration and Three Canopies With Simulated Variable Canopy Inflation at a Mach Number of 6.6. NASA TN D-1022, 1962.

7. Polhamus, Edward C., and Naeseth, Rodger L.: Experimental and Theoretical Studies of the Effects of Camber and Twist on the Aerodynamic Characteristics of Parawings Having Nominal Aspect Ratios of 3 and 6. NASA TN D-972, 1963.

8. Fournier, Paul G., and Bell, B. Ann: Low Subsonic Pressure Distributions on Three Rigid Wings Simulating Paragliders With Varied Canopy Curvature and Leading-Edge Sweep. NASA TN D-983, 1961.

9. Fournier, Paul G., and Bell, B. Ann: Transonic Pressure Distributions on Three Rigid Wings Simulating Paragliders With Varied Canopy Curvature and Leading-Edge Sweep. NASA TN D-1009, 1962.

10. Anon.: Manual for Users of the Unitary Plan Wind Tunnel Facilities of the National Advisory Committee for Aeronautics. NACA, 1956.

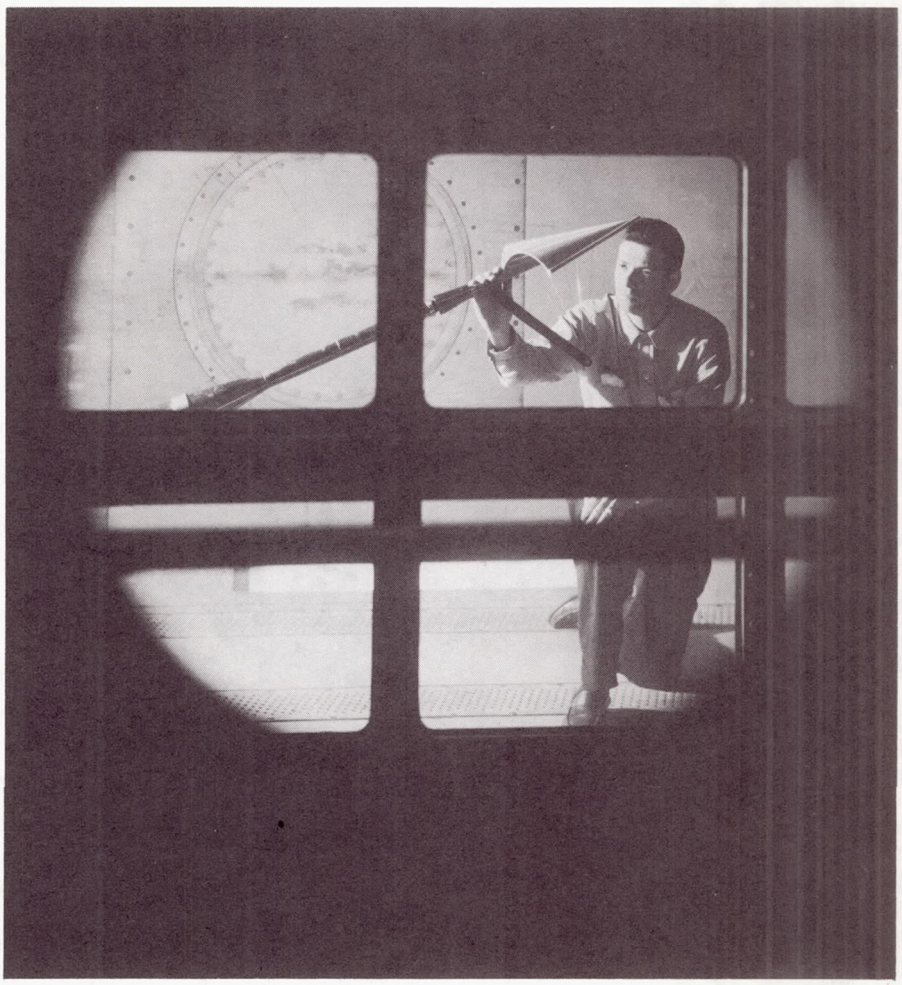

(a) Side view. L-61-1732

Figure 1.- Typical test setup.

(b) One-quarter front view. L-61-1731

Figure 1.- Concluded.

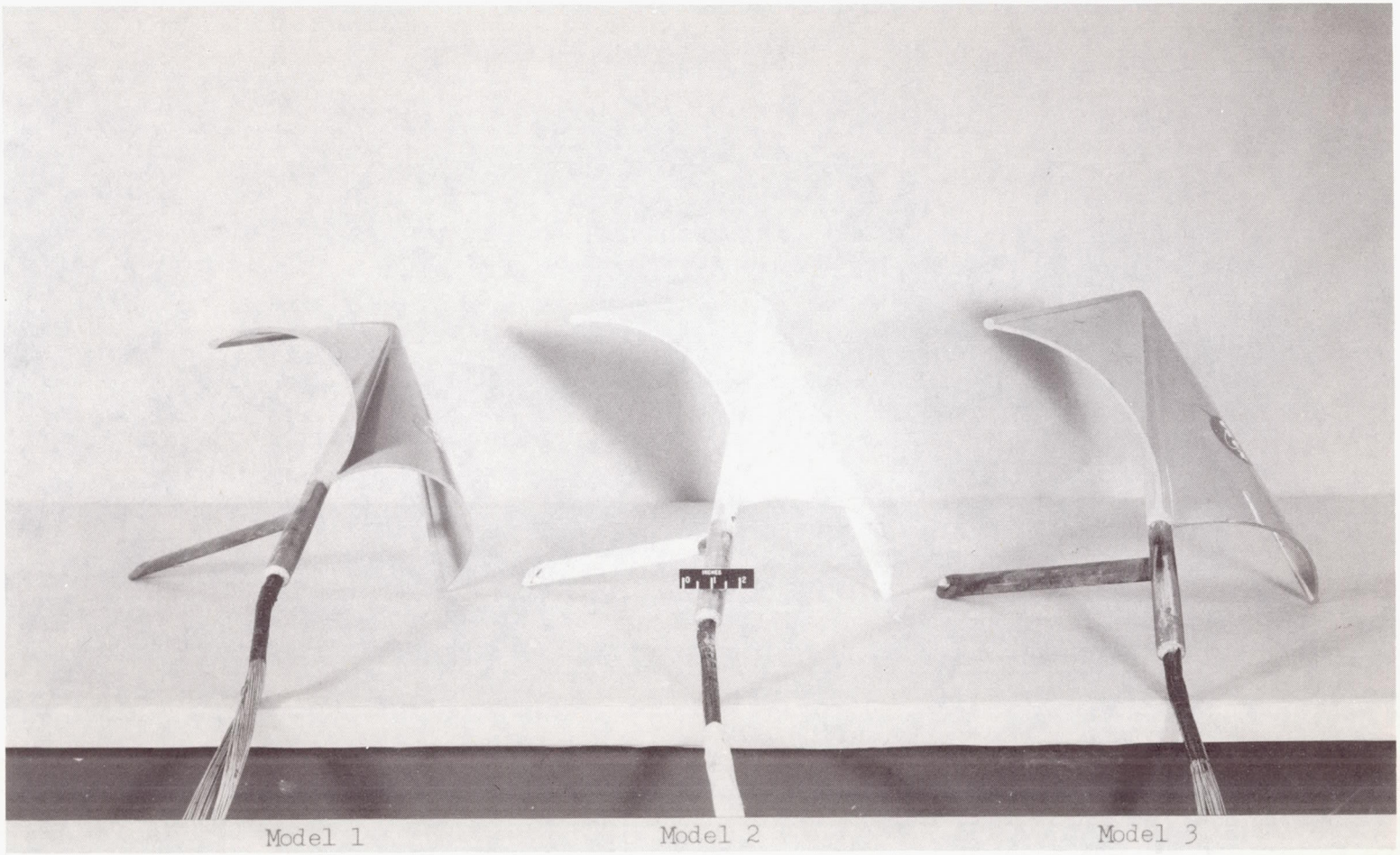

(a) One-quarter rear view. L-61-4687

Figure 2.- Photographs of three models tested.

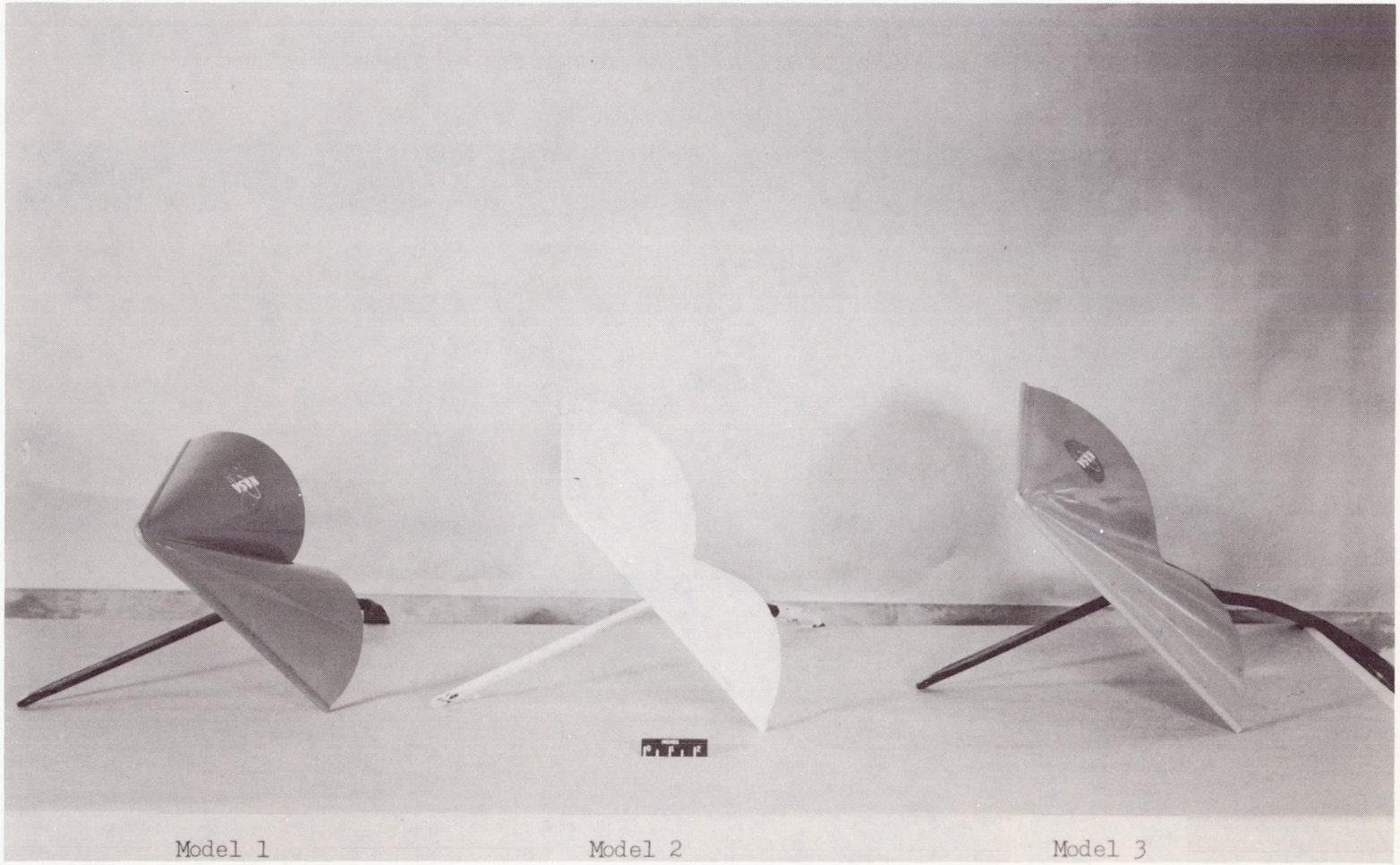

(b) Three-quarter front view. L-61-4689

Figure 2.- Concluded.

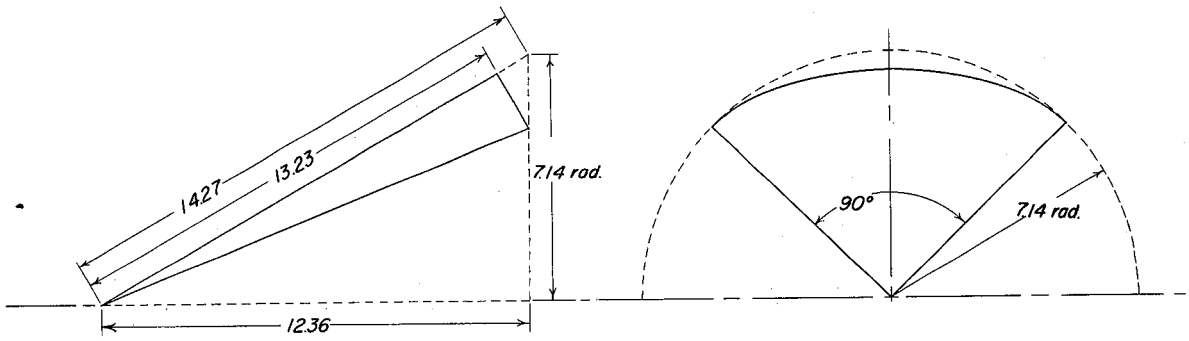

Model 3

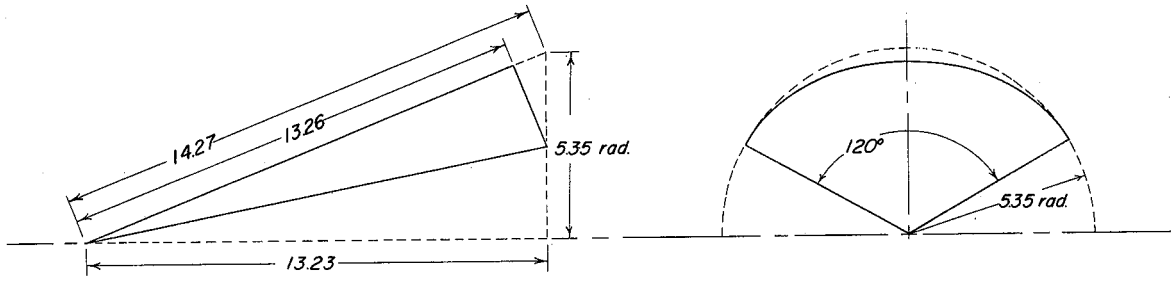

Model 2

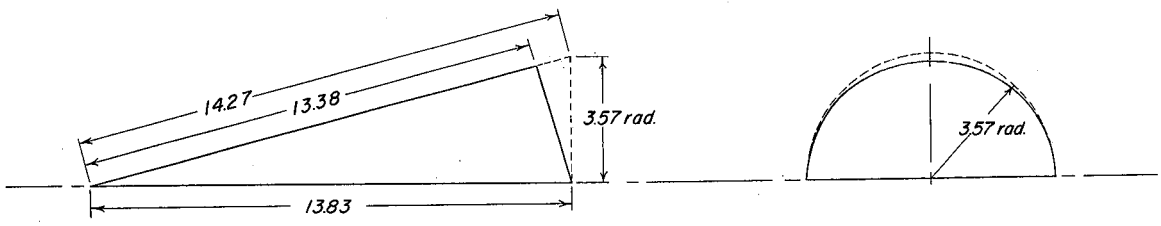

Model 1

Figure 3.- Development of paraglider panels. Linear dimensions are in inches.

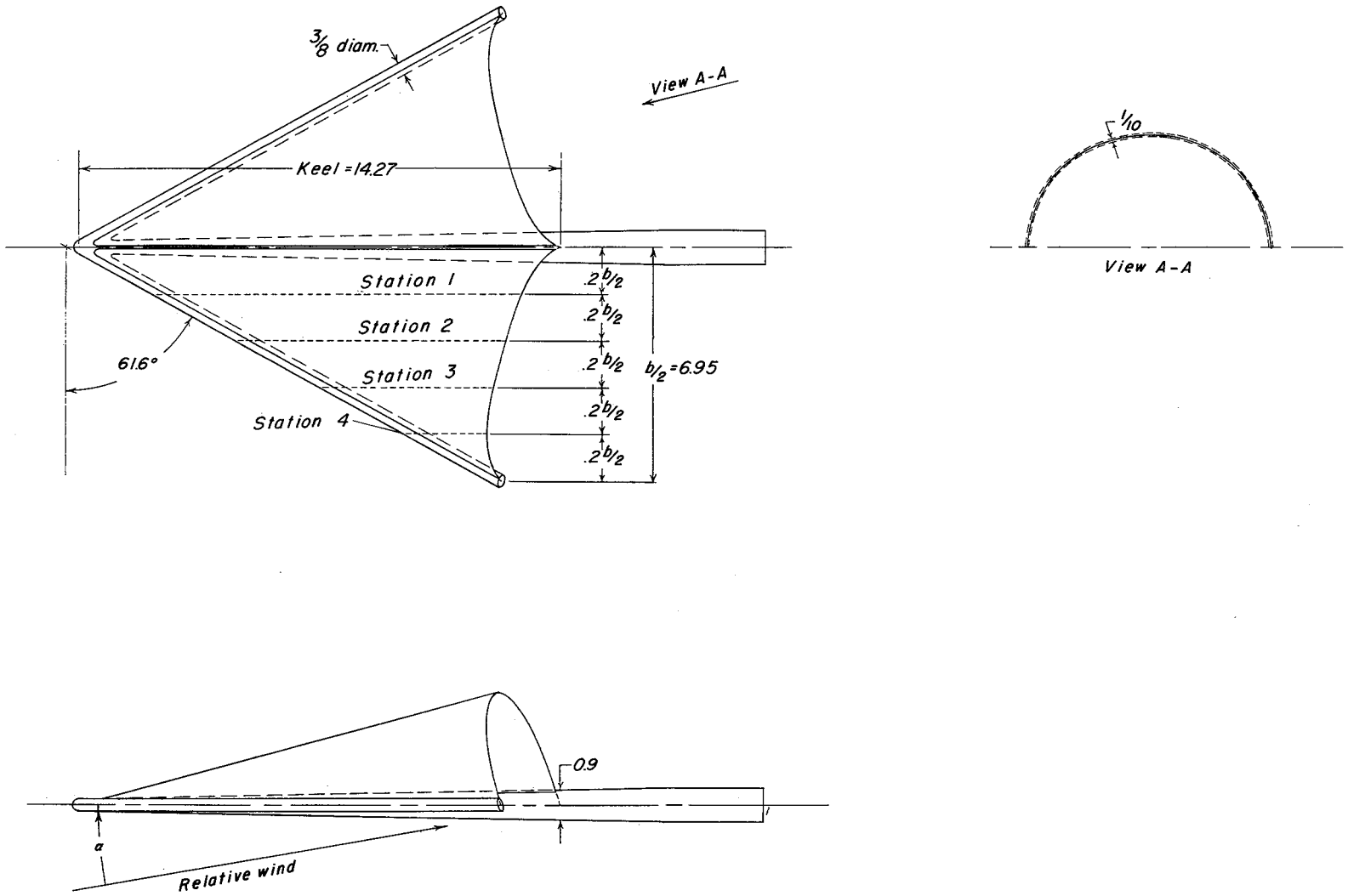

(a) Model 1.

Figure 4.- Geometric characteristics of rigid paraglider models. Linear dimensions are in inches.

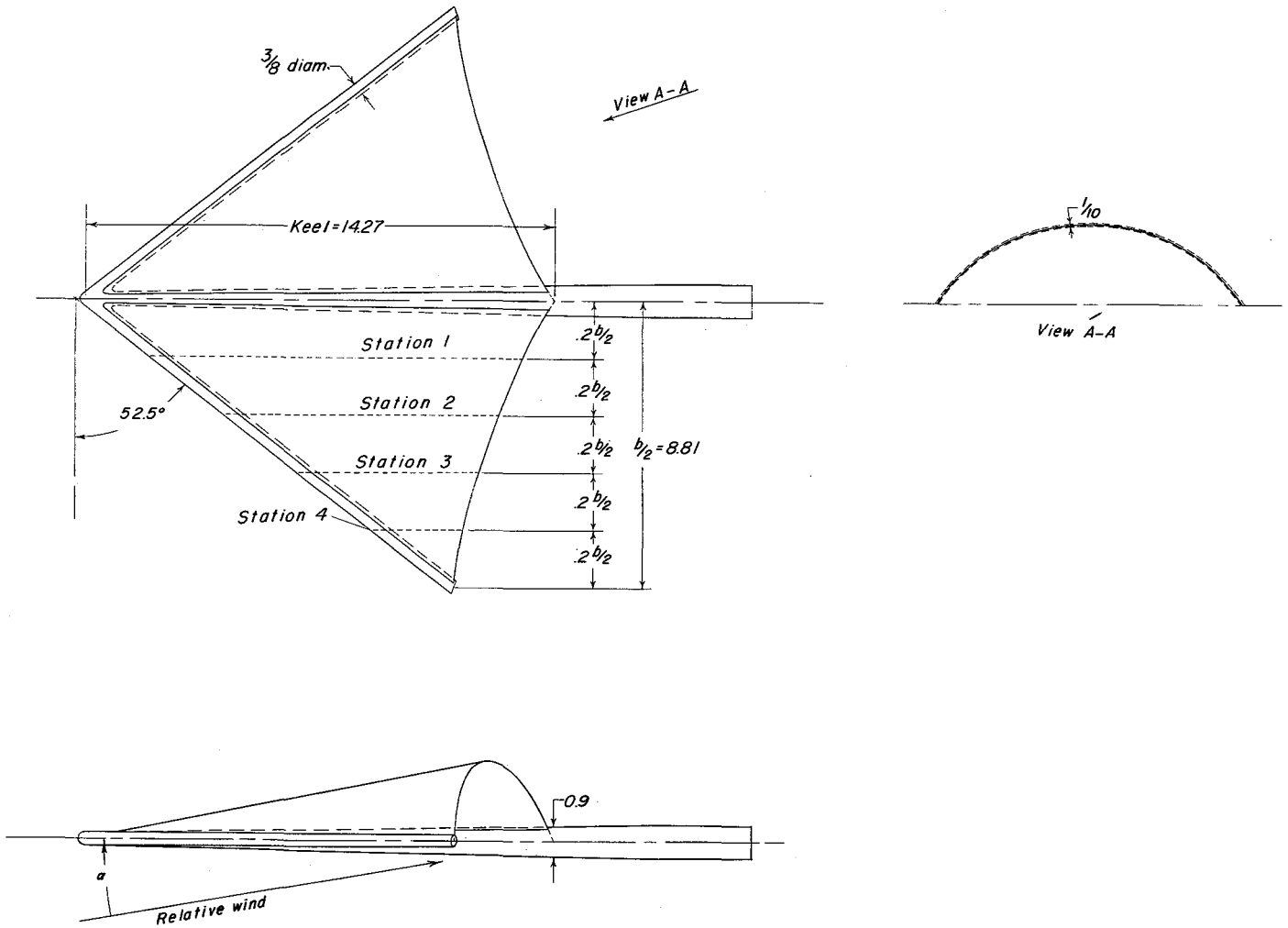

(b) Model 2.

Figure 4.- Continued.

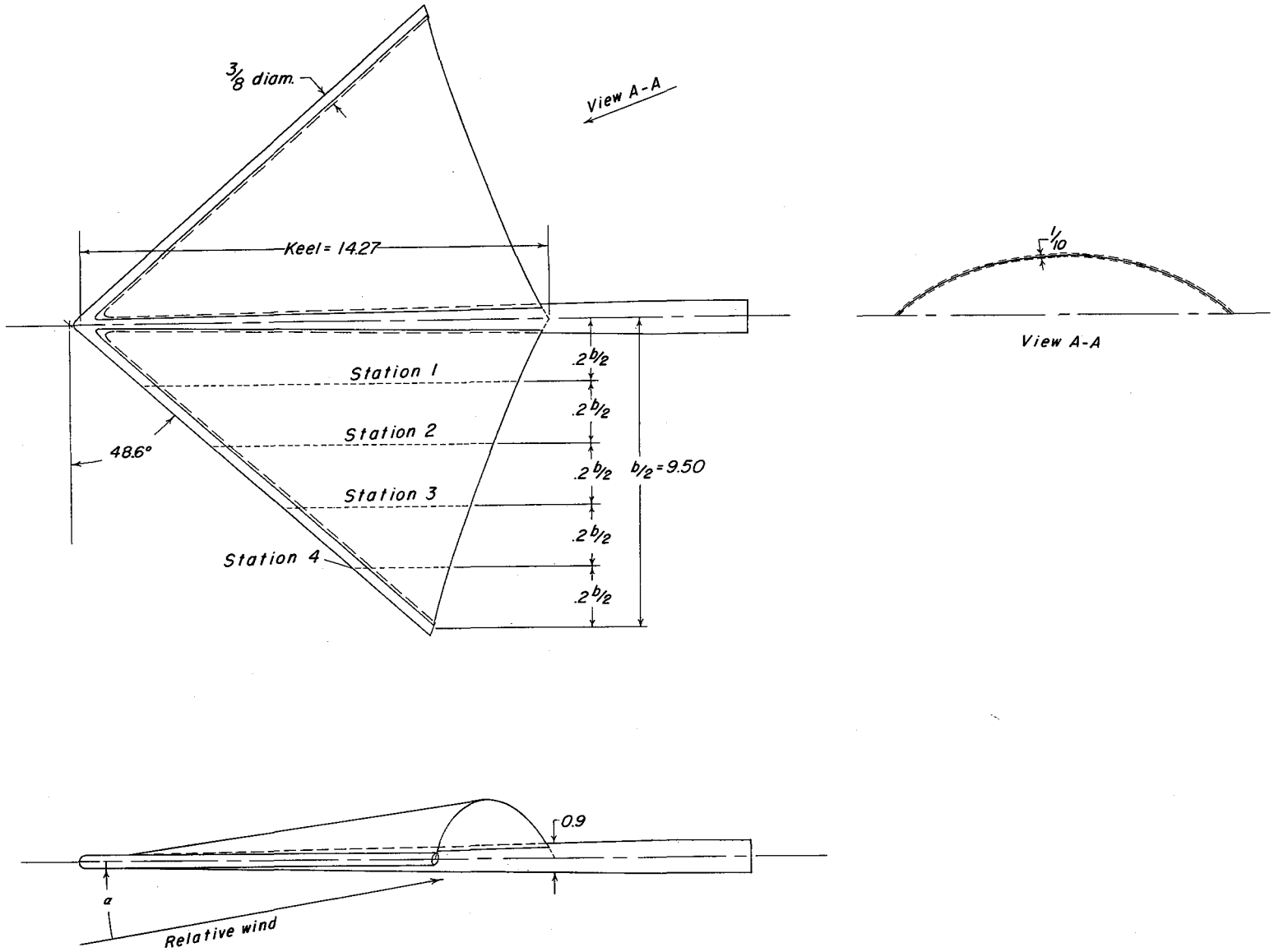

(c) Model 3.

Figure 4.- Concluded.

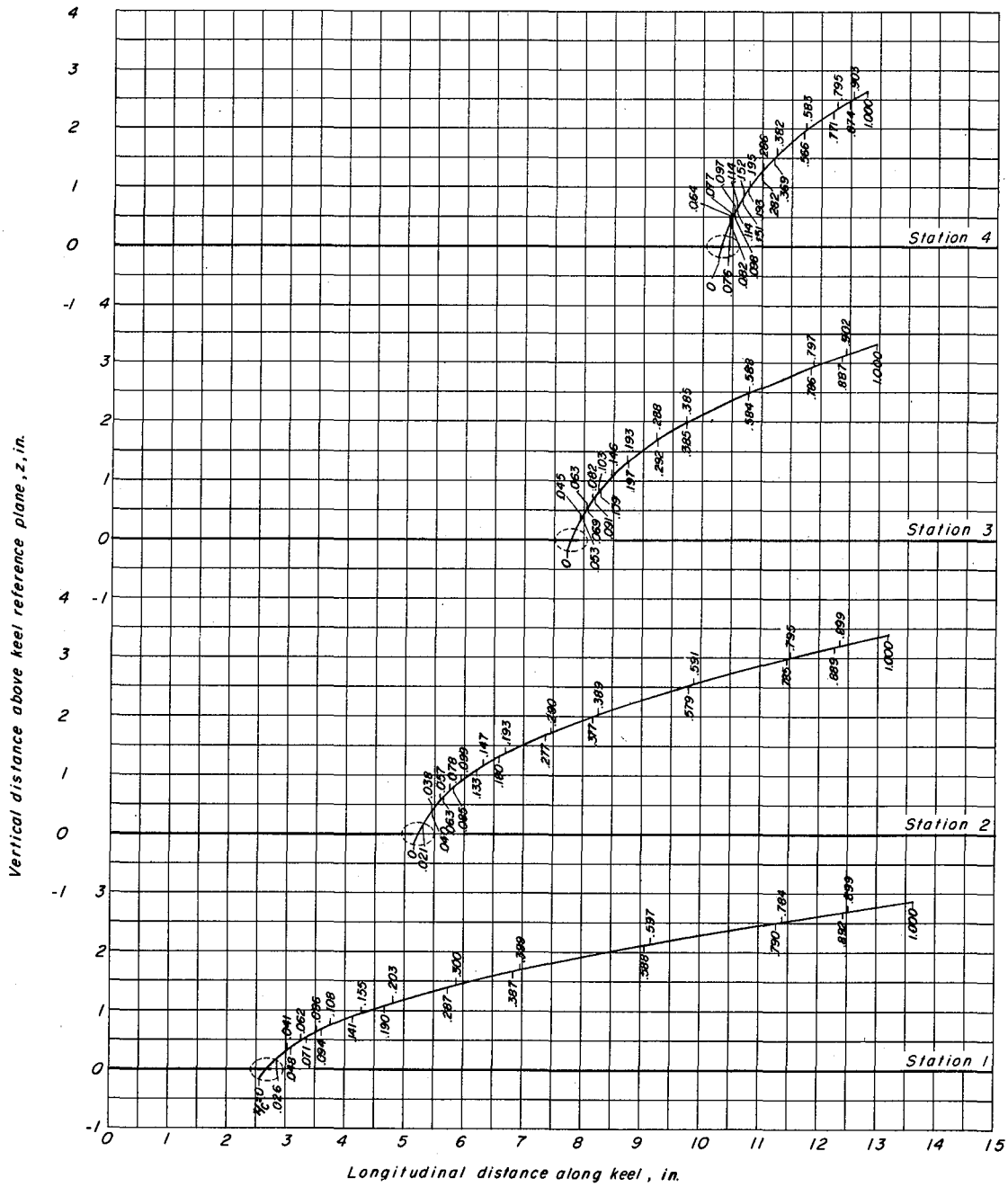

(a) Model 1.

Figure 5.- Location of lower and upper surface orifices designated in fraction of local projected chord c.

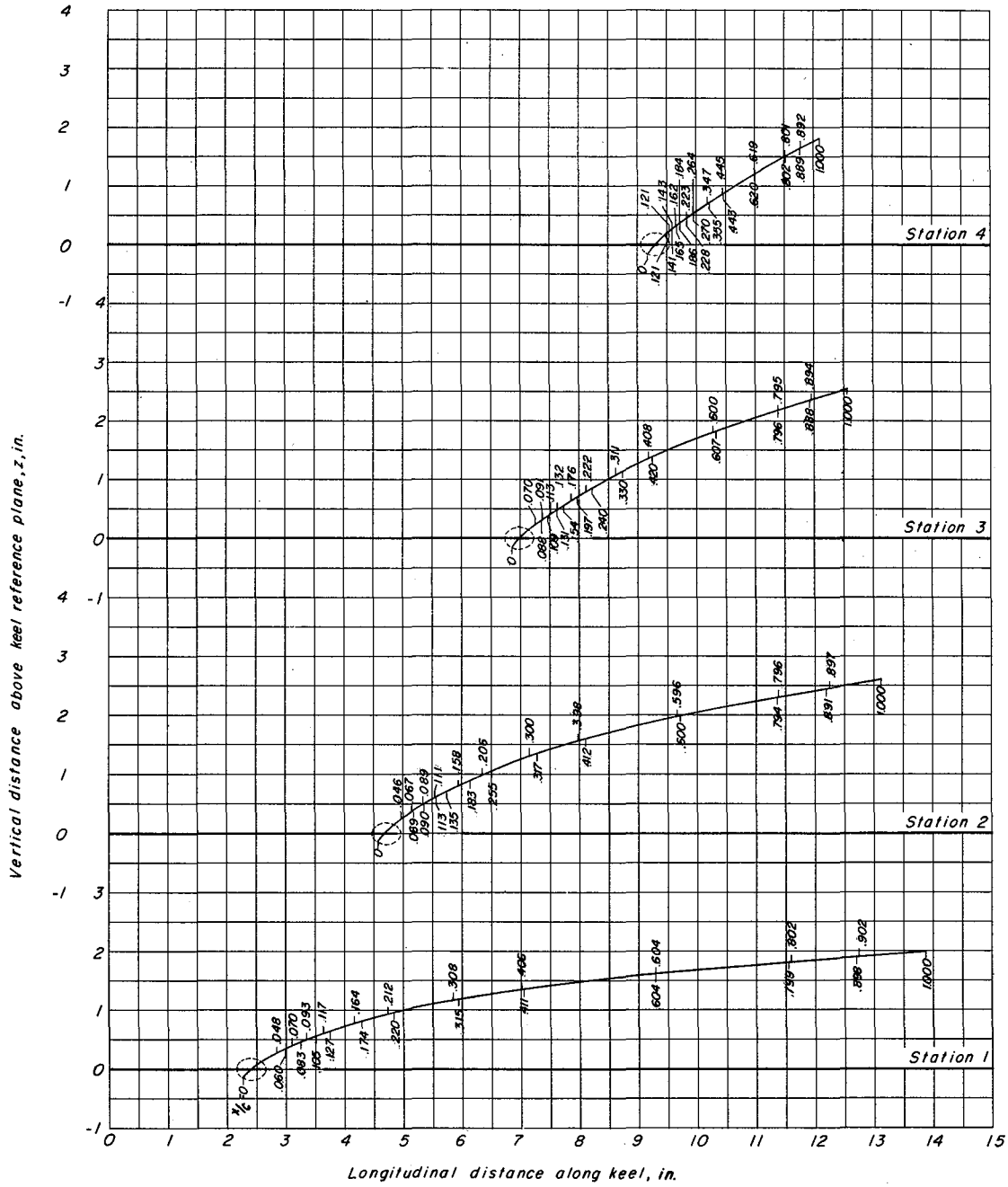

(b) Model 2.

Figure 5.- Continued.

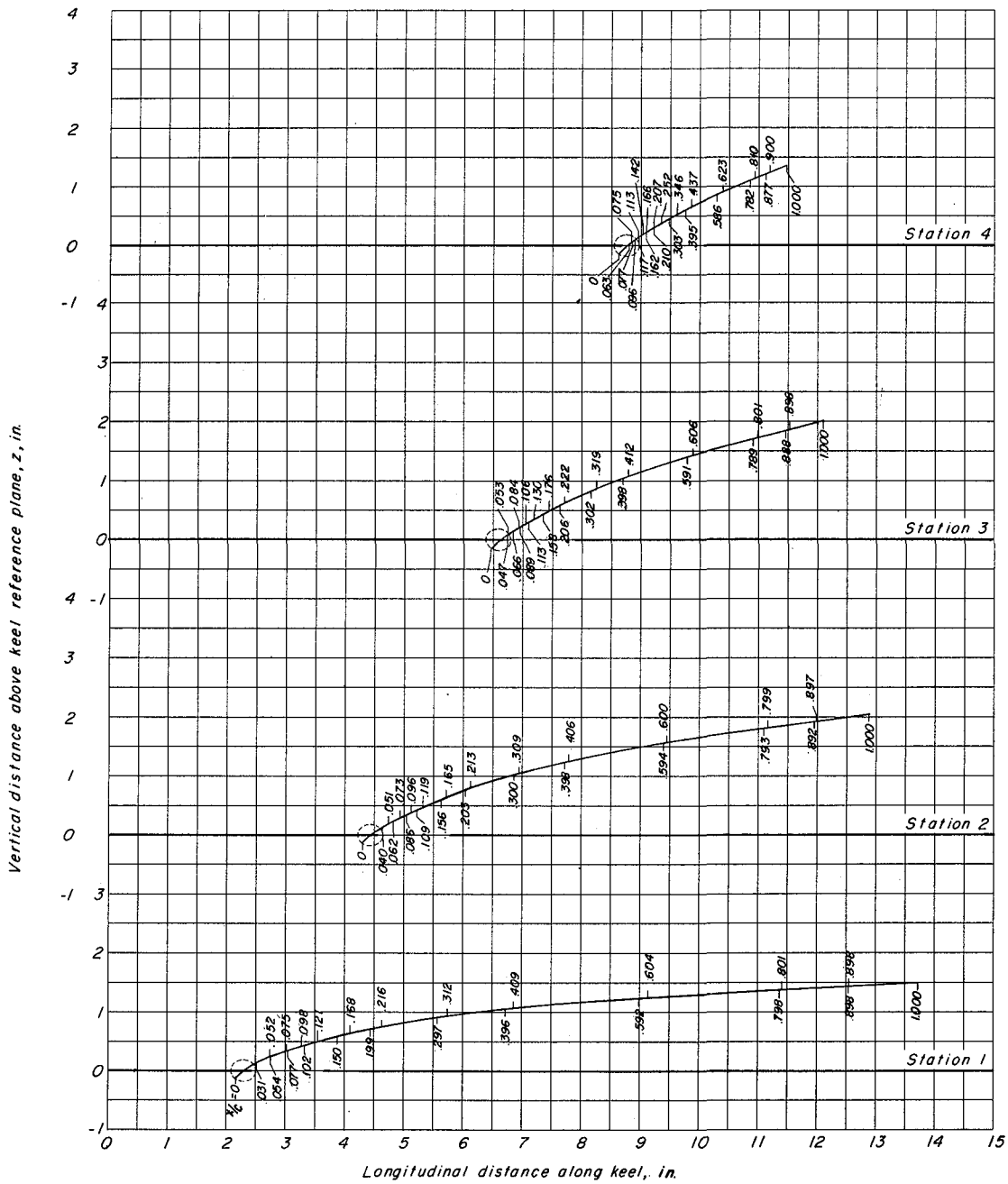

(c) Model 3.

Figure 5.- Concluded.

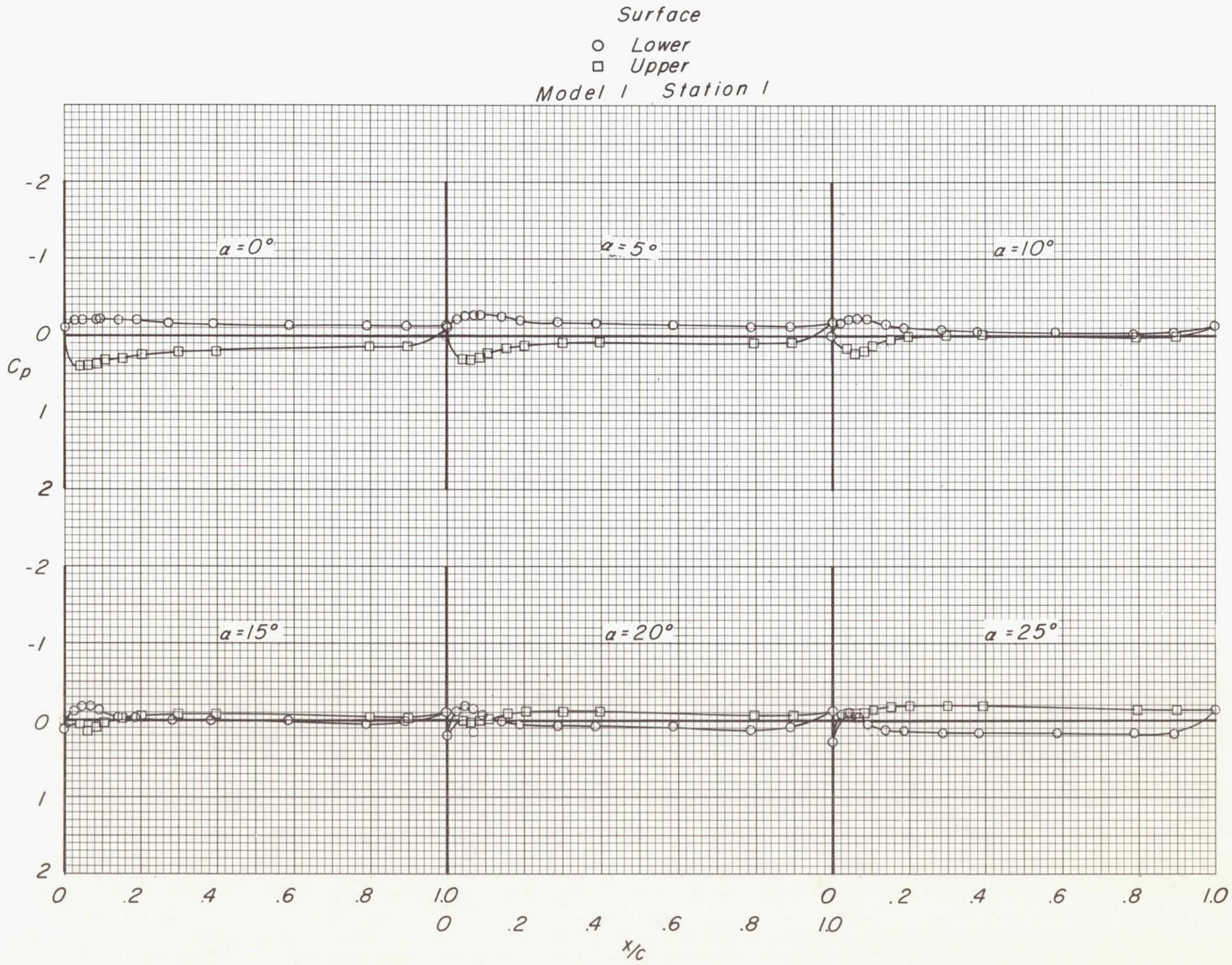

(a) M = 2.29.

Figure 6.- Pressure distributions on model 1 at various angles of attack and Mach numbers.

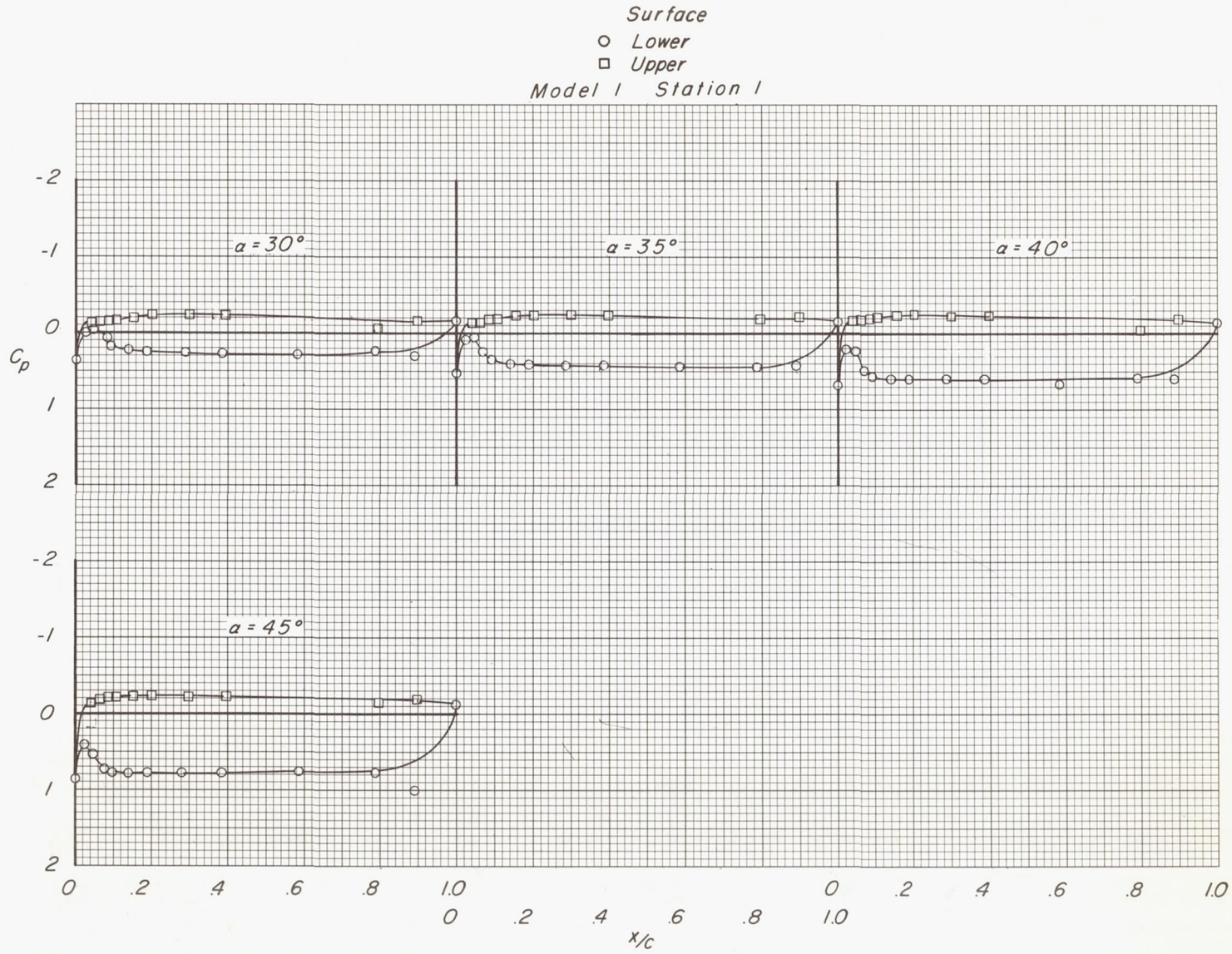

(a) M = 2.29. Continued.

Figure 6.- Continued.

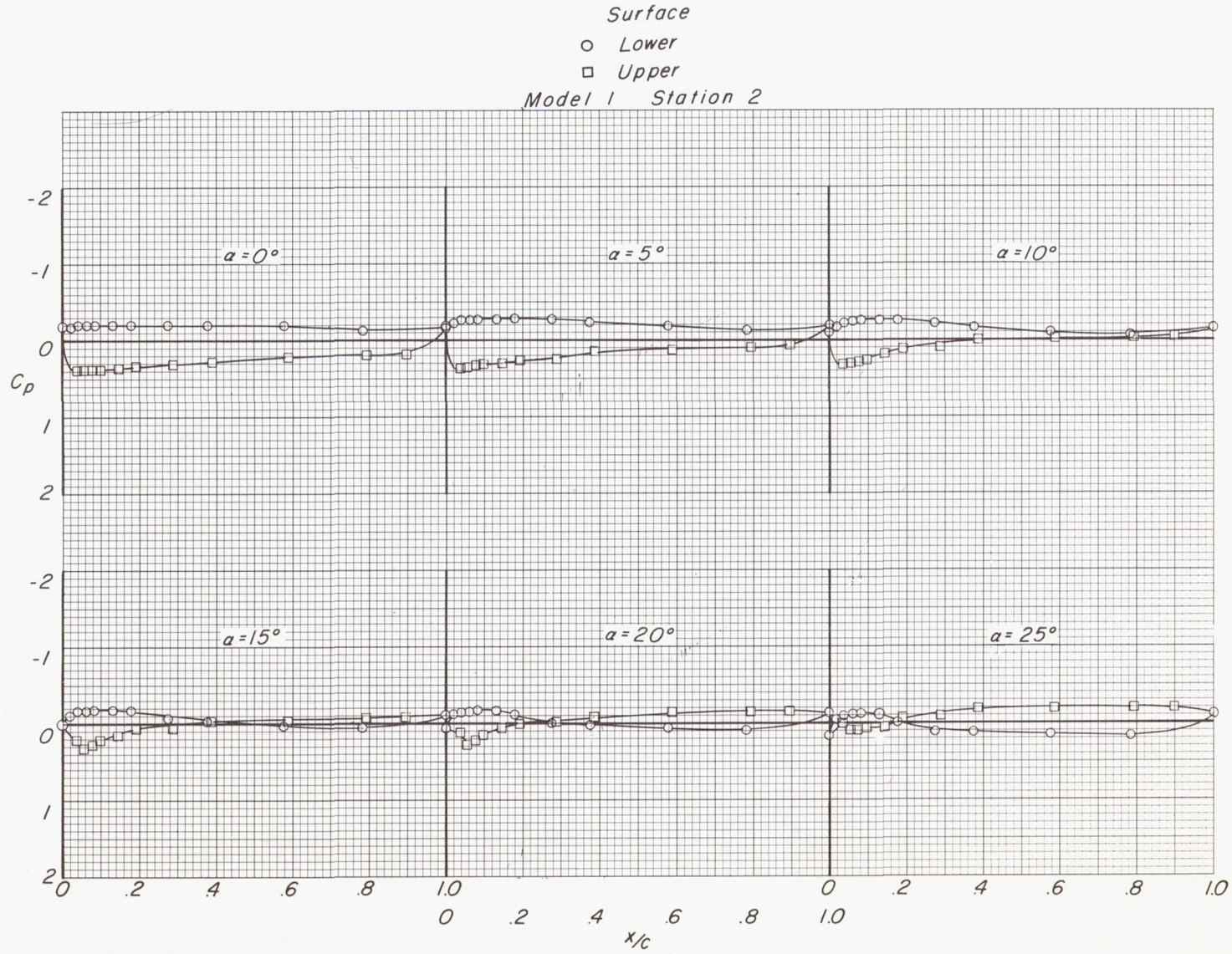

(a) M = 2.29. Continued.

Figure 6.- Continued.

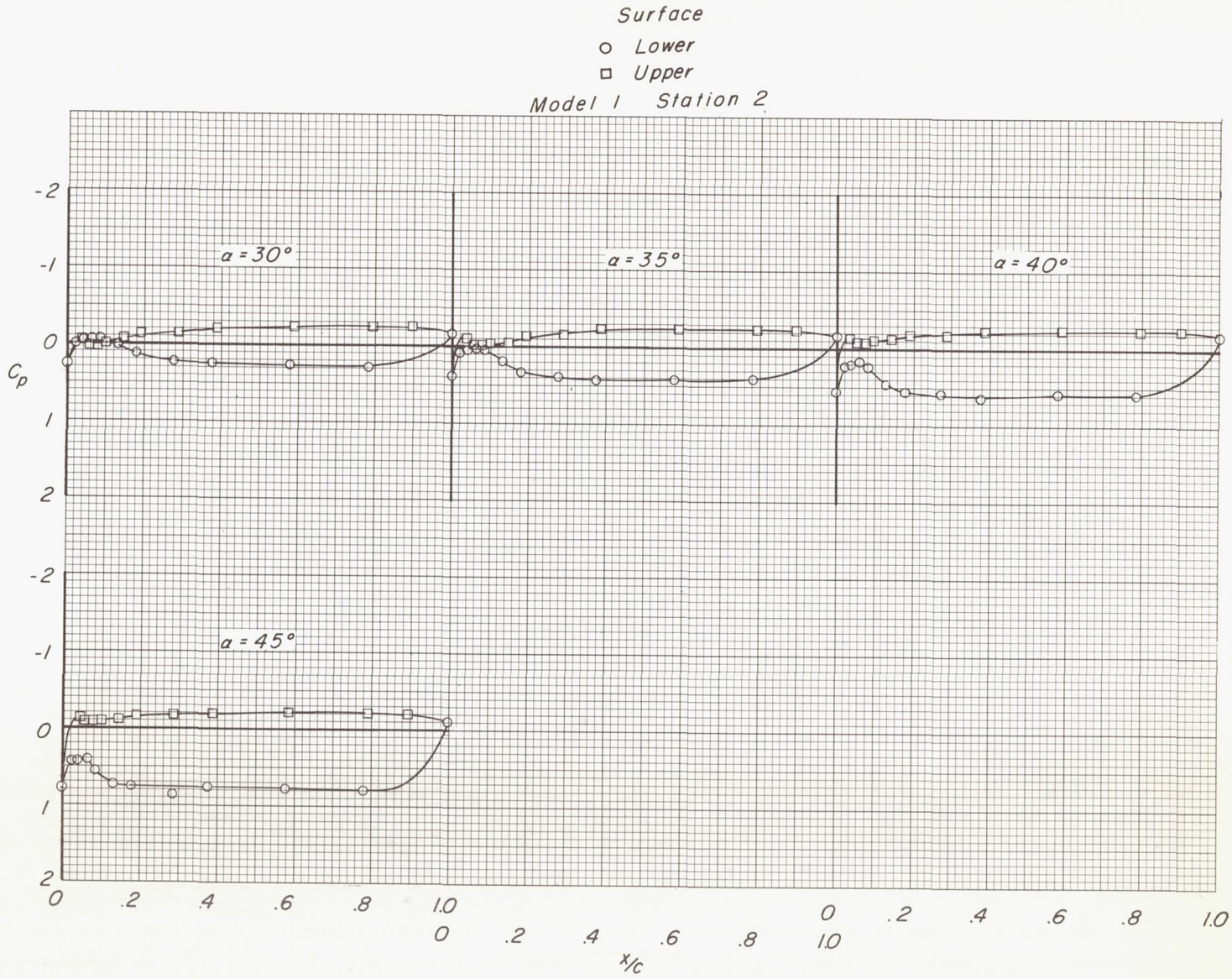

(a) M = 2.29. Continued.

Figure 6.- Continued.

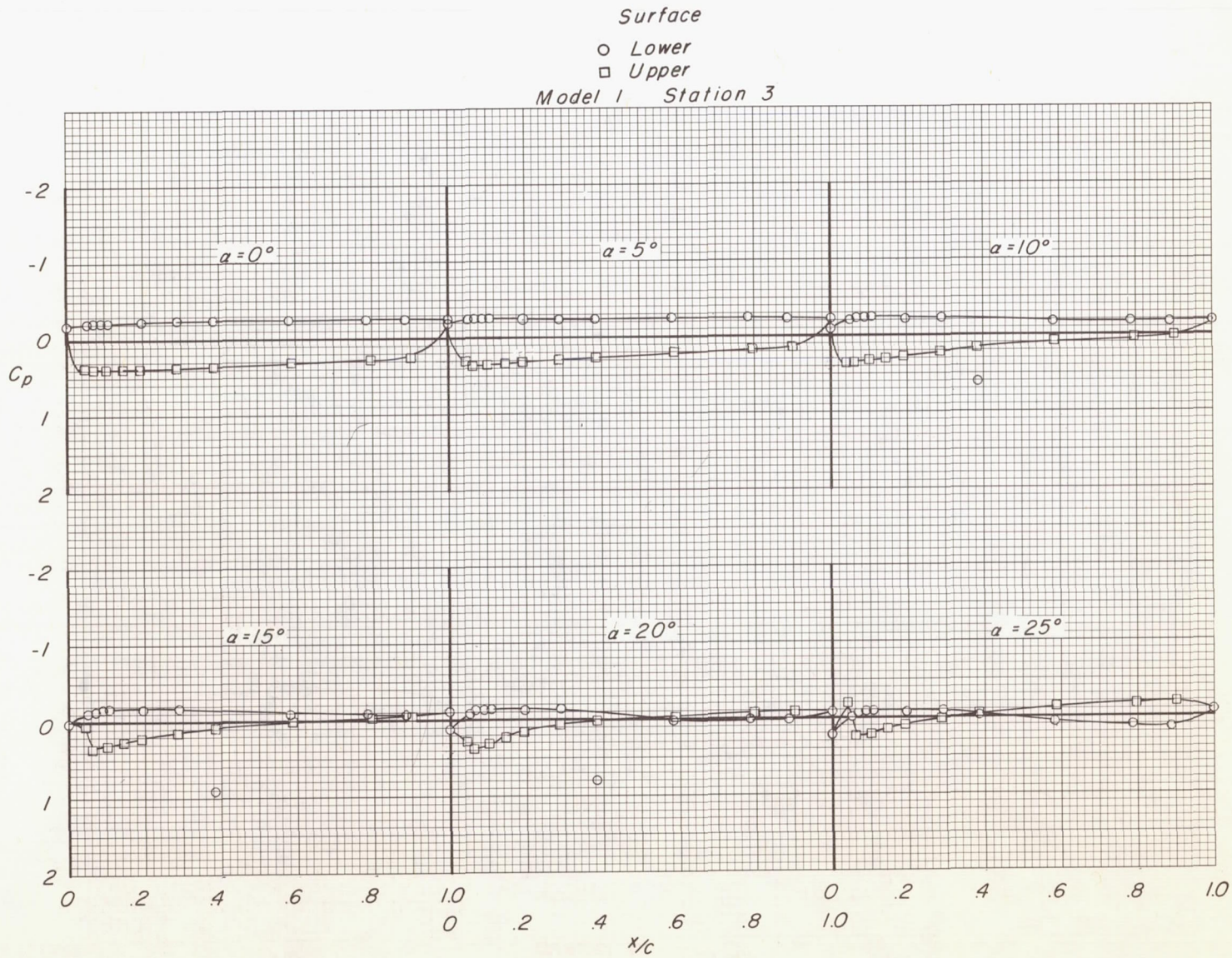

(a) M = 2.29. Continued.

Figure 6.- Continued.

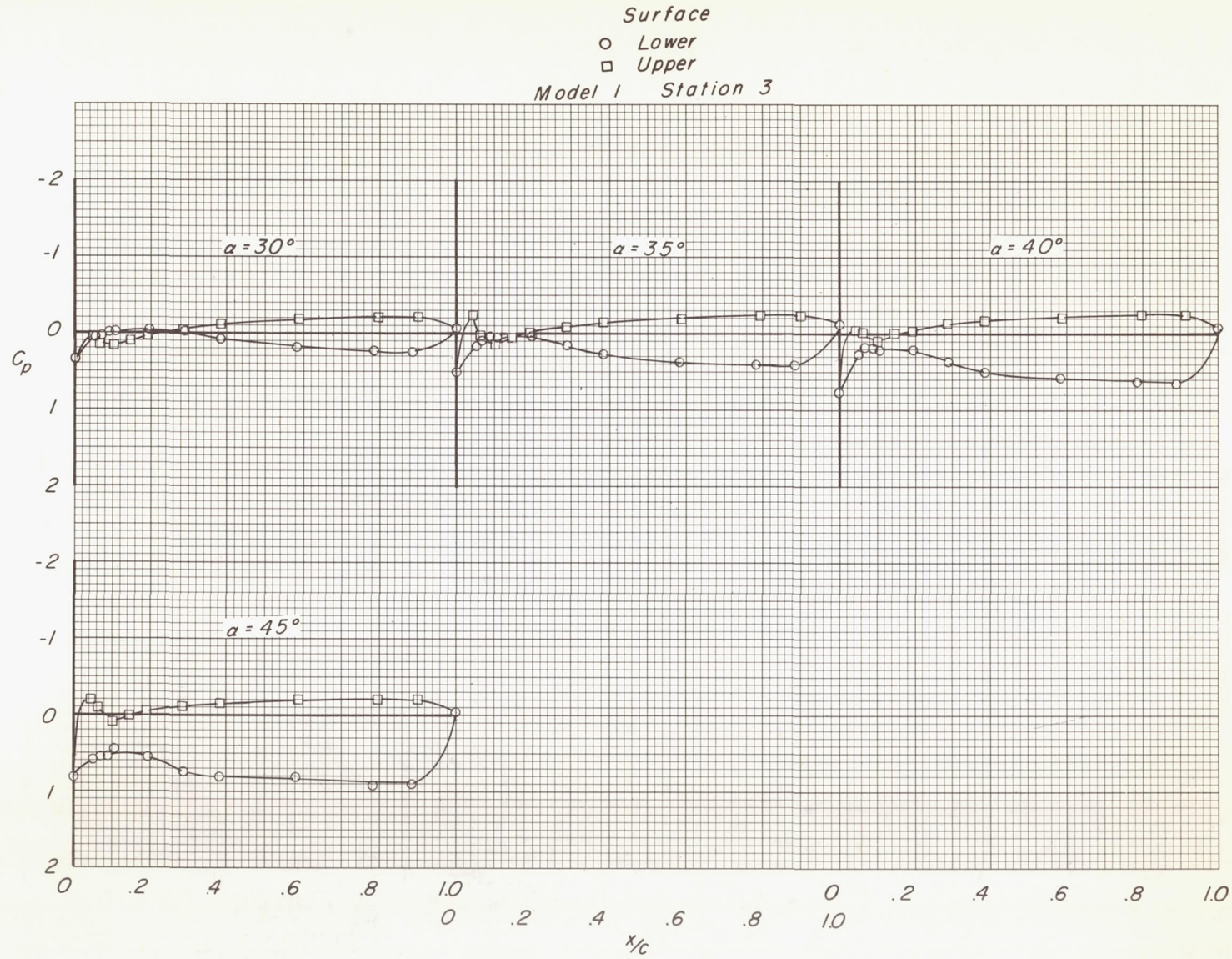

(a) M = 2.29. Continued.

Figure 6.- Continued.

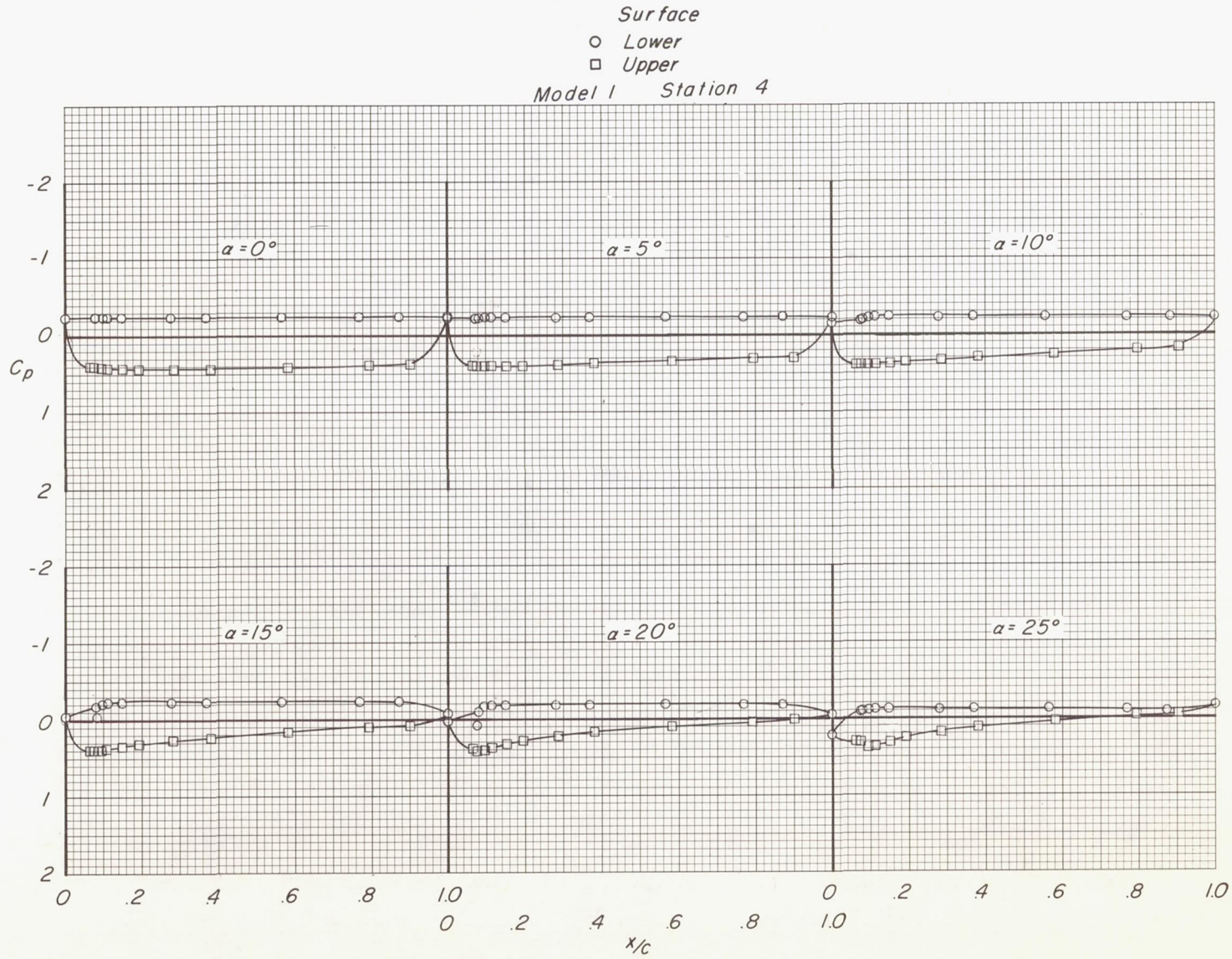

(a) M = 2.29. Continued.

Figure 6.- Continued.

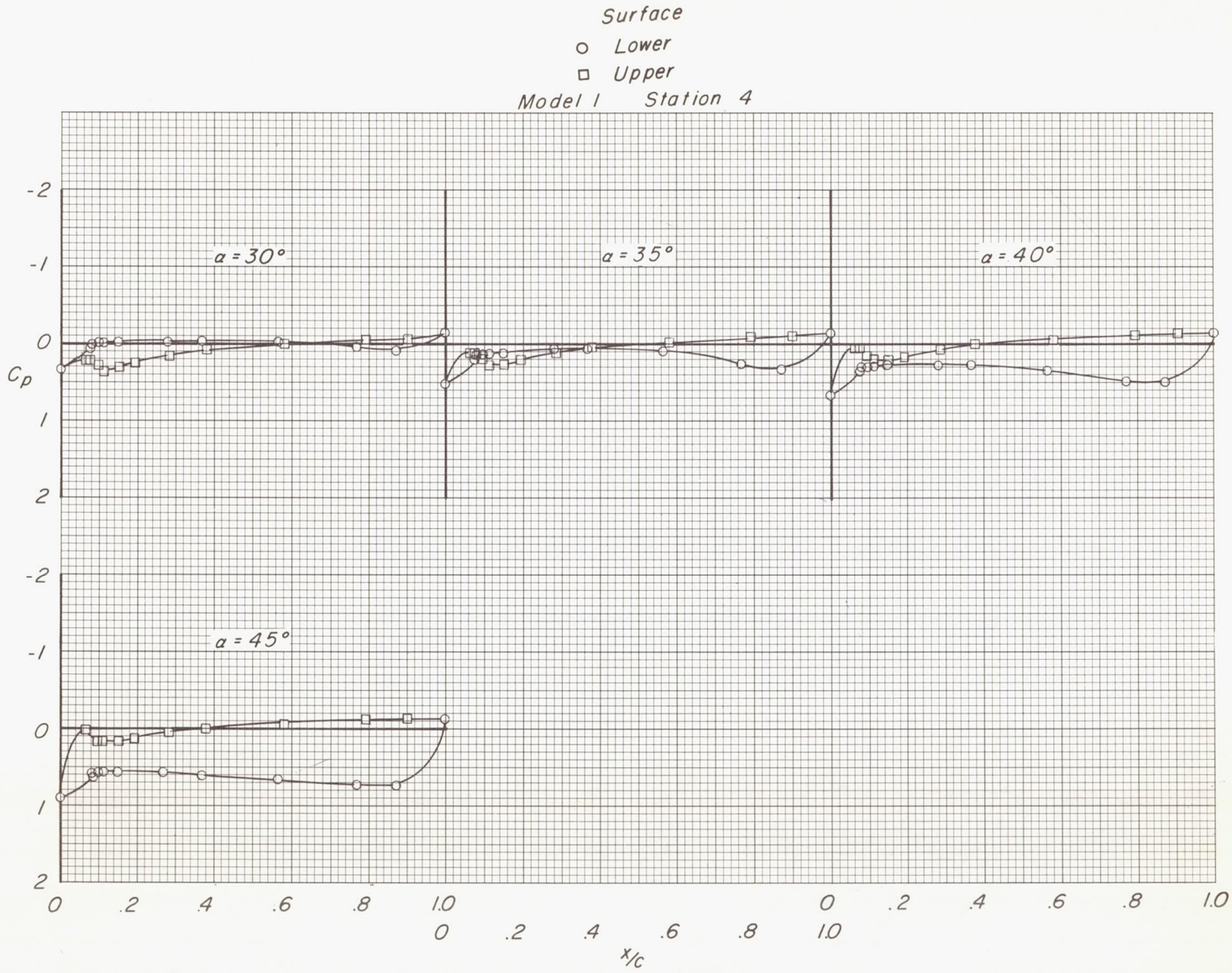

(a) M = 2.29. Concluded.

Figure 6.- Continued.

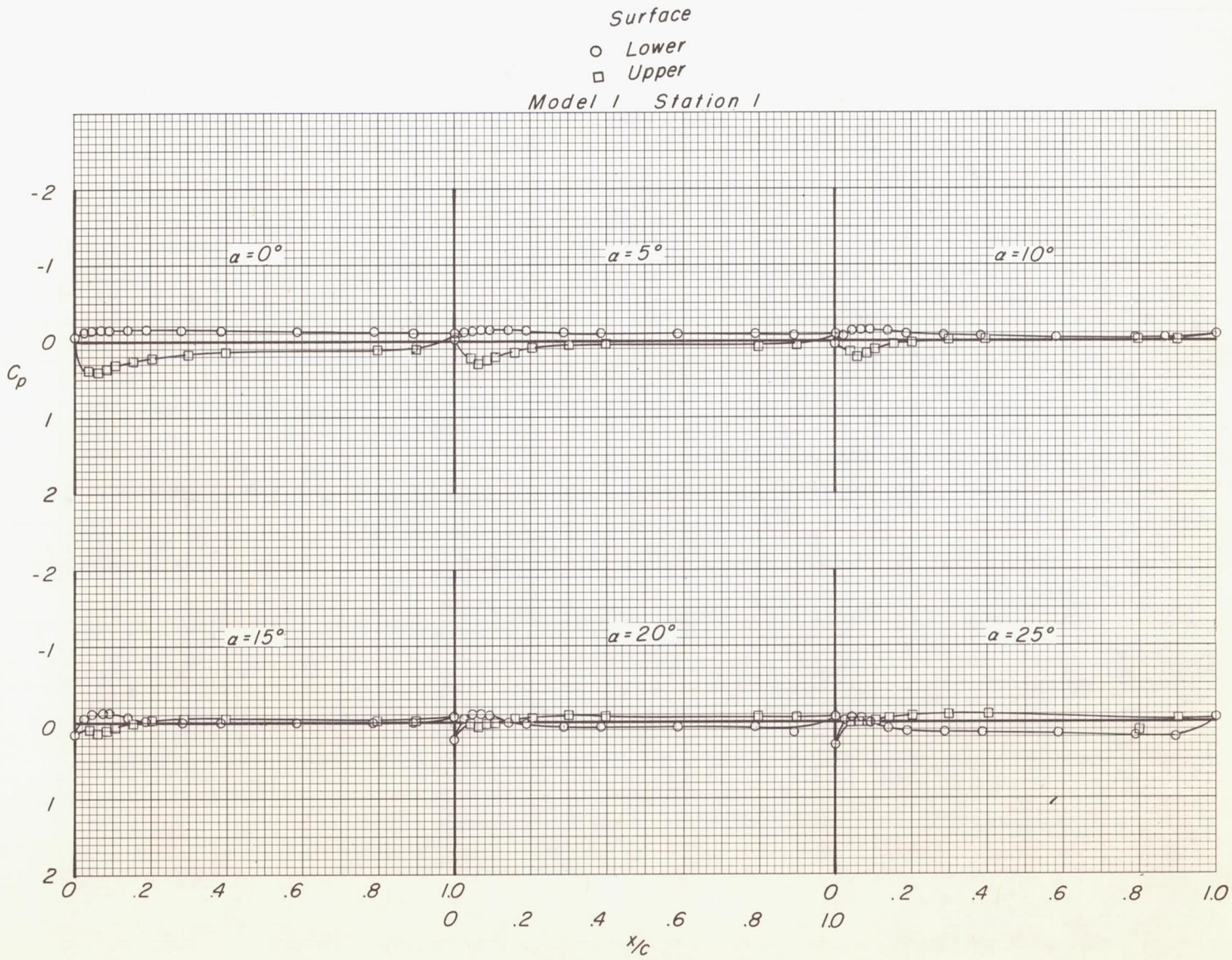

(b) M = 2.96.

Figure 6.- Continued.

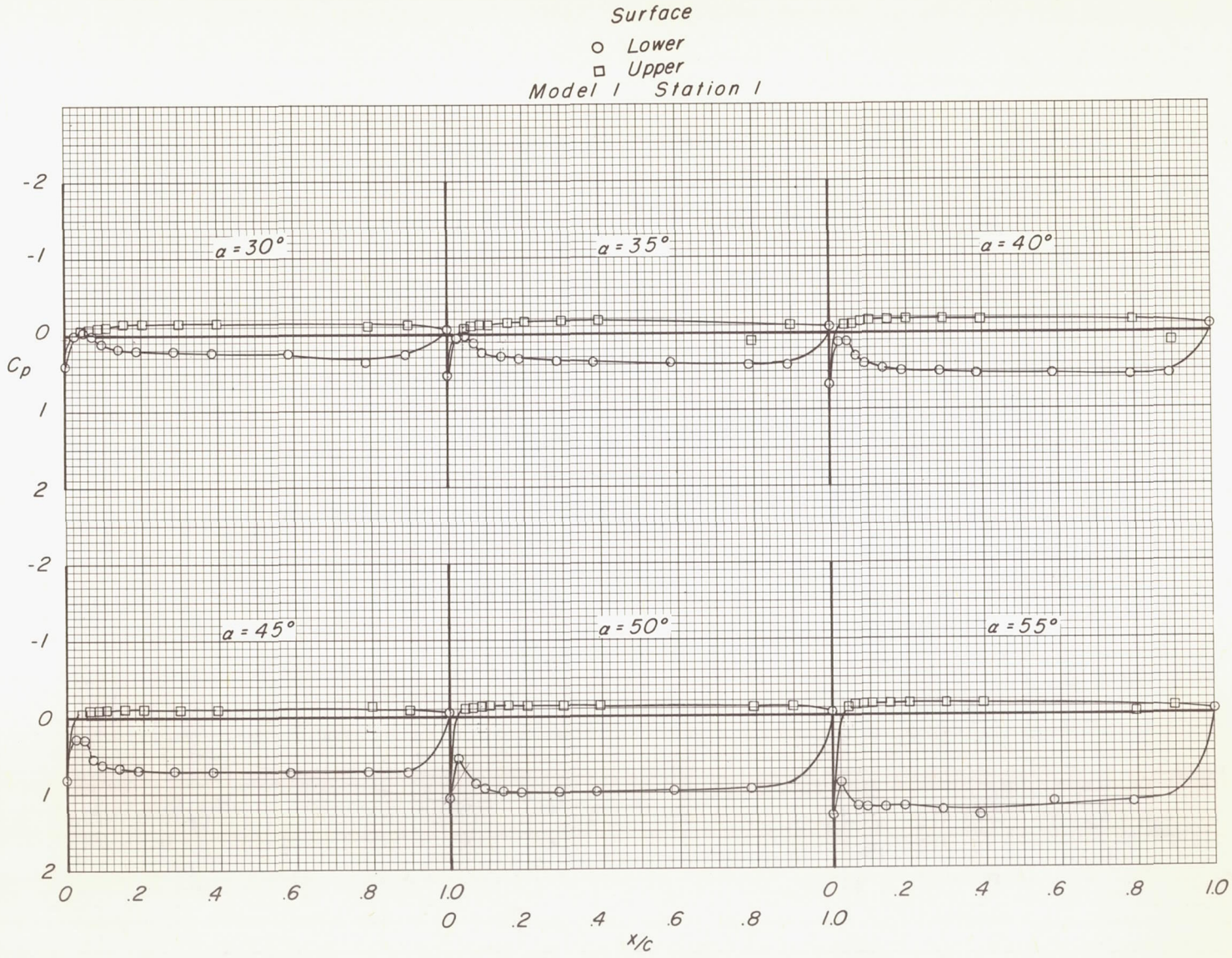

(b) M = 2.96. Continued.

Figure 6.- Continued.

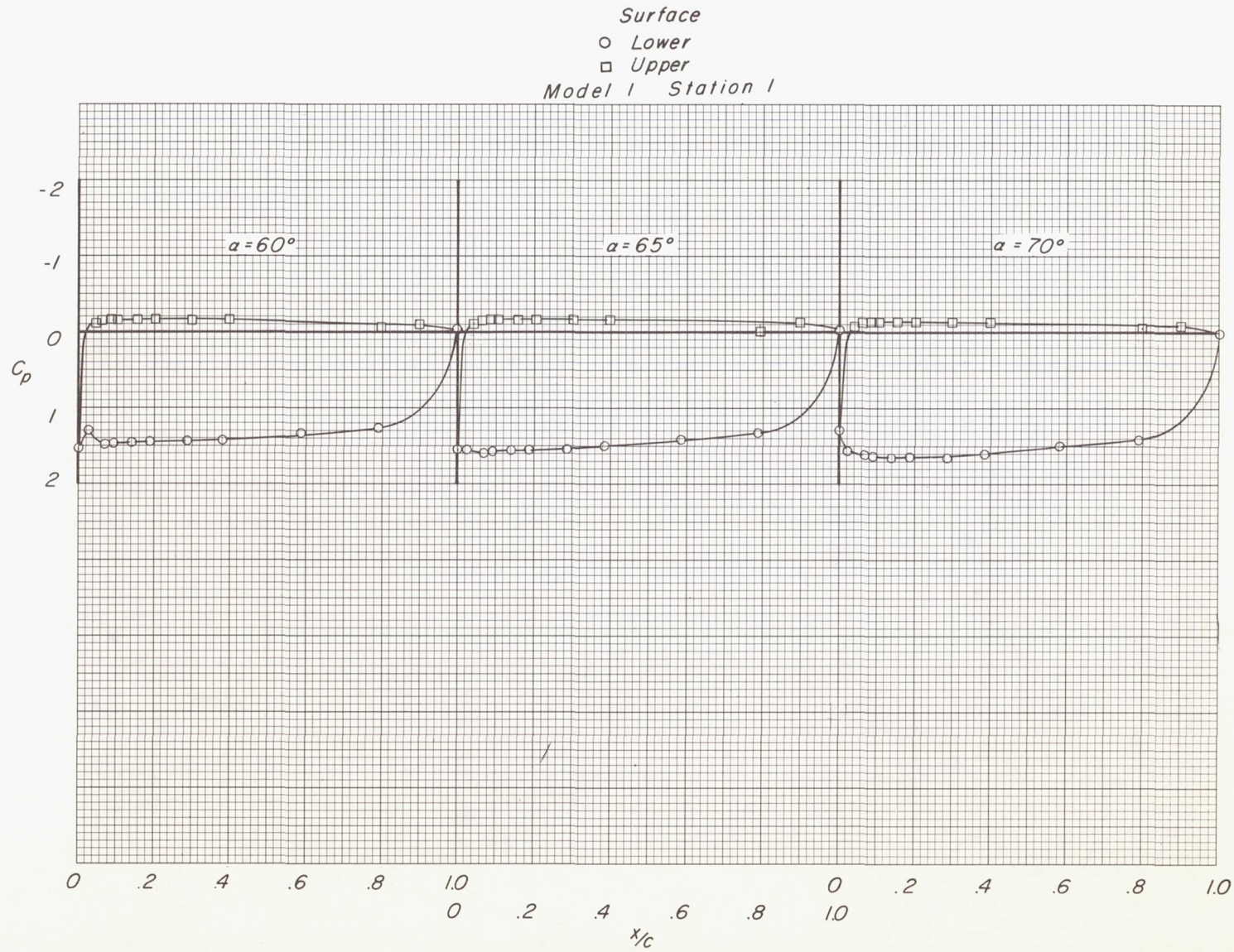

(b) M = 2.96. Continued.

Figure 6.- Continued.

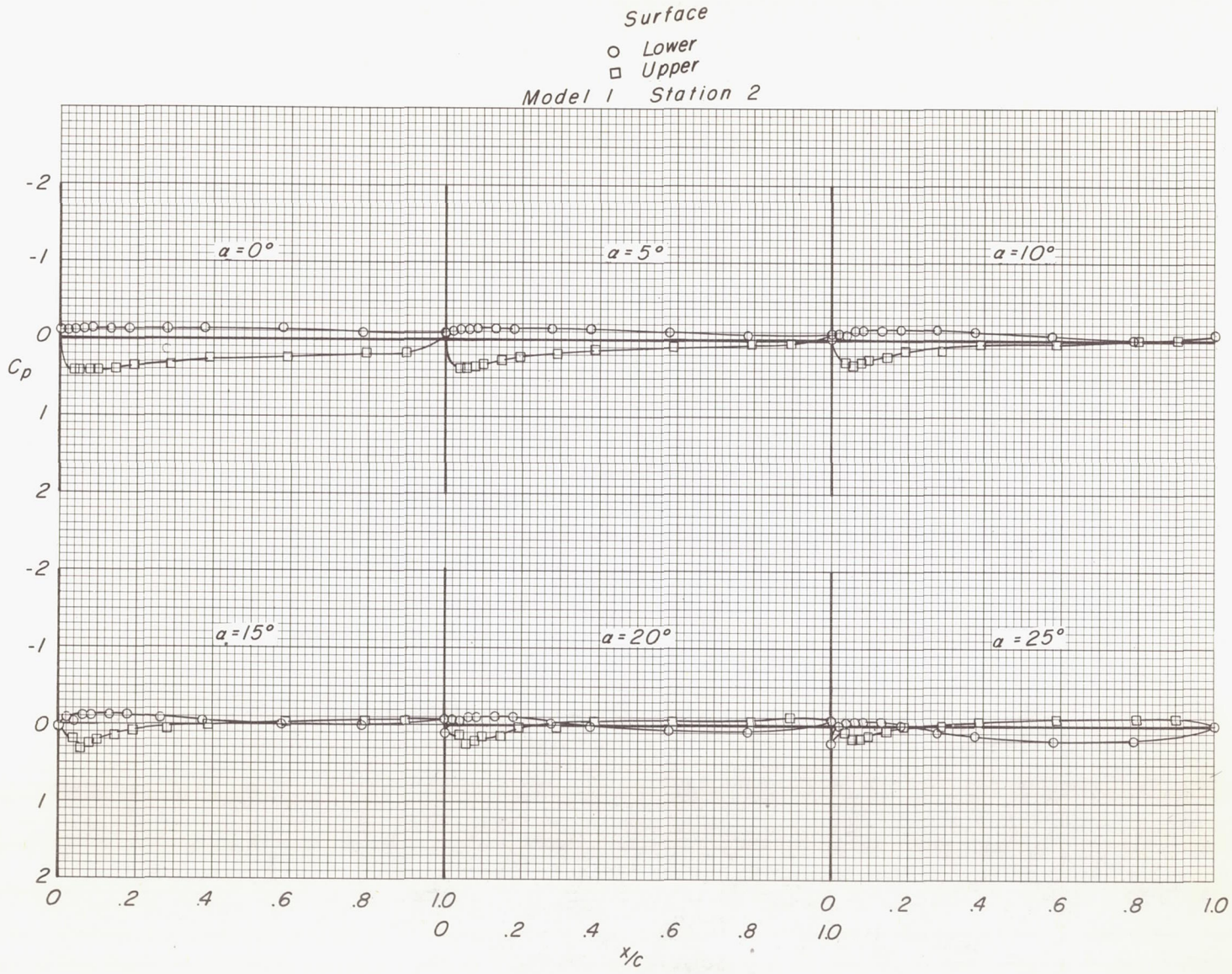

(b) M = 2.96. Continued.

Figure 6.- Continued.

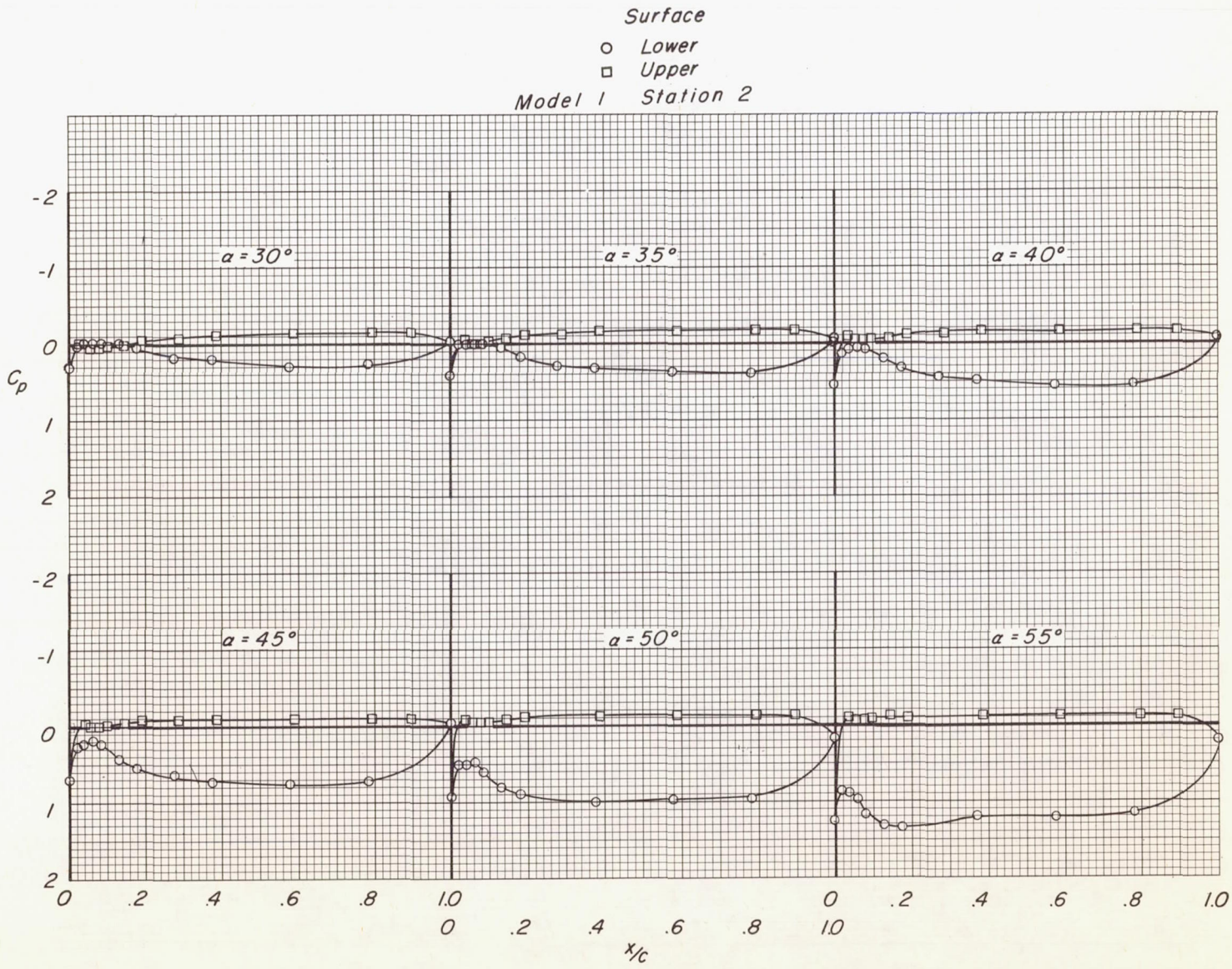

(b) M = 2.96. Continued.

Figure 6.- Continued.

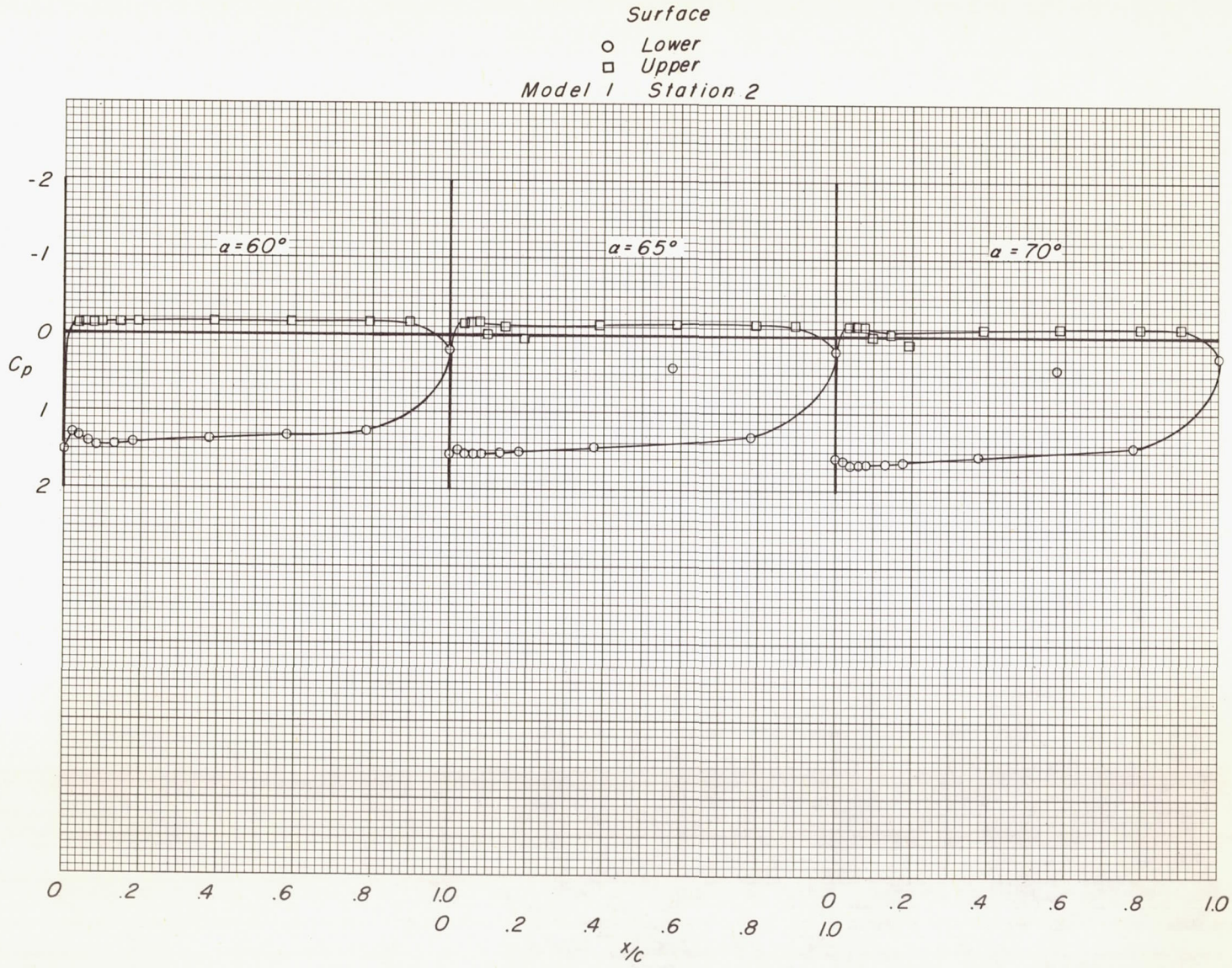

(b) M = 2.96. Continued.

Figure 6.- Continued.

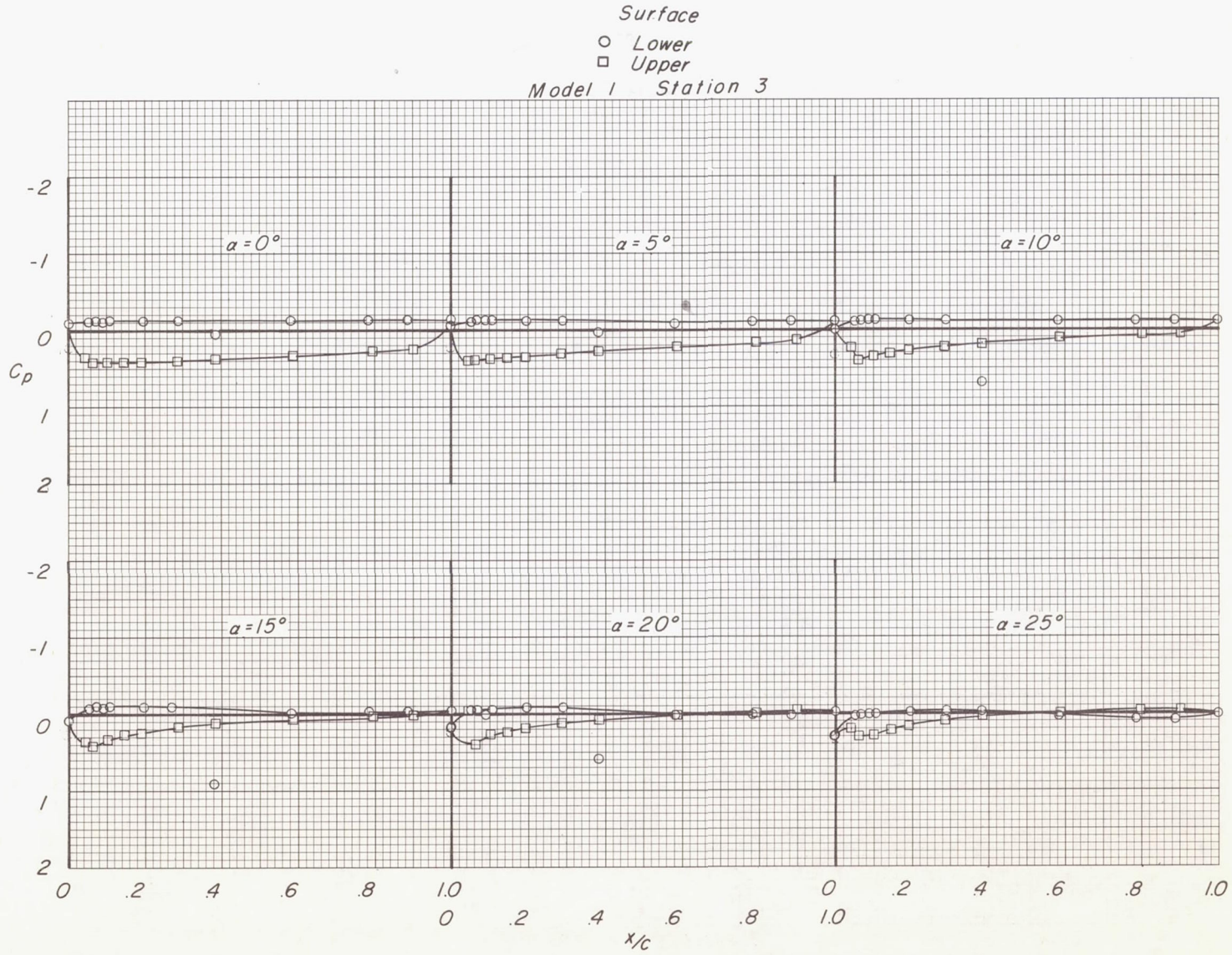

(b) M = 2.96. Continued.

Figure 6.- Continued.

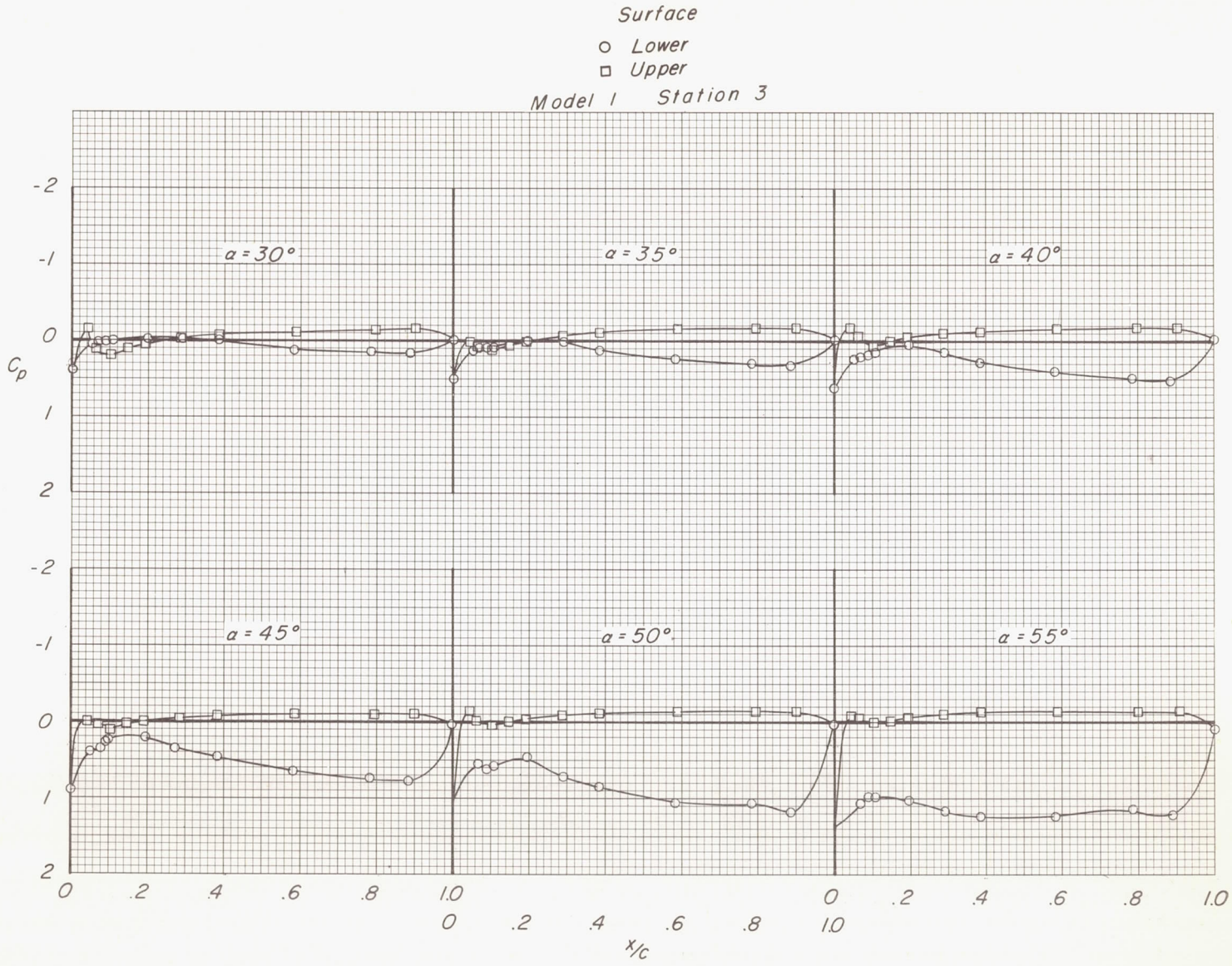

(b) M = 2.96. Continued.

Figure 6.- Continued.

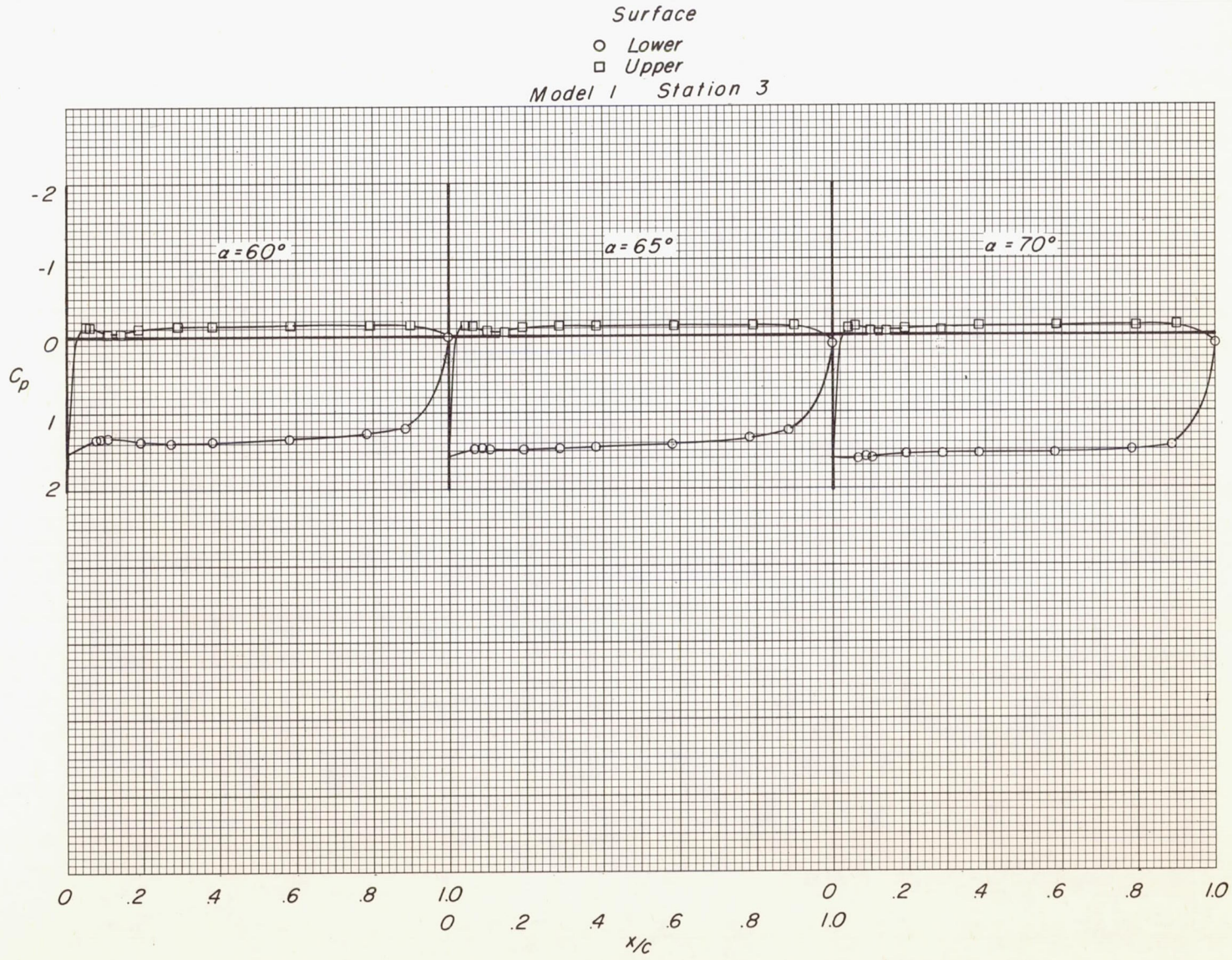

(b) M = 2.96. Continued.

Figure 6.- Continued.

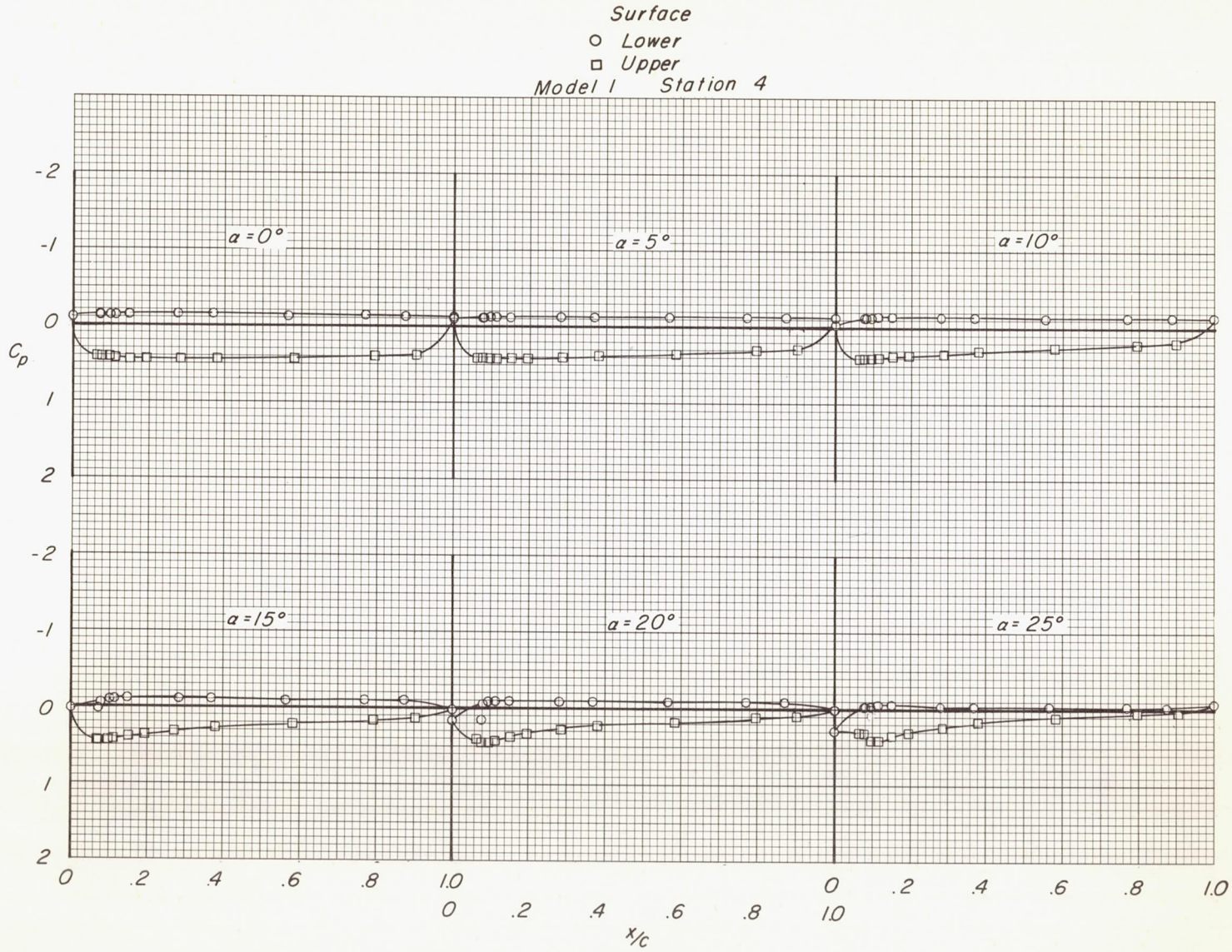

(b) M = 2.96. Continued.

Figure 6.- Continued.

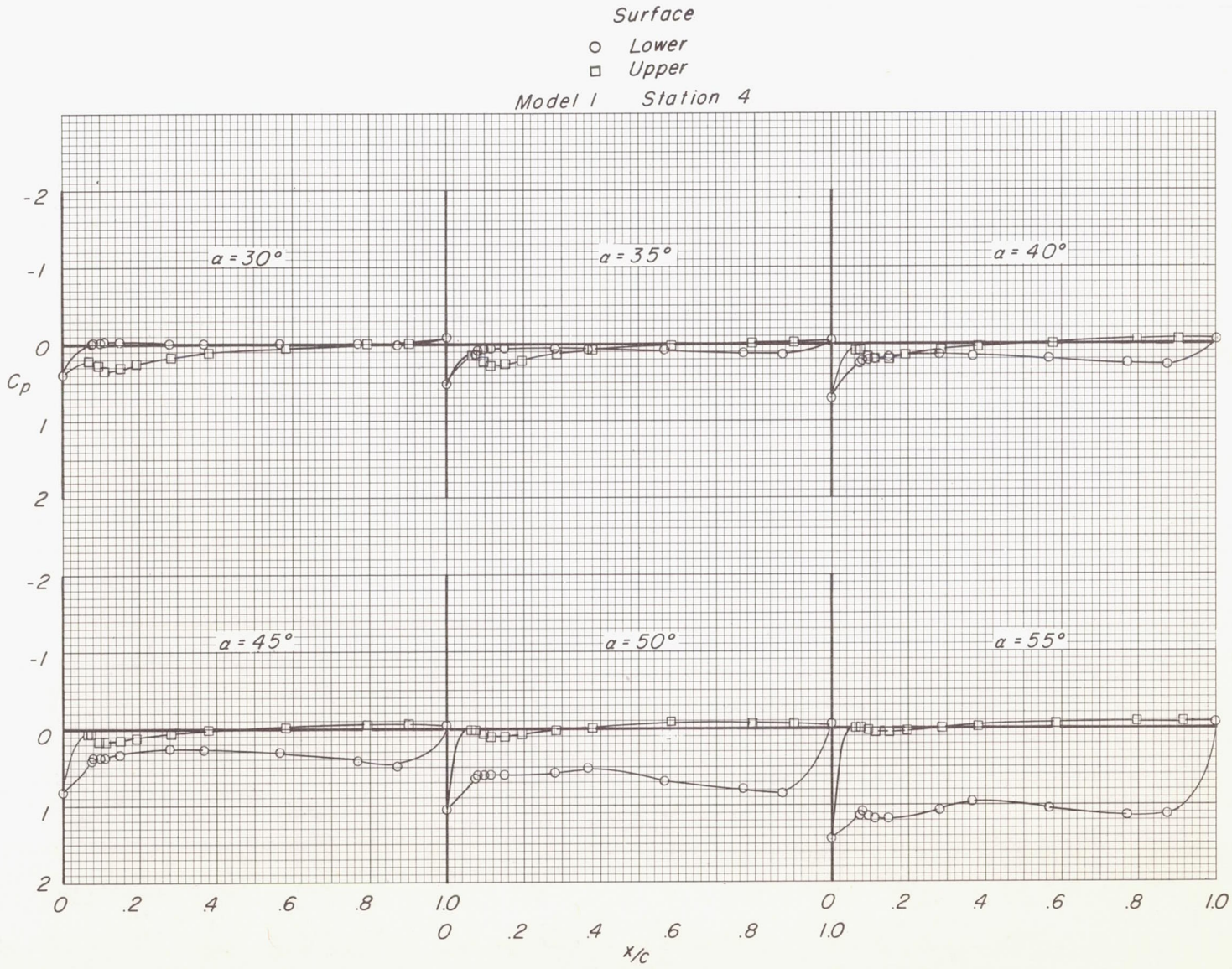

(b) M = 2.96. Continued.

Figure 6.- Continued.

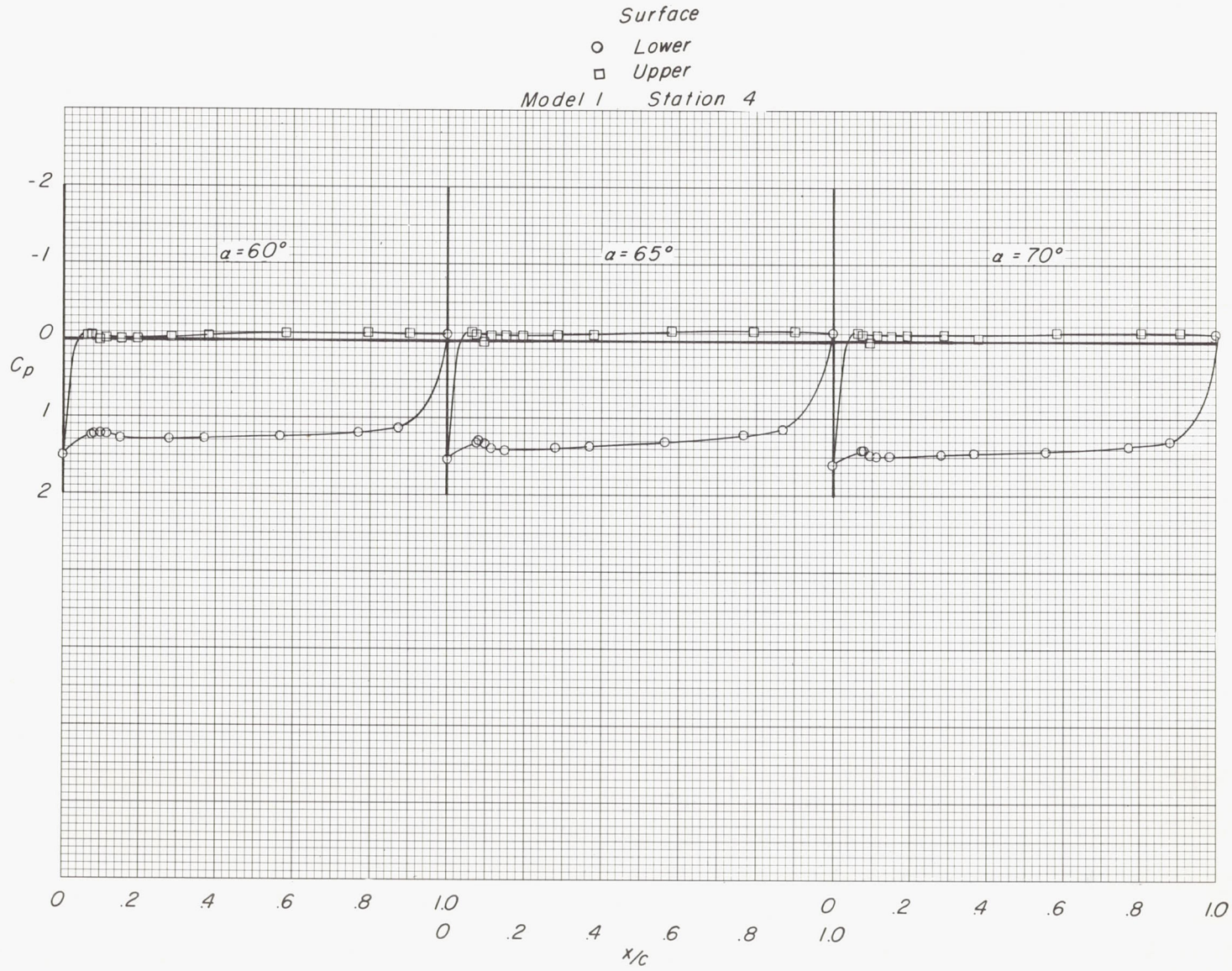

(b) M = 2.96. Concluded.

Figure 6.- Continued.

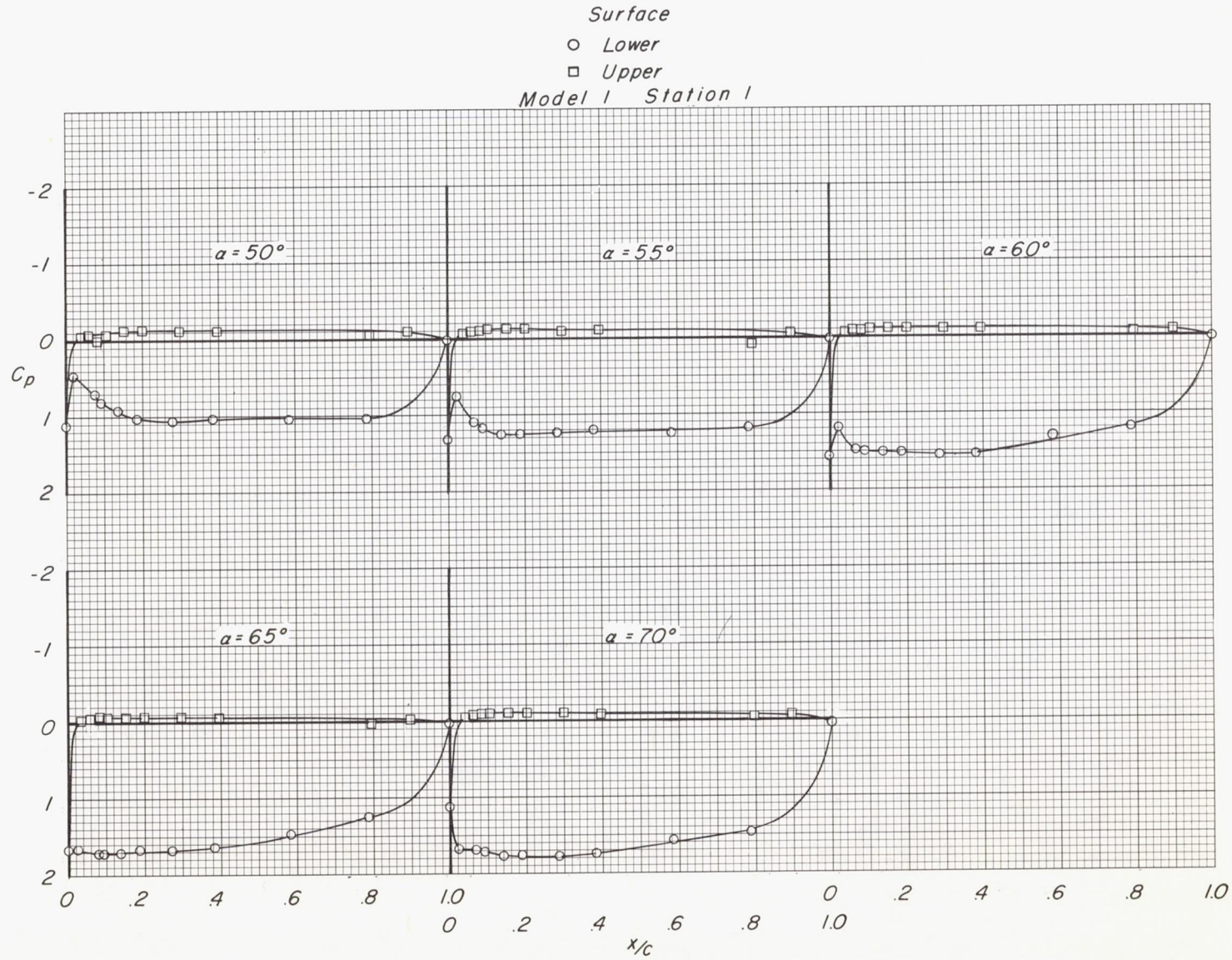

(c) M = 3.95.

Figure 6.- Continued.

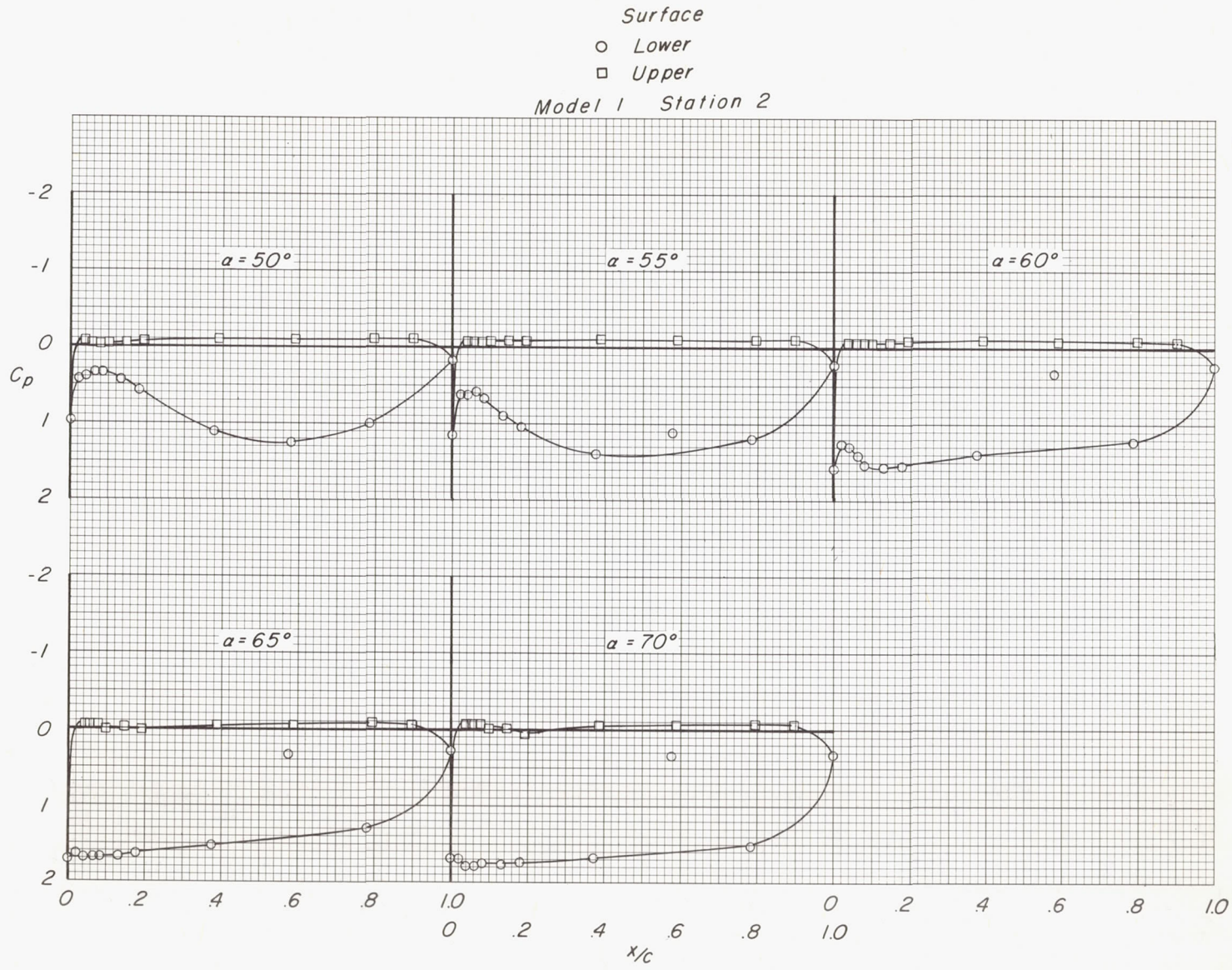

(c) M = 3.95. Continued.

Figure 6.- Continued.

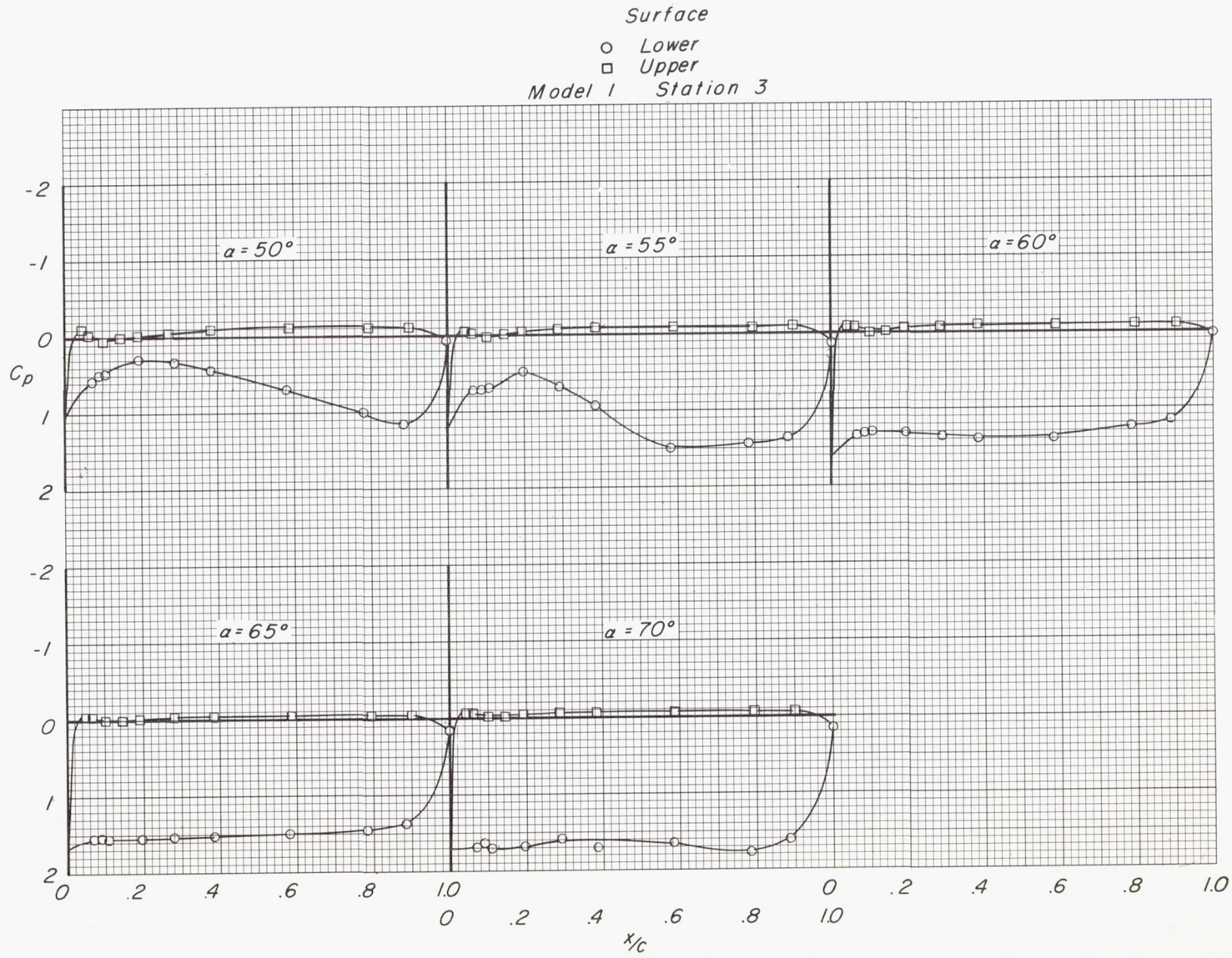

(c) M = 3.95. Continued.

Figure 6.- Continued.

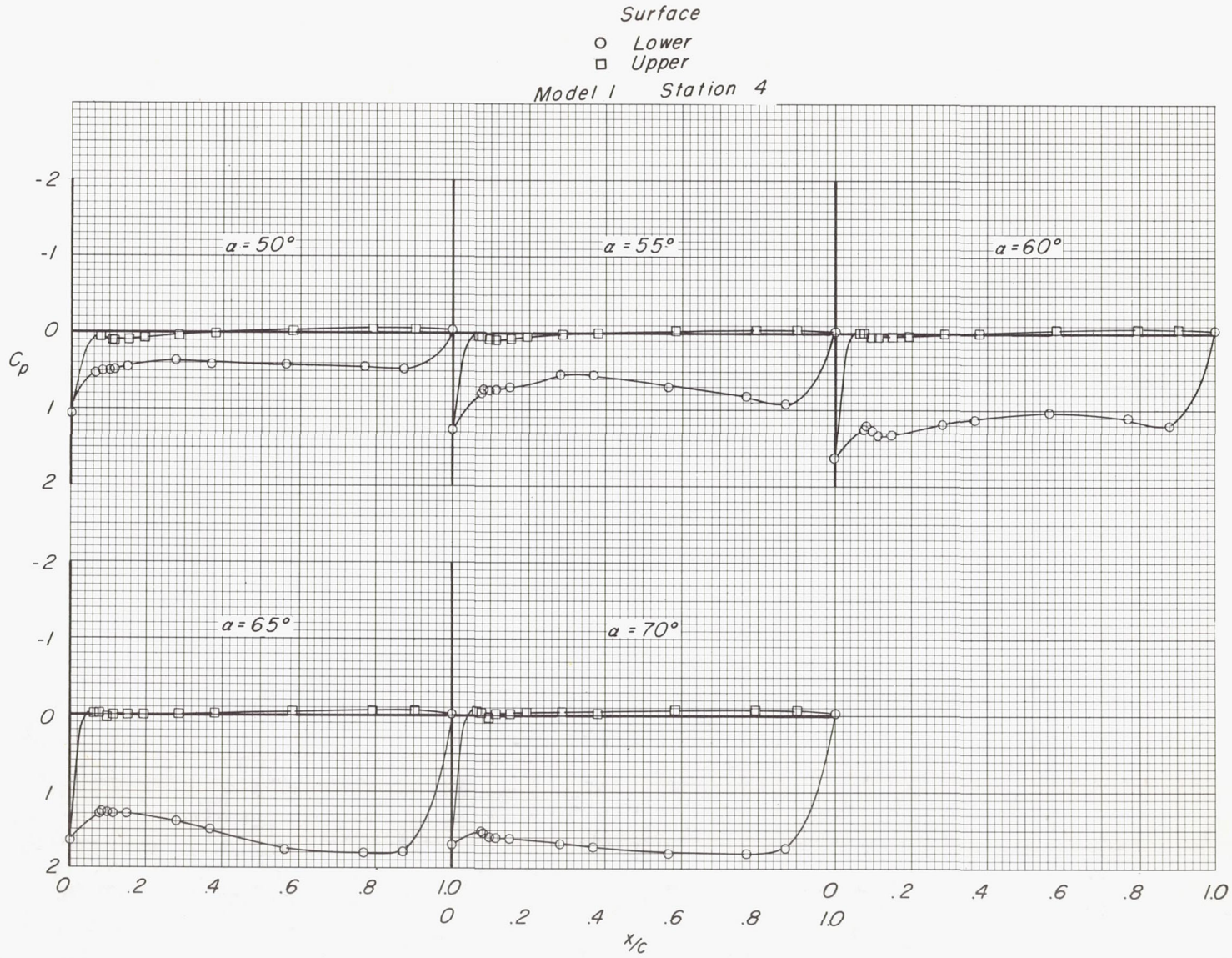

(c) M = 3.95. Concluded.

Figure 6.- Continued.

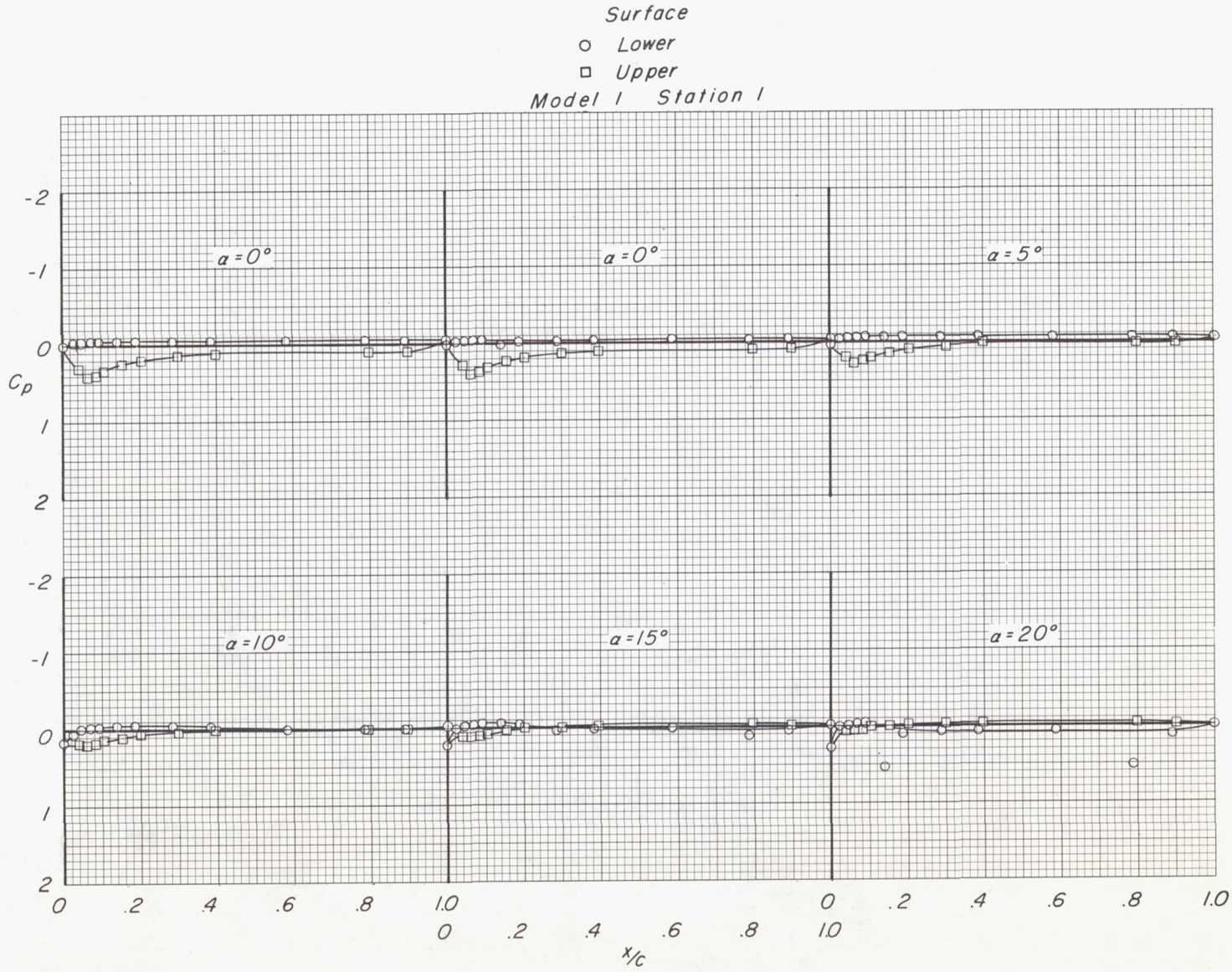

(d) M = 4.65.

Figure 6.- Continued.

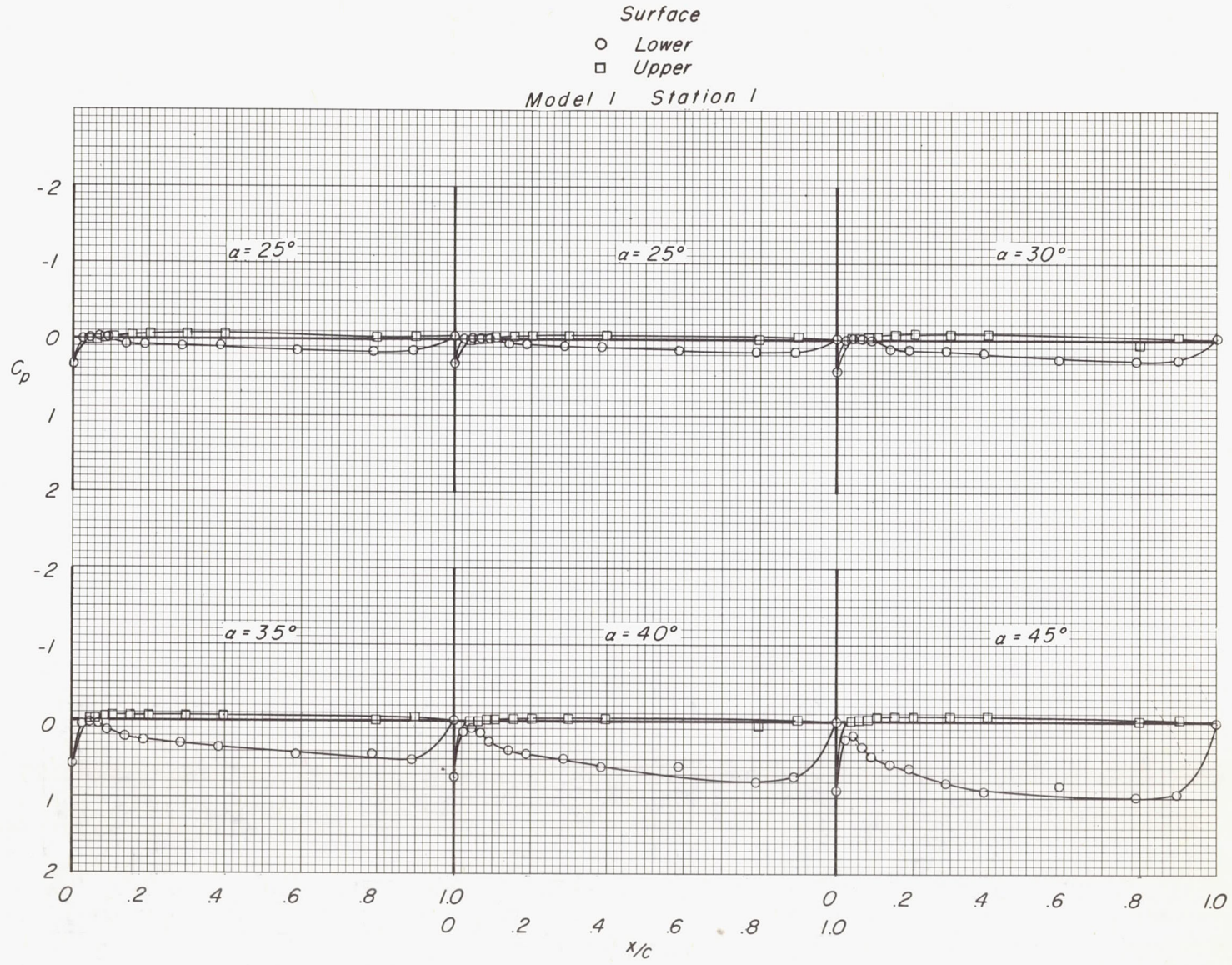

(d) M = 4.65. Continued.

Figure 6.- Continued.

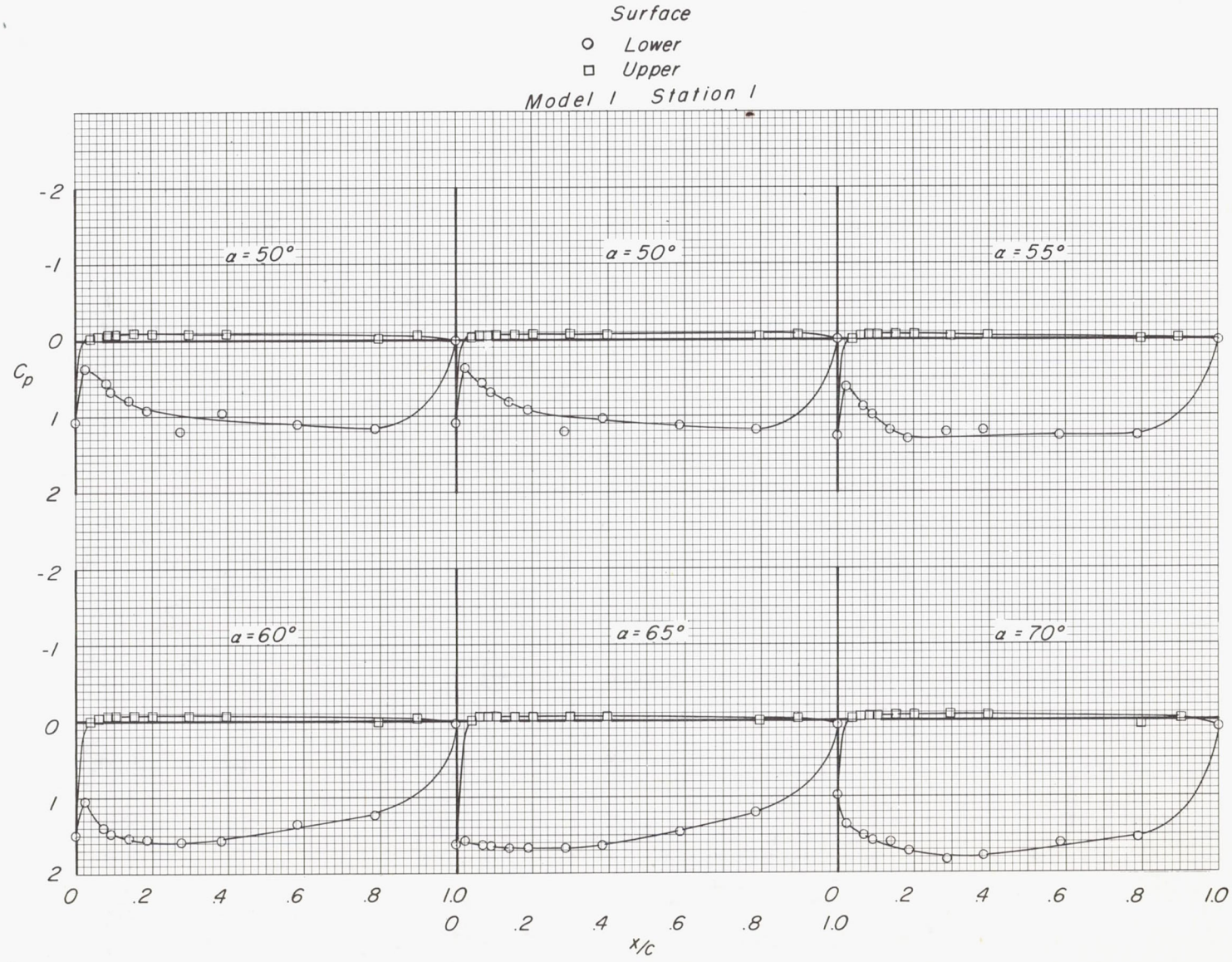

(d) M = 4.65. Continued.

Figure 6.- Continued.

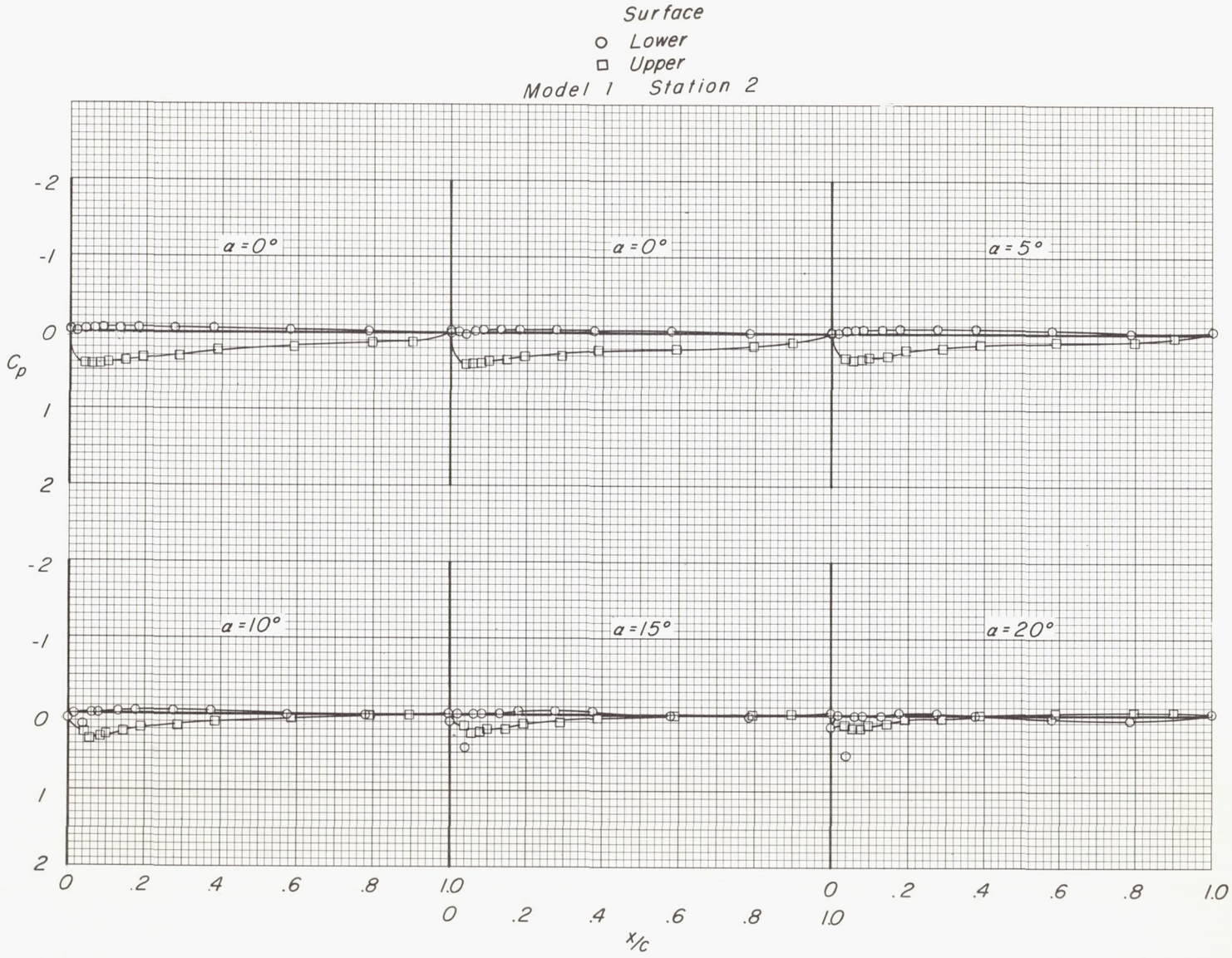

(d) M = 4.65. Continued.

Figure 6.- Continued.

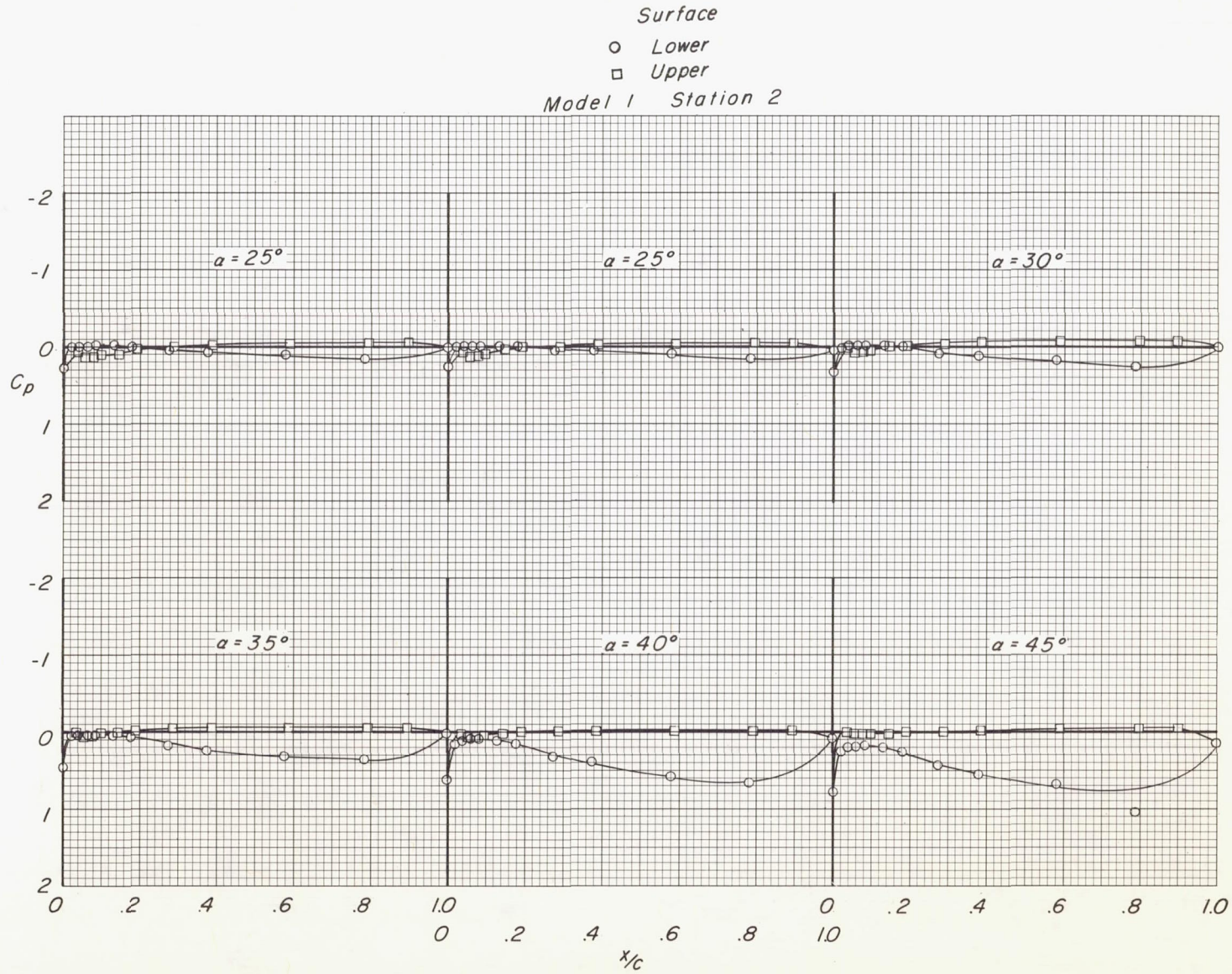

(d) M = 4.65. Continued.

Figure 6.- Continued.

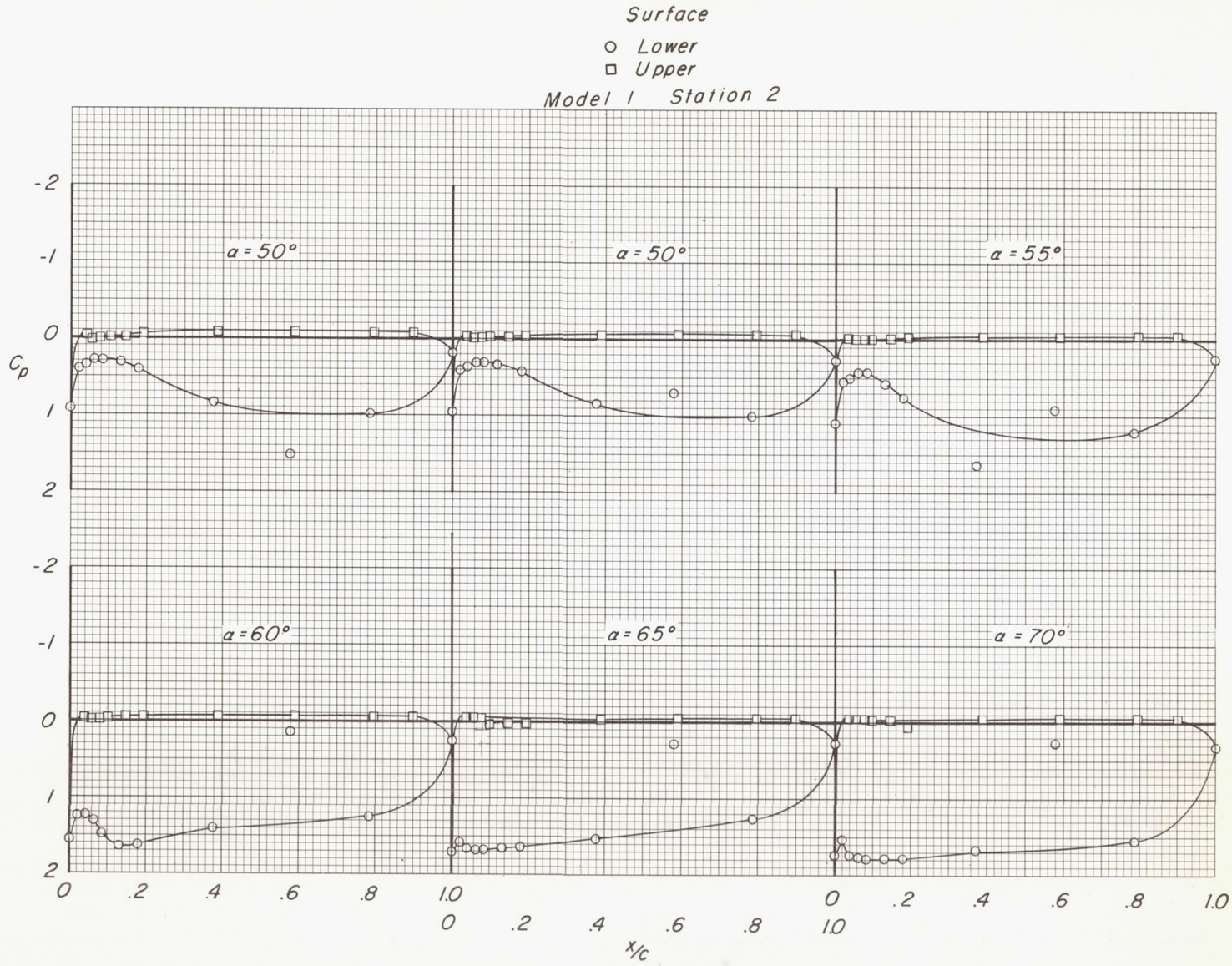

(d) M = 4.65. Continued.

Figure 6.- Continued.

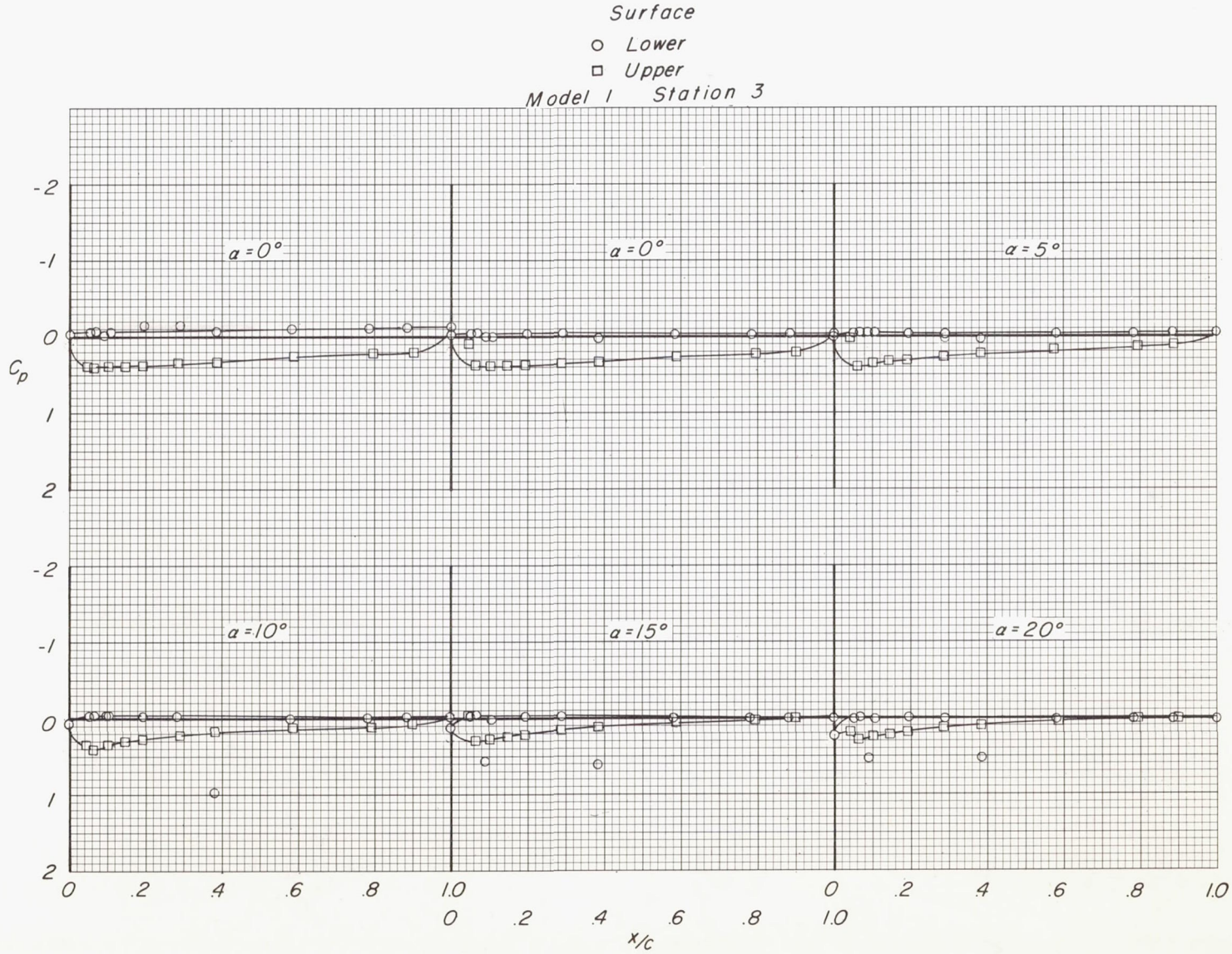

(d) M = 4.65. Continued.

Figure 6.- Continued.

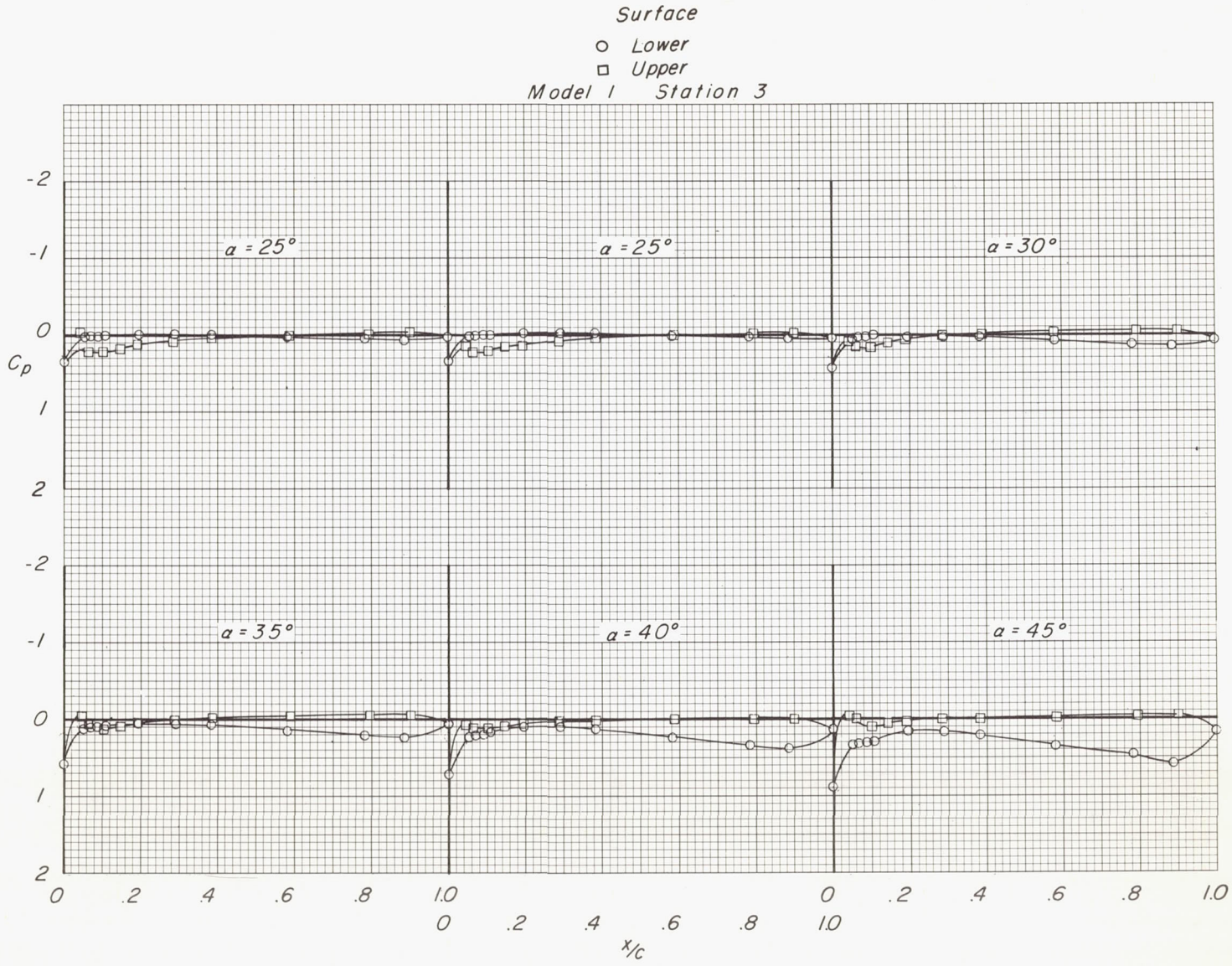

(d) M = 4.65. Continued.

Figure 6.- Continued.

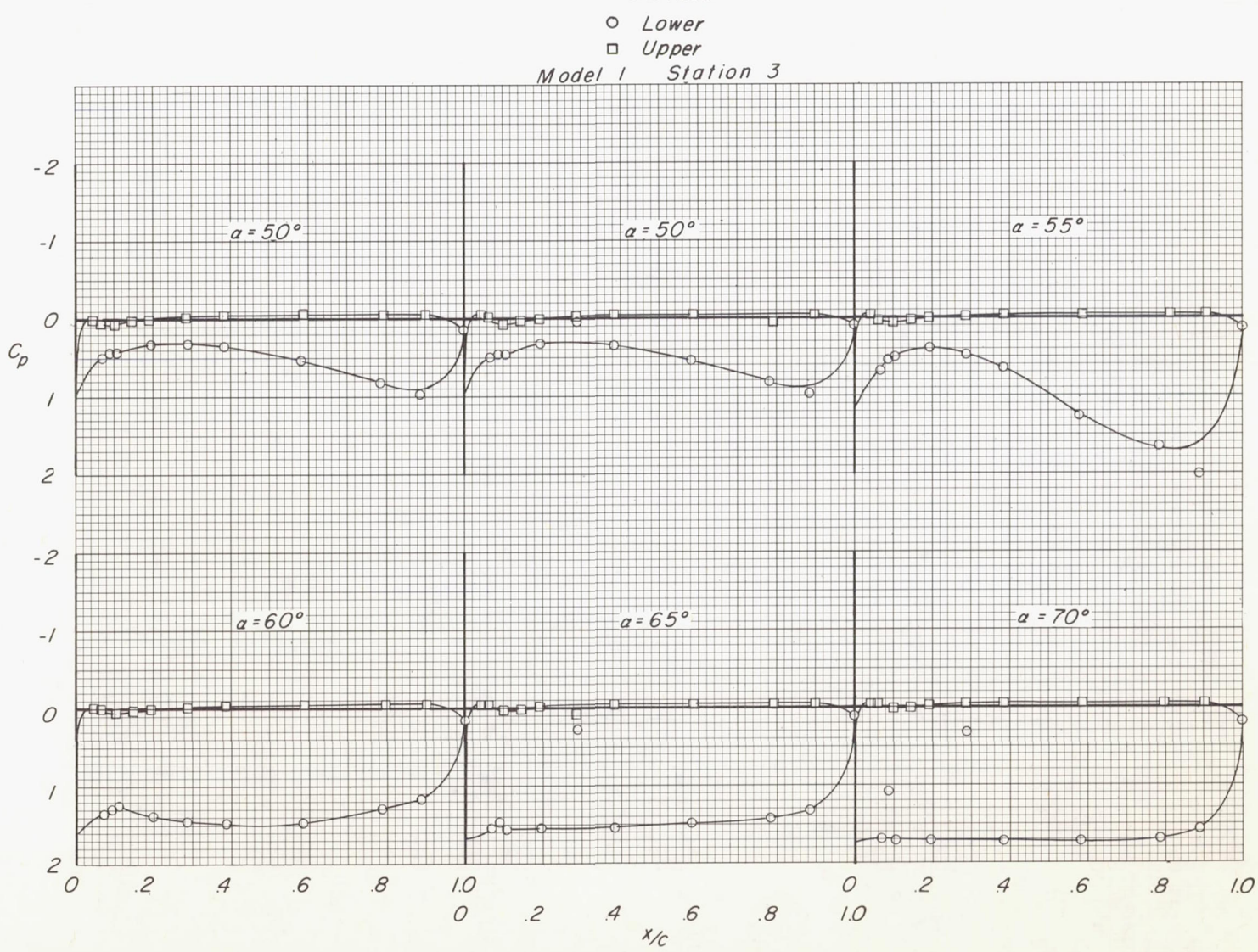

(d) M = 4.65. Continued.

Figure 6.- Continued.

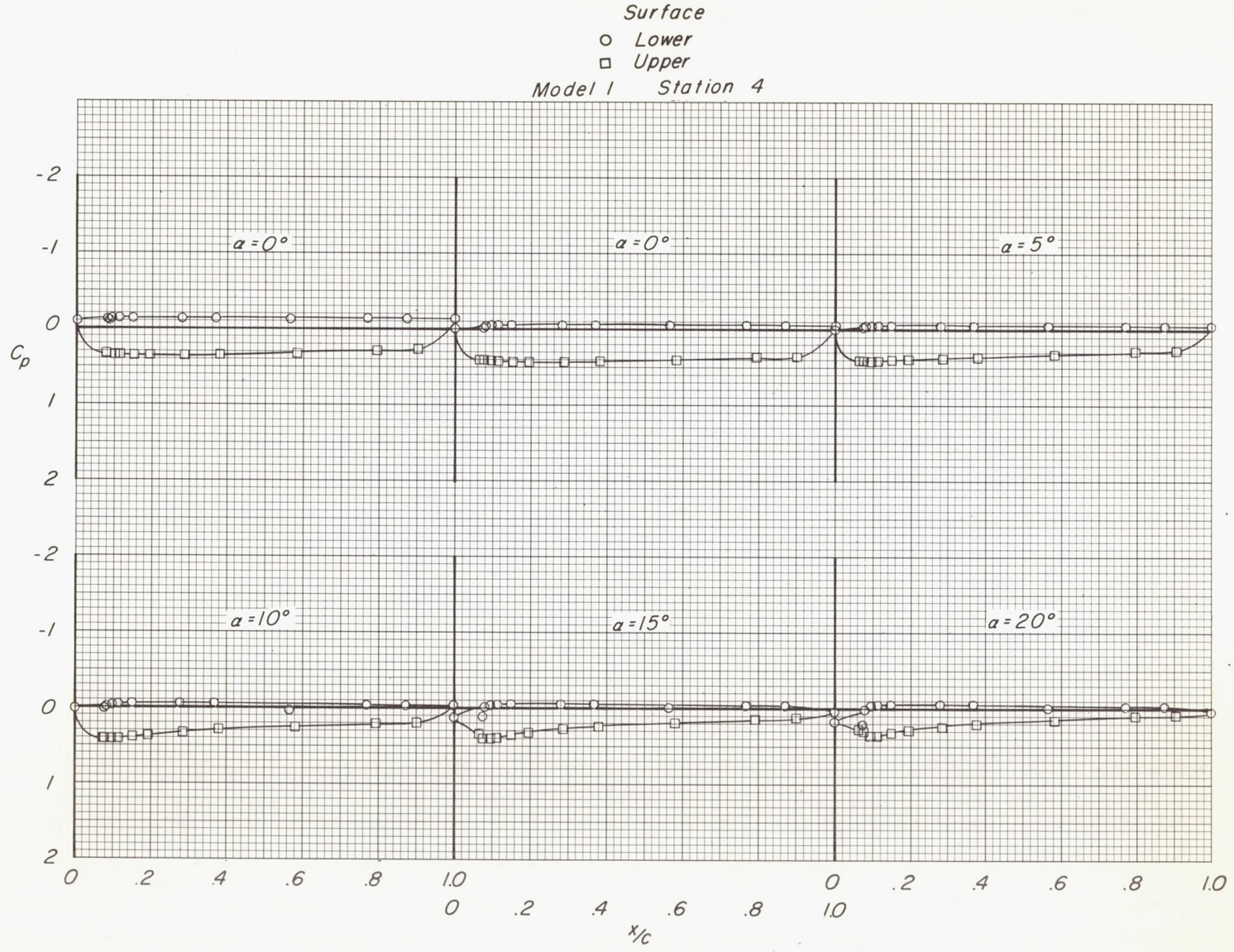

(d) M = 4.65. Continued.

Figure 6.- Continued.

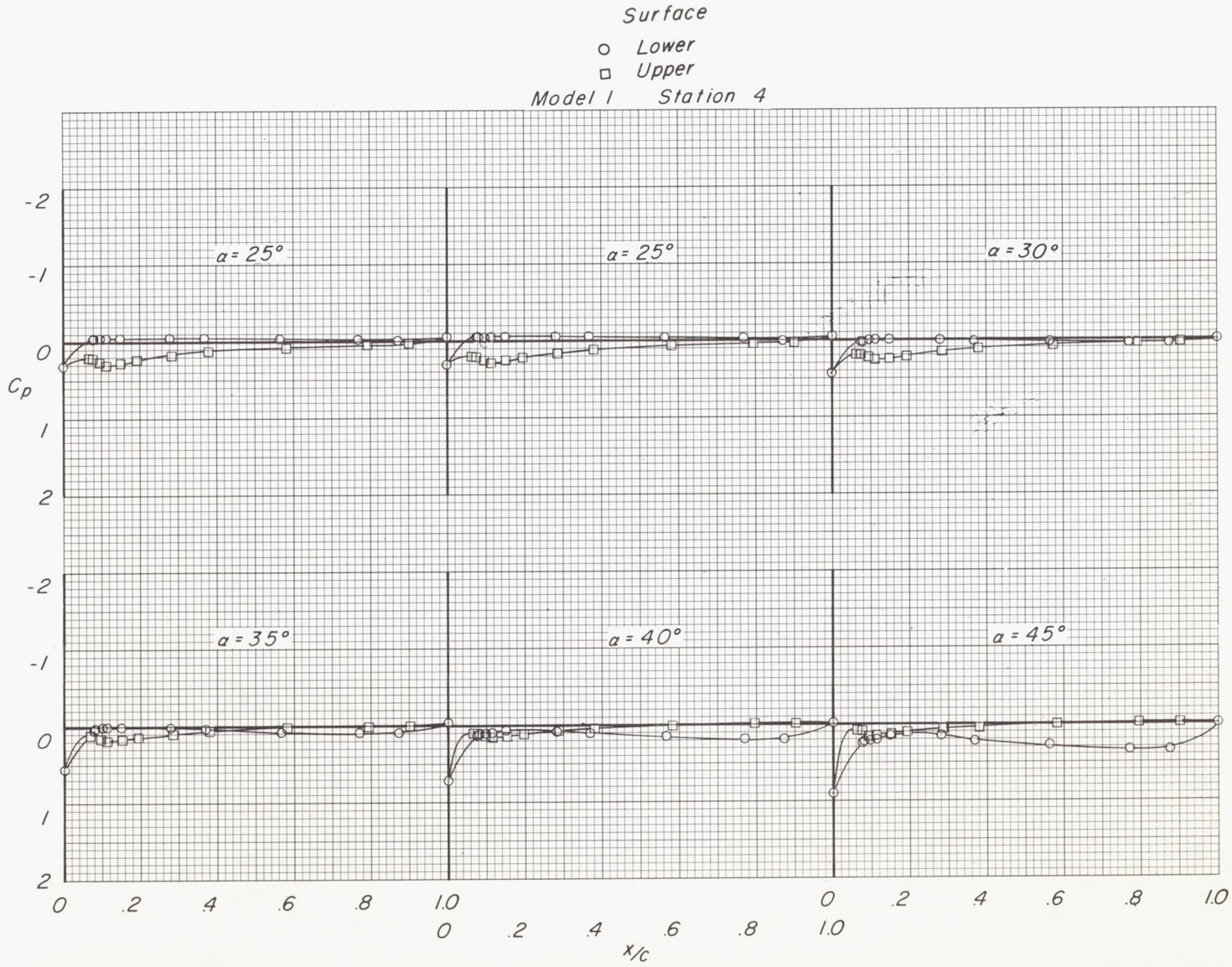

(d) M = 4.65. Continued.

Figure 6.- Continued.

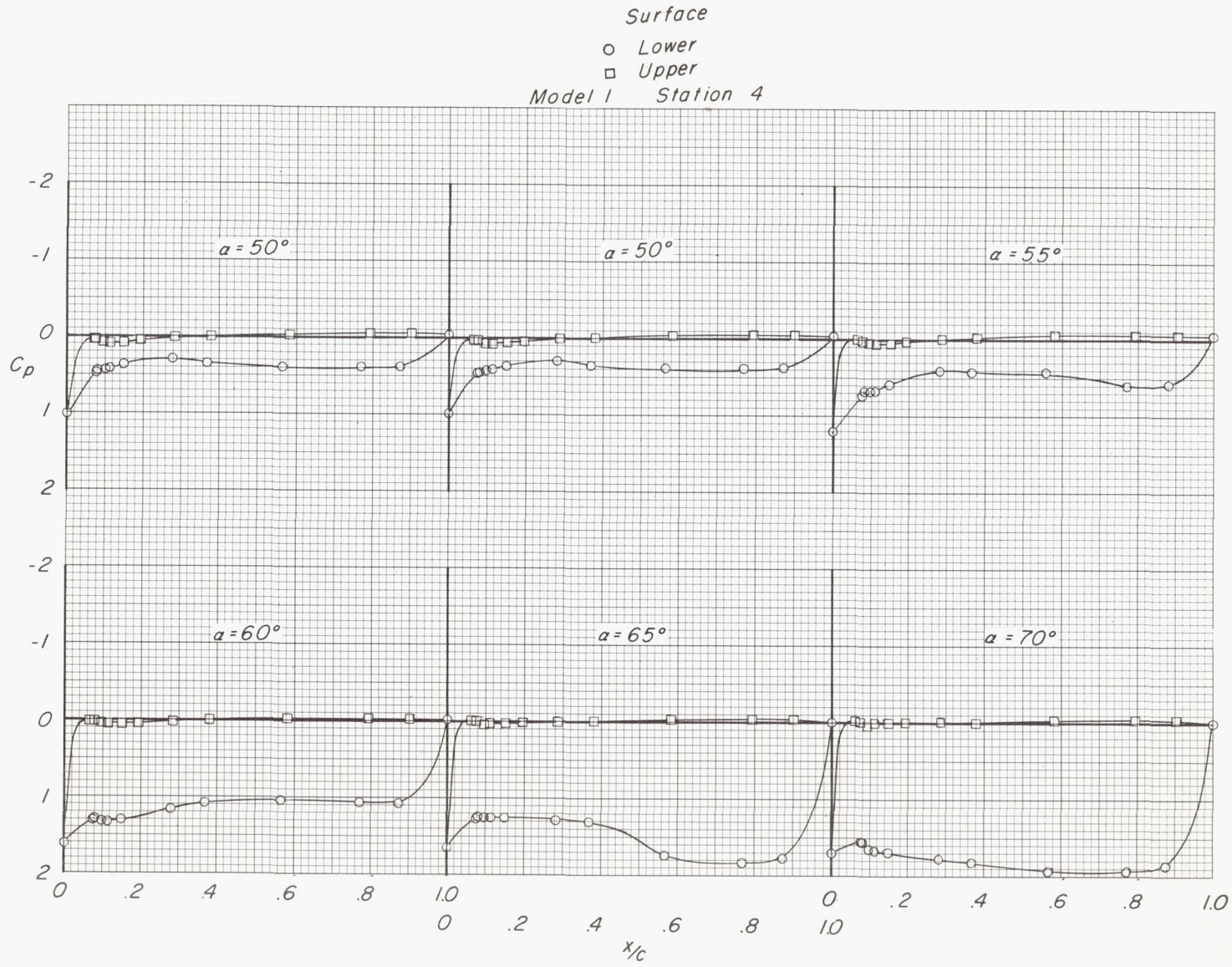

(d) M = 4.65. Concluded.

Figure 6.- Concluded.

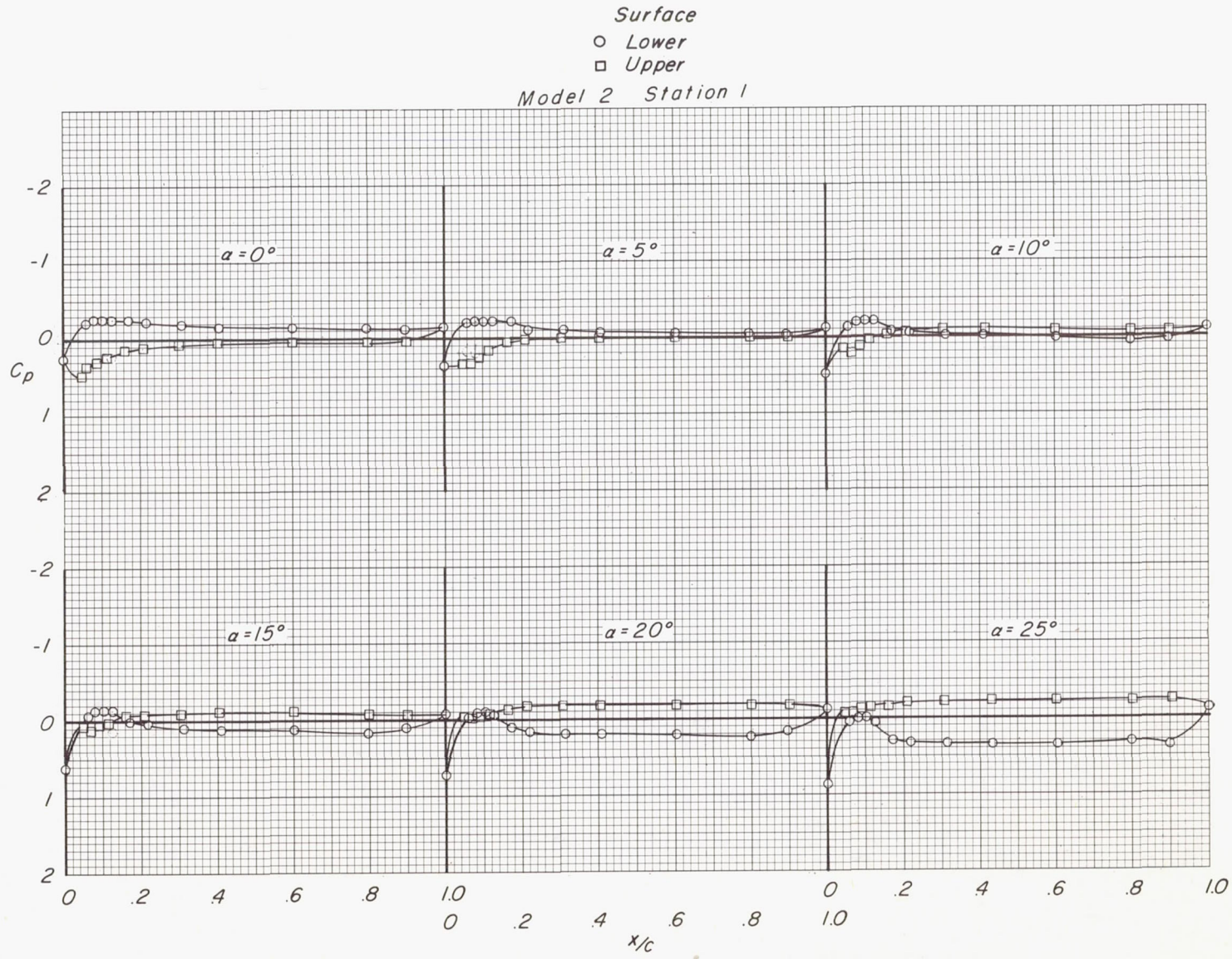

(a) M = 2.29.

Figure 7.- Pressure distributions on model 2 at various angles of attack and Mach numbers.

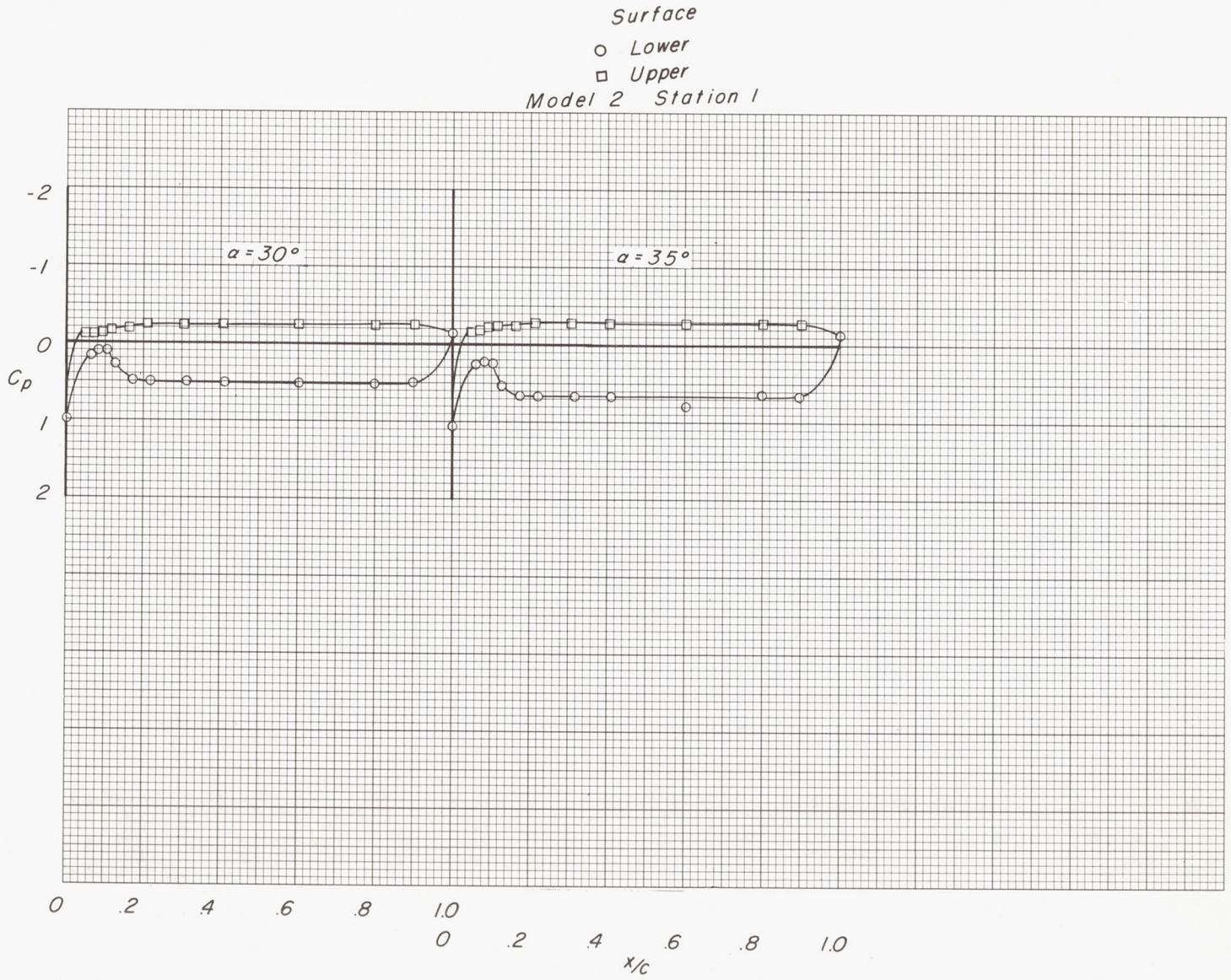

(a) M = 2.29. Continued.

Figure 7.- Continued.

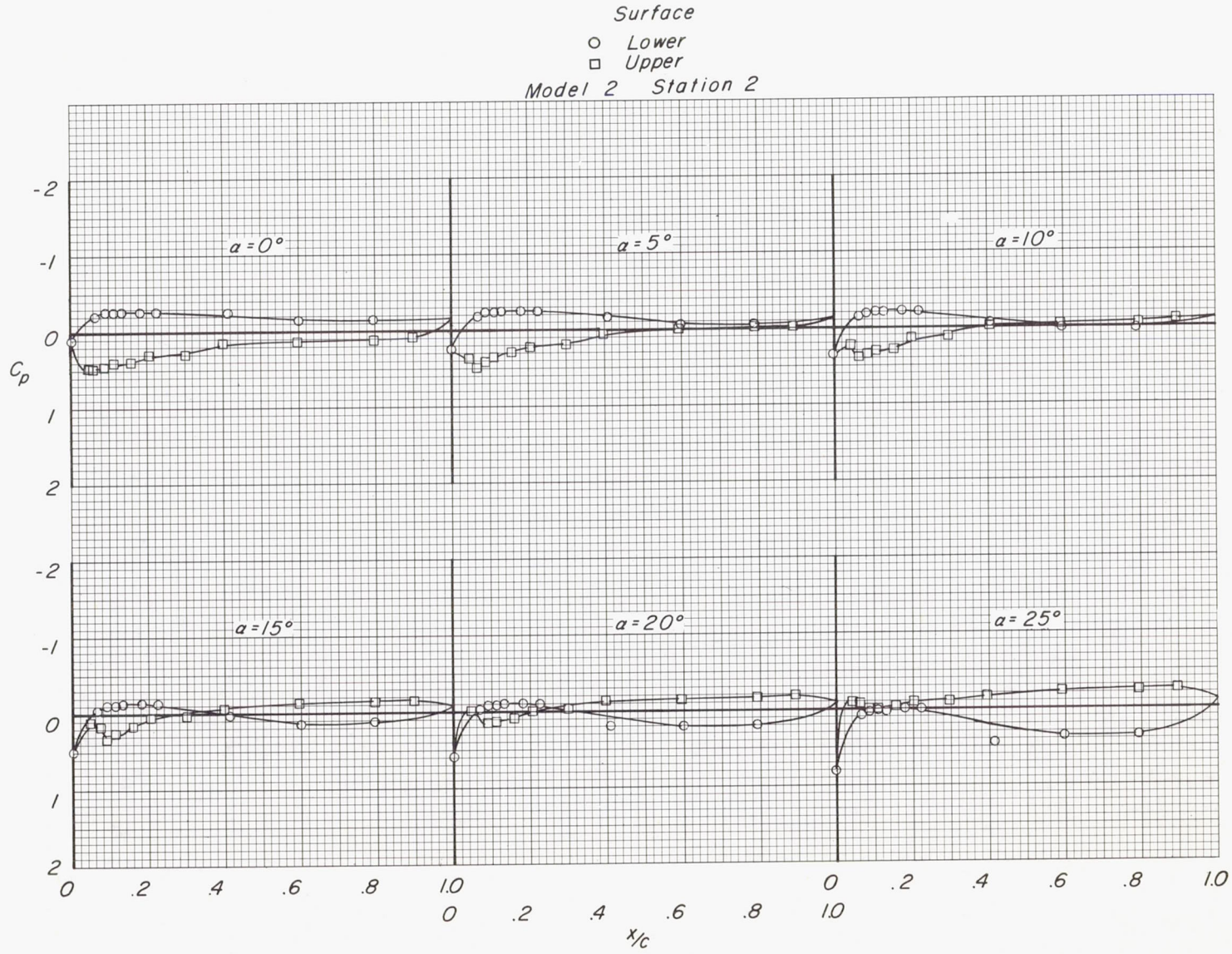

(a) M = 2.29. Continued.

Figure 7.- Continued.

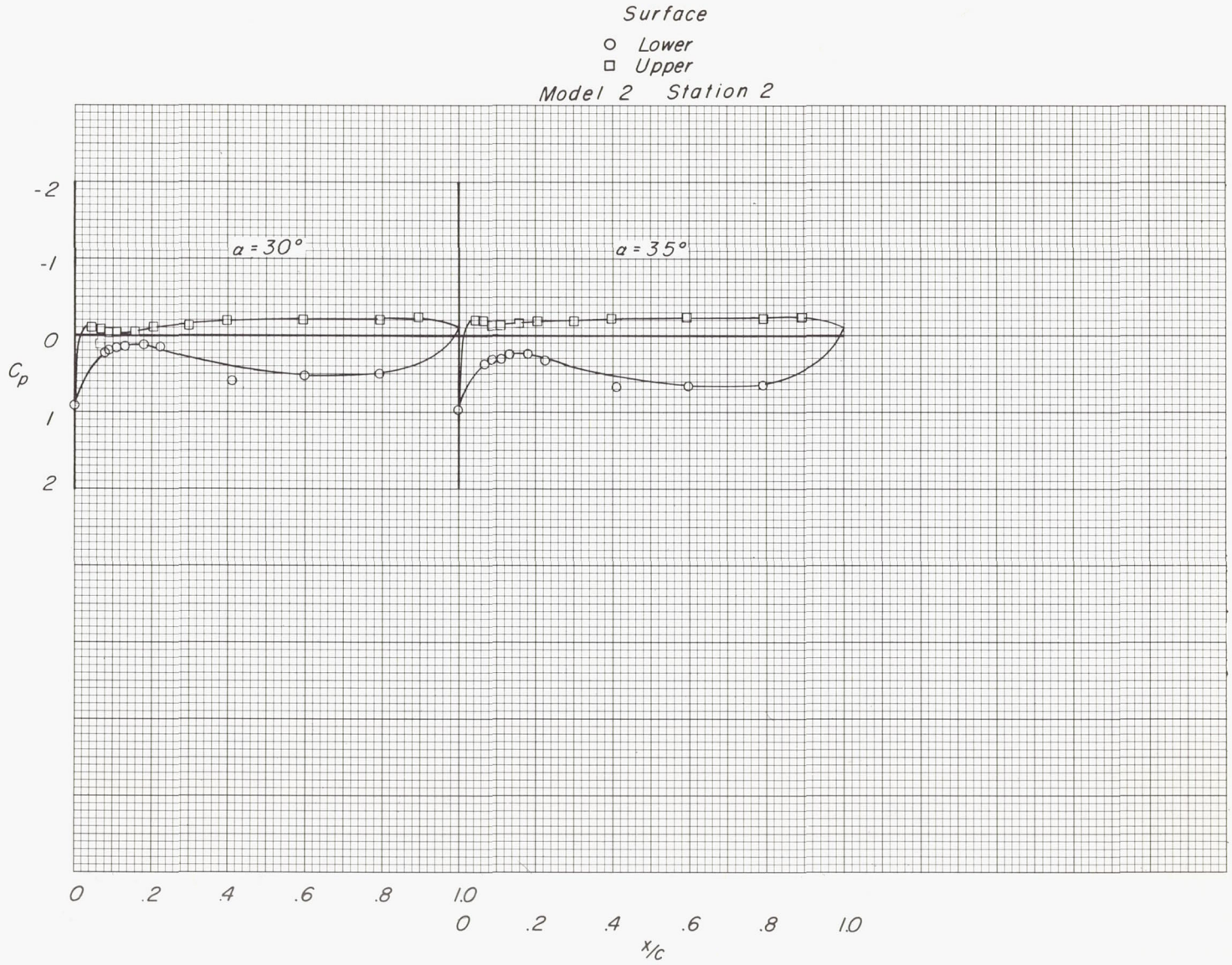

(a) M = 2.29. Continued.

Figure 7.- Continued.

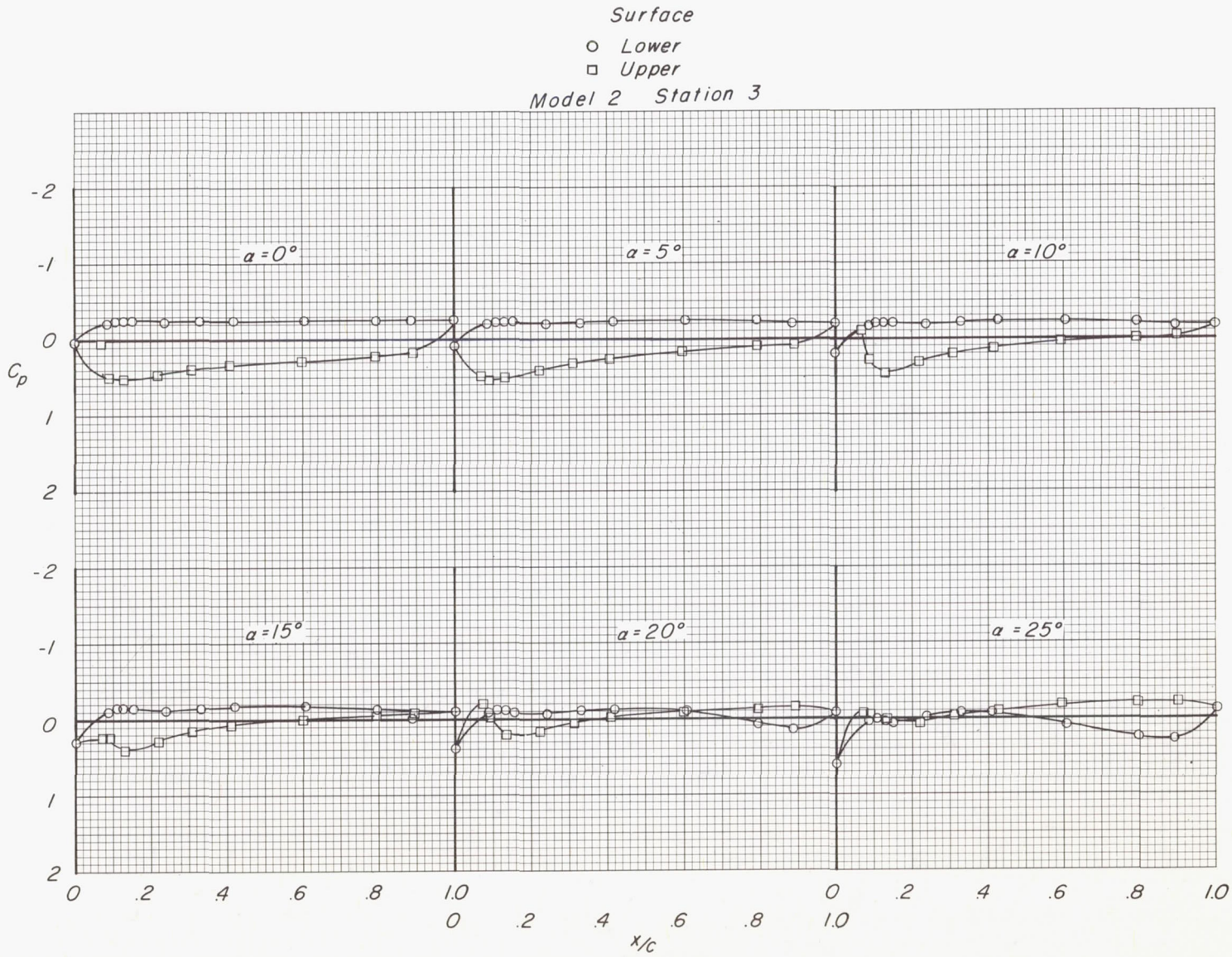

(a) M = 2.29. Continued.

Figure 7.- Continued.

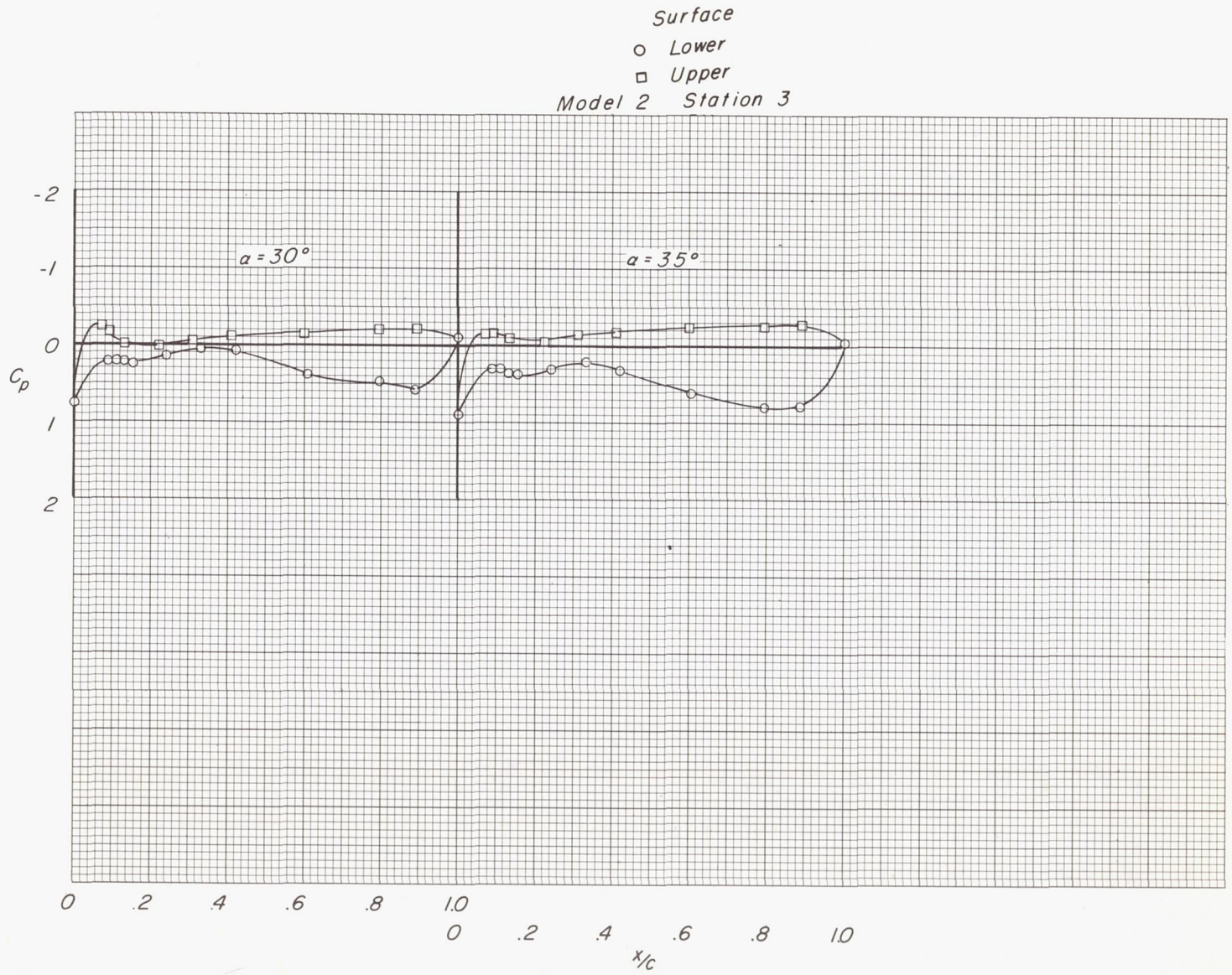

(a) M = 2.29. Continued.

Figure 7.- Continued.

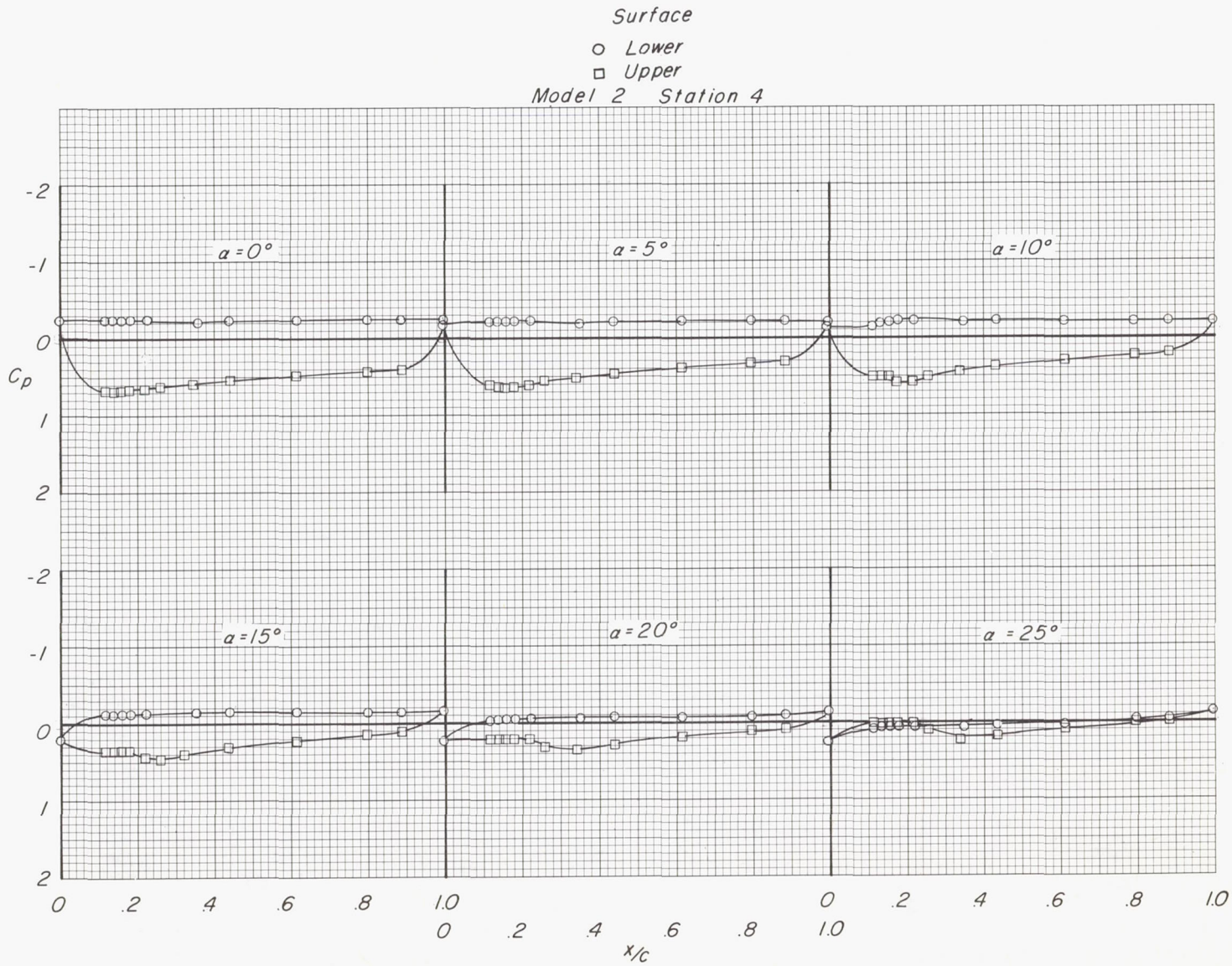

(a) M = 2.29. Continued.

Figure 7.- Continued.

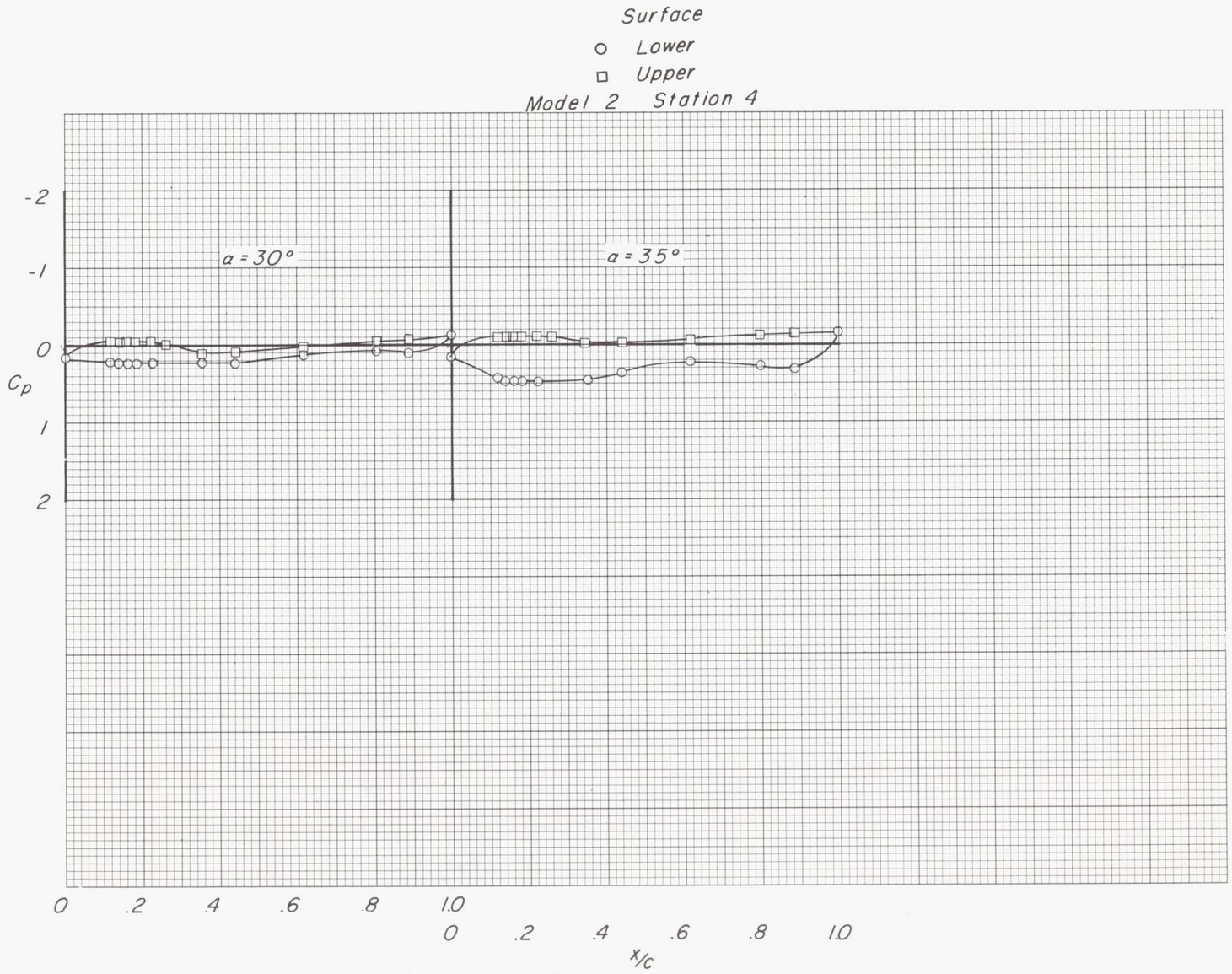

(a) M = 2.29. Concluded.

Figure 7.- Continued.

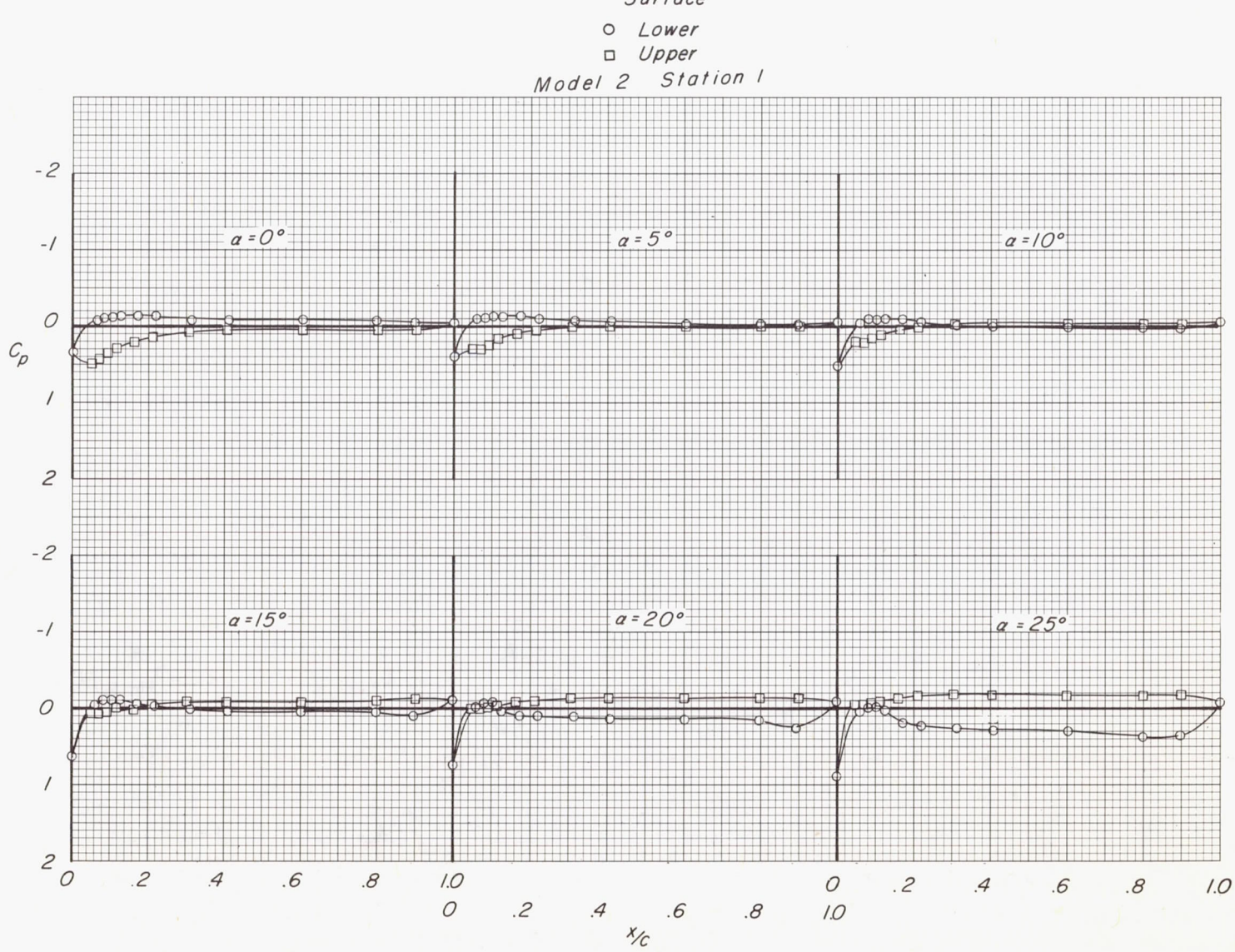

(b) M = 2.96.

Figure 7.- Continued.

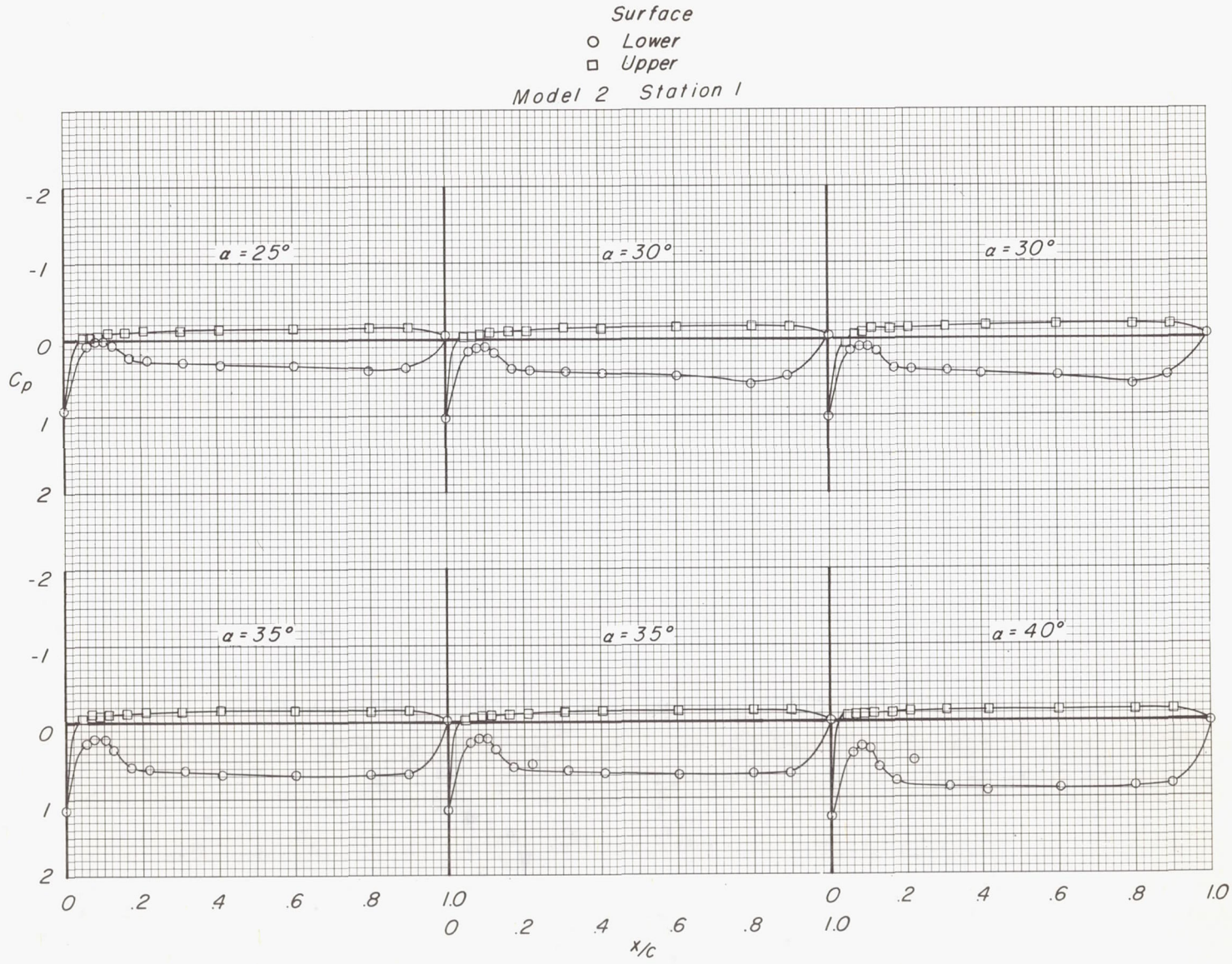

(b) M = 2.96. Continued.

Figure 7.- Continued.

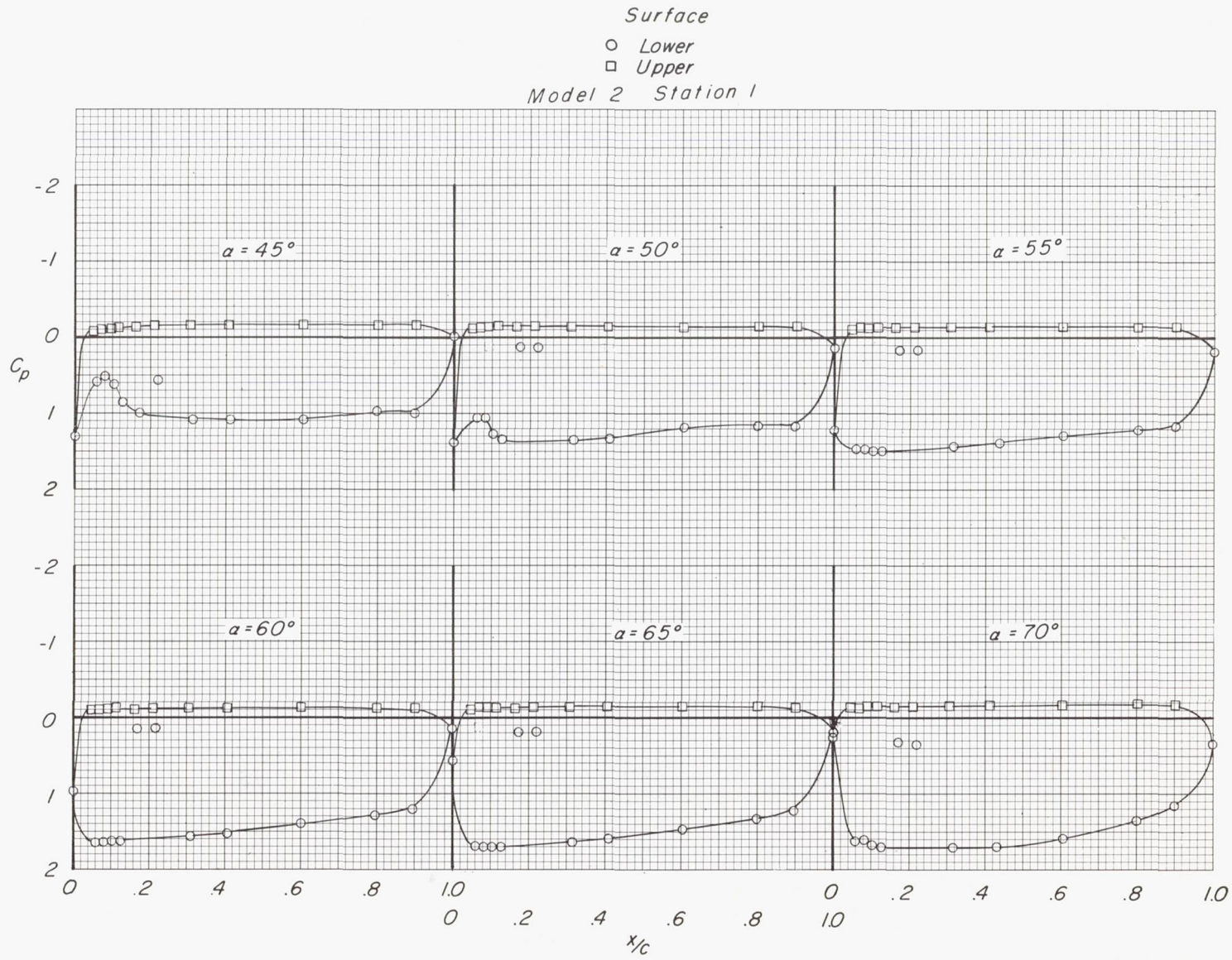

(b) M = 2.96. Continued.

Figure 7.- Continued.

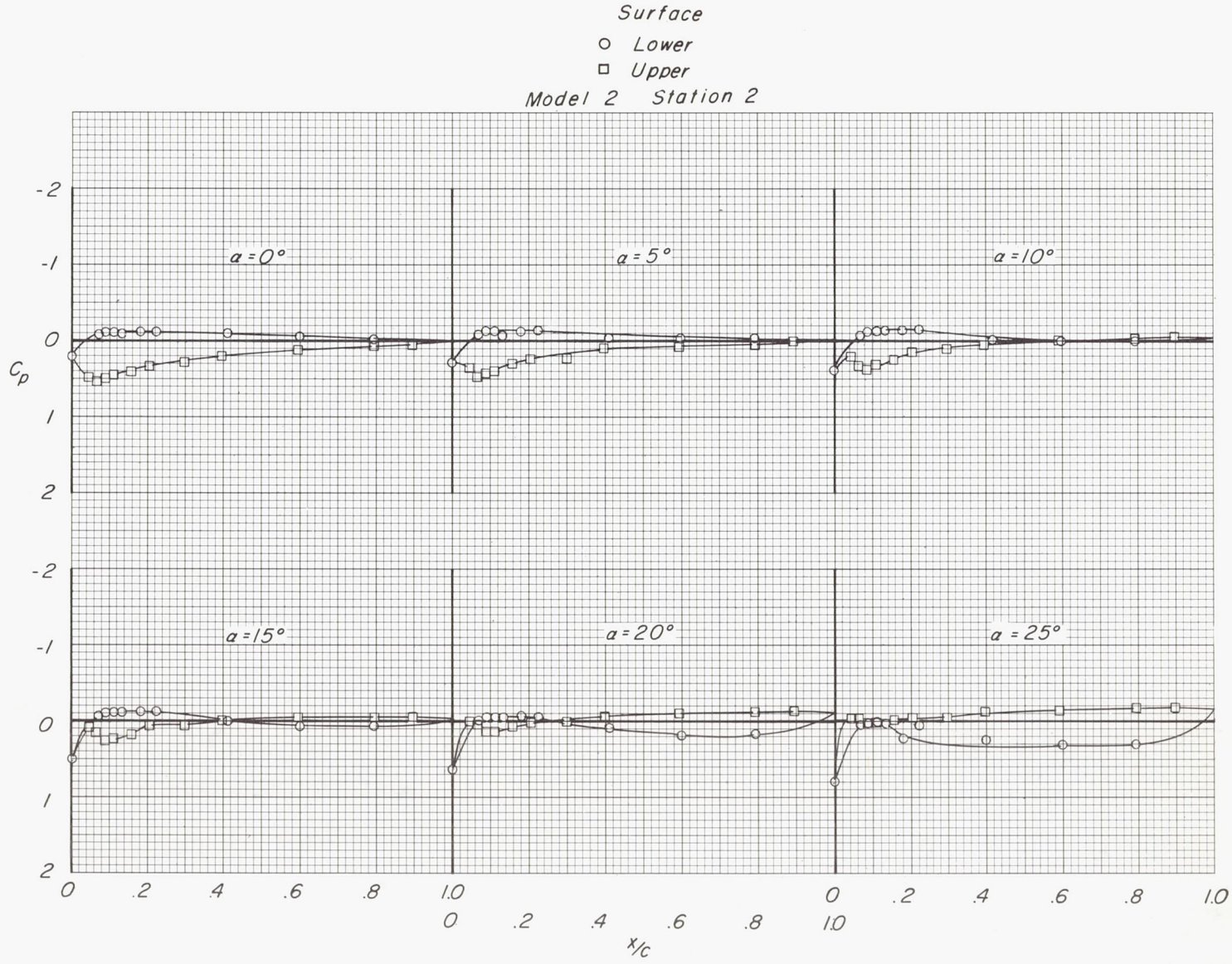

(b) M = 2.96. Continued.

Figure 7.- Continued.

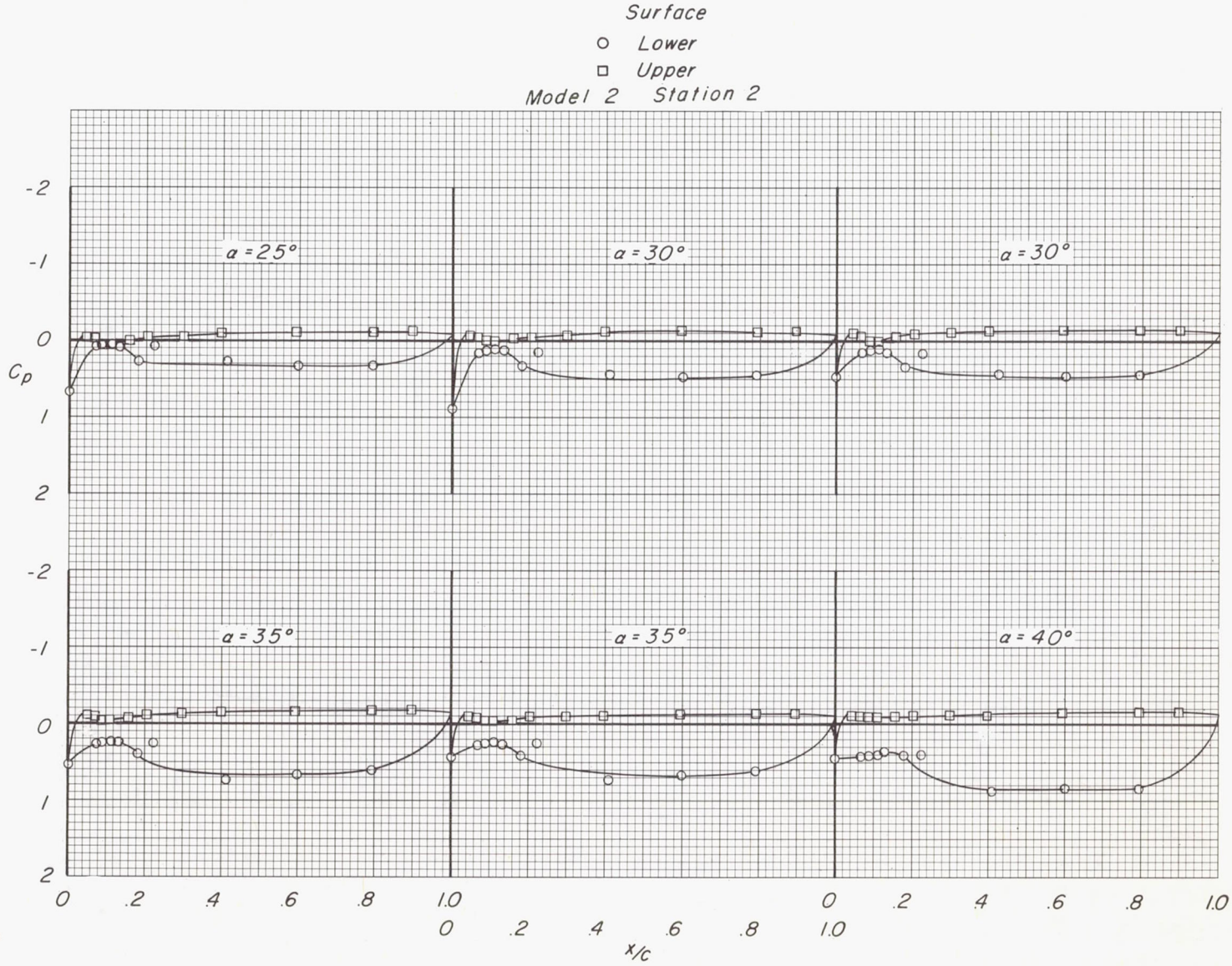

(b) M = 2.96. Continued.

Figure 7.- Continued.

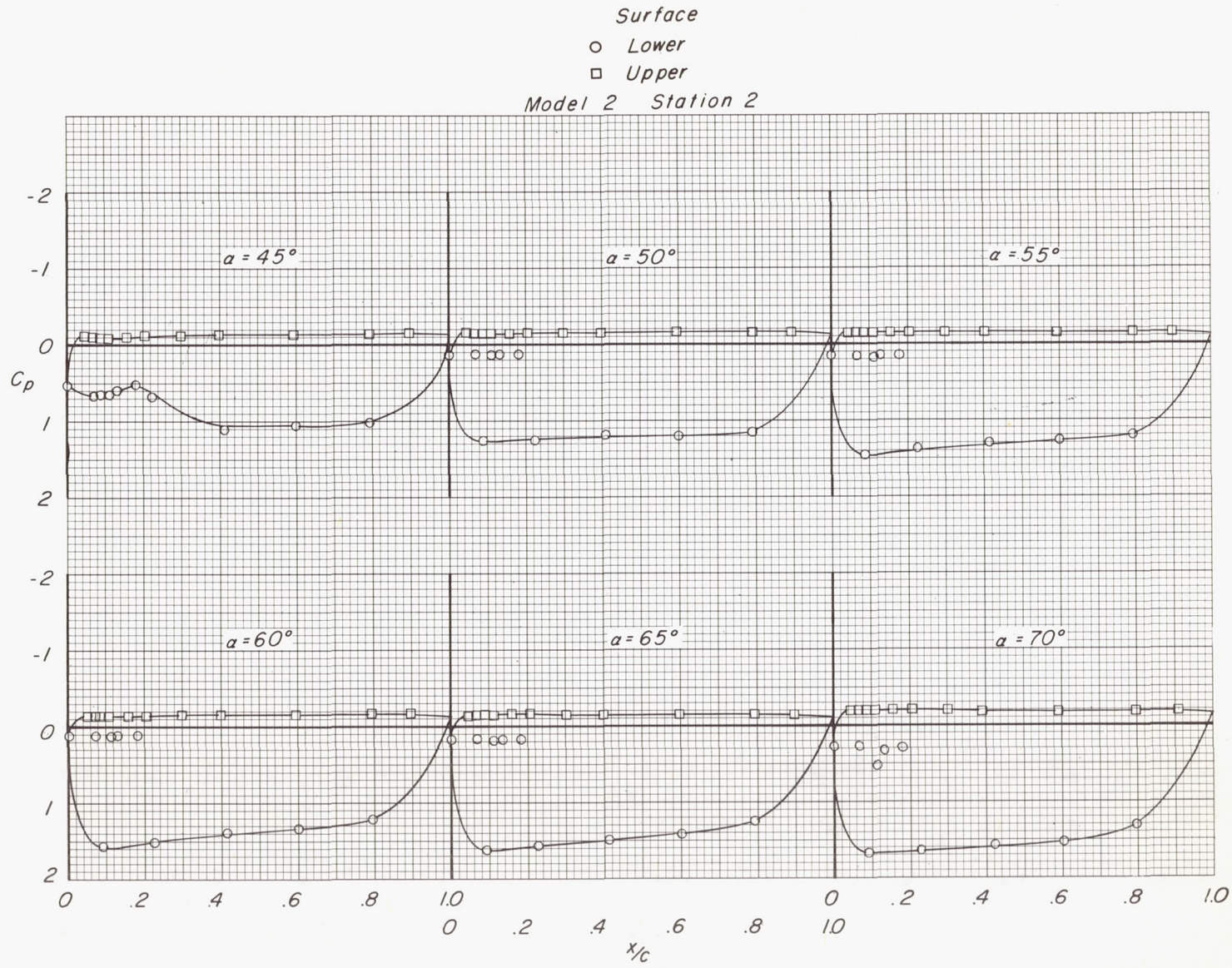

(b) M = 2.96. Continued.

Figure 7.- Continued.

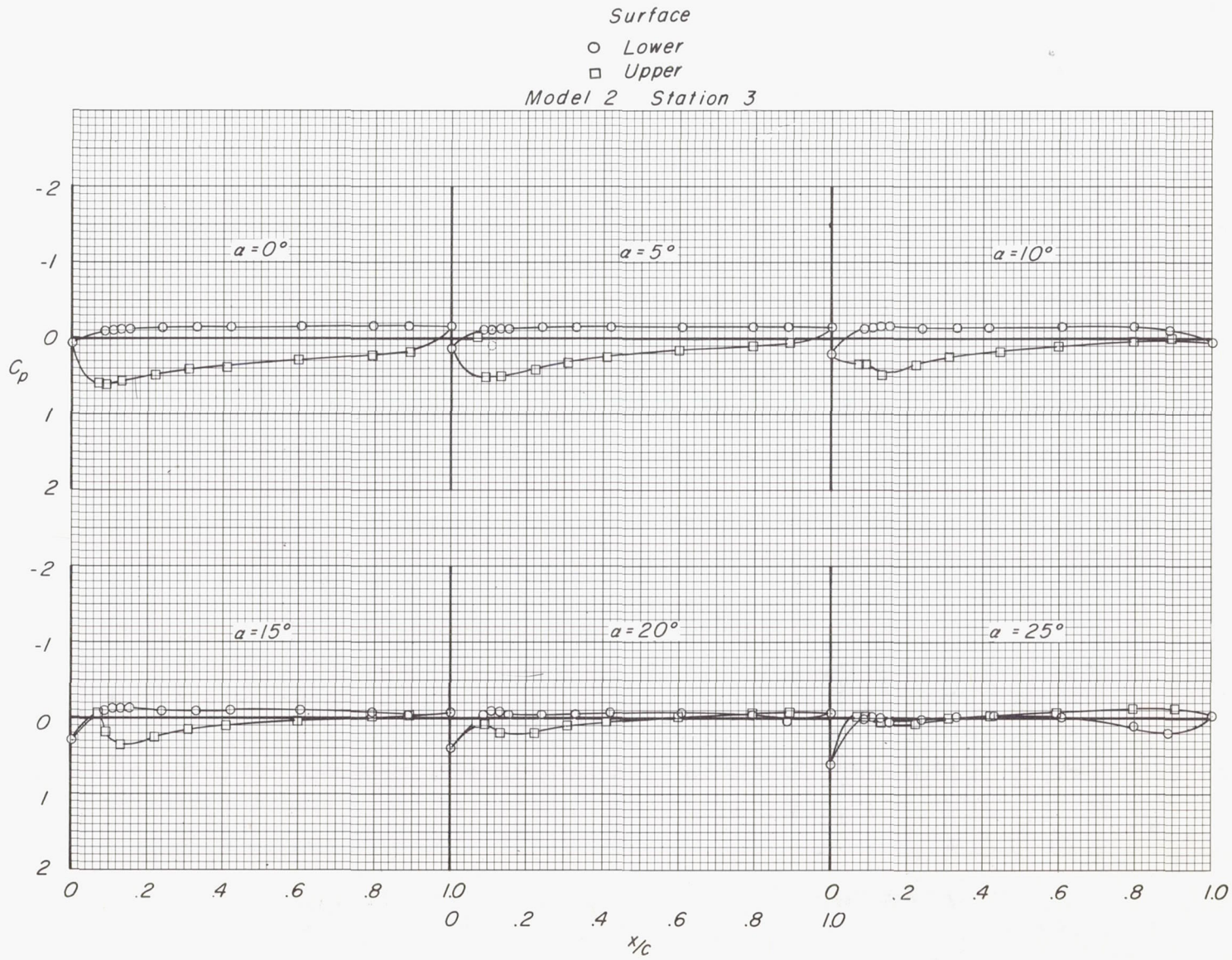

(b) M = 2.96. Continued.

Figure 7.- Continued.

(b) M = 2.96. Continued.

Figure 7.- Continued.

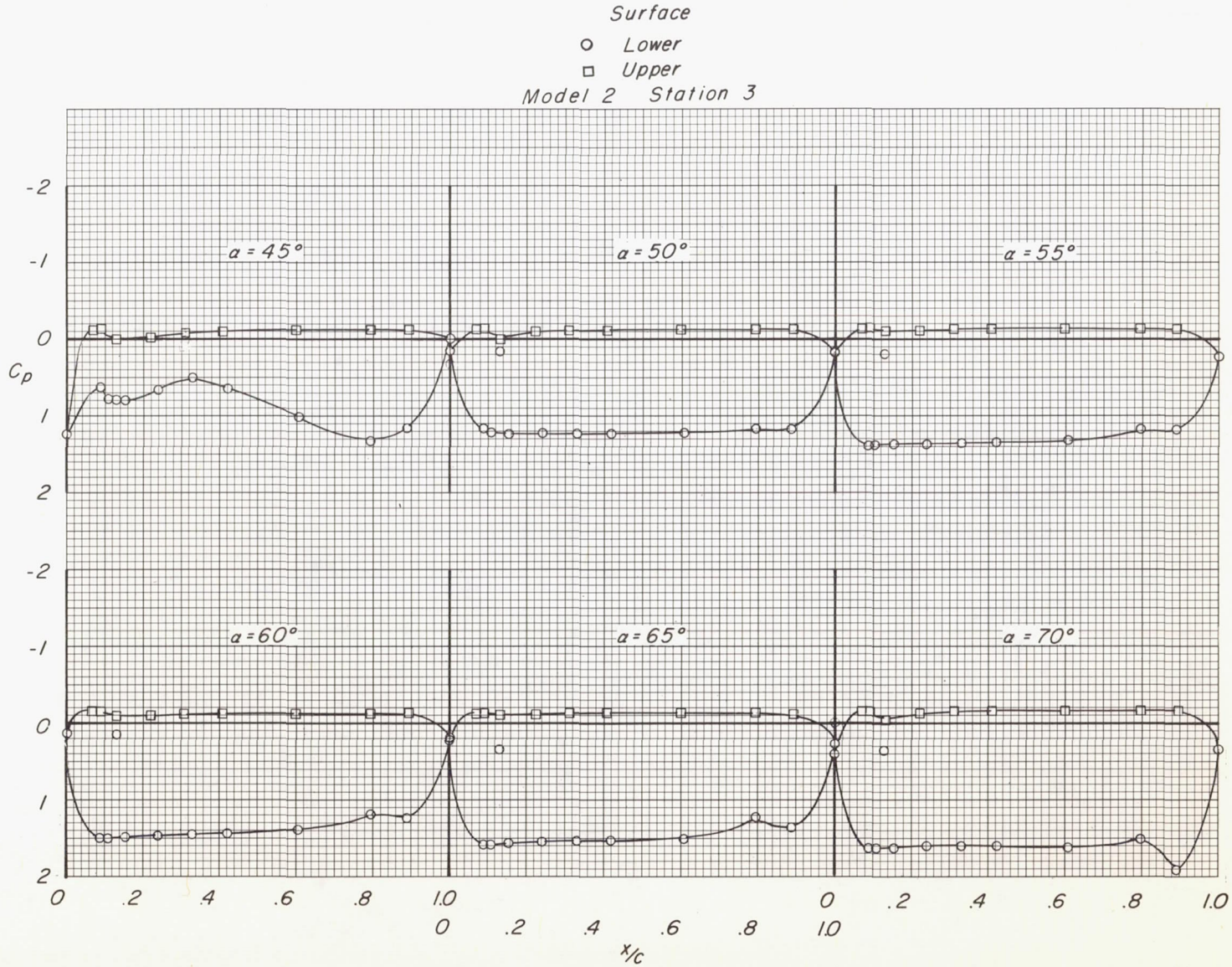

(b) M = 2.96. Continued.

Figure 7.- Continued.

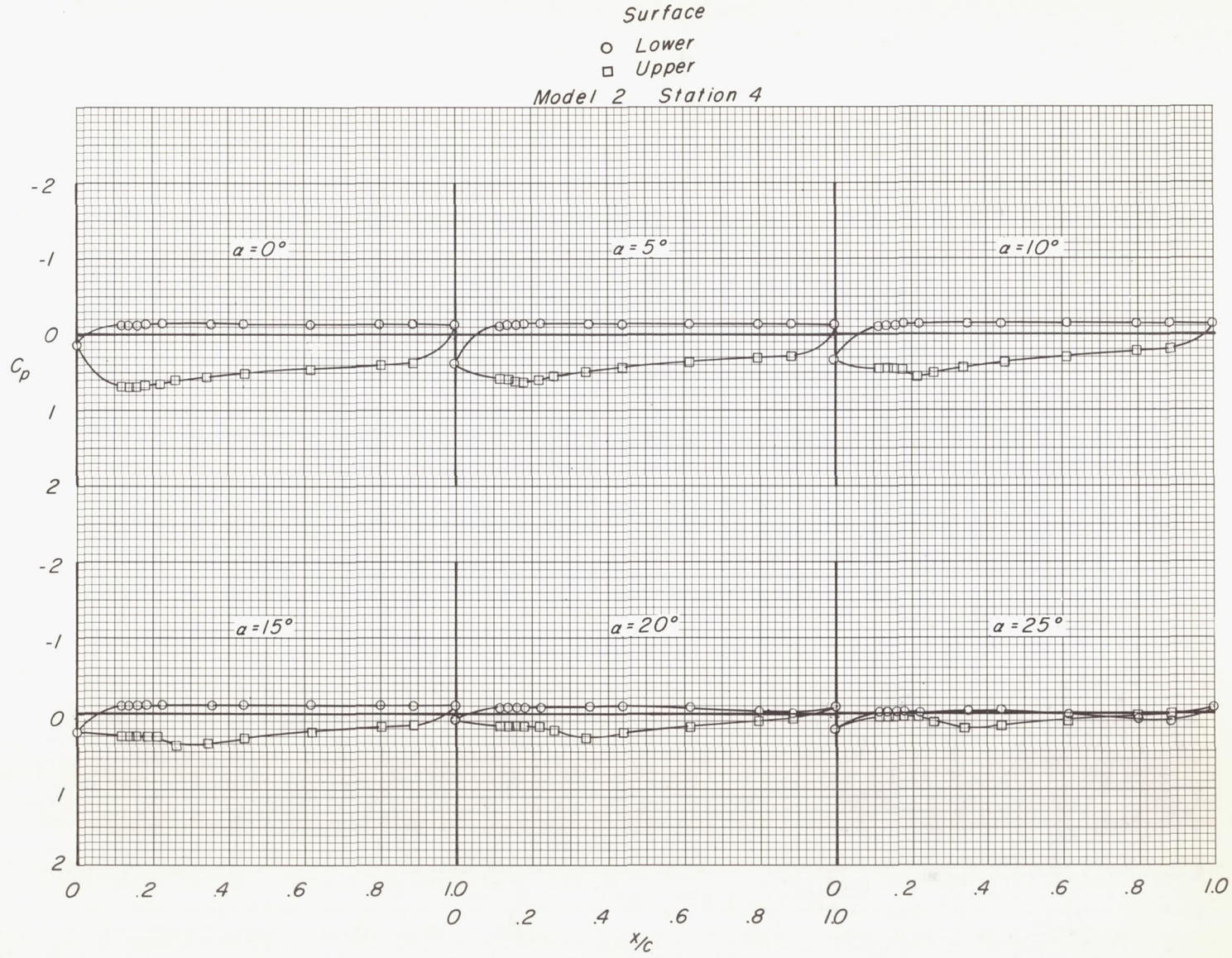

(b) M = 2.96. Continued.

Figure 7.- Continued.

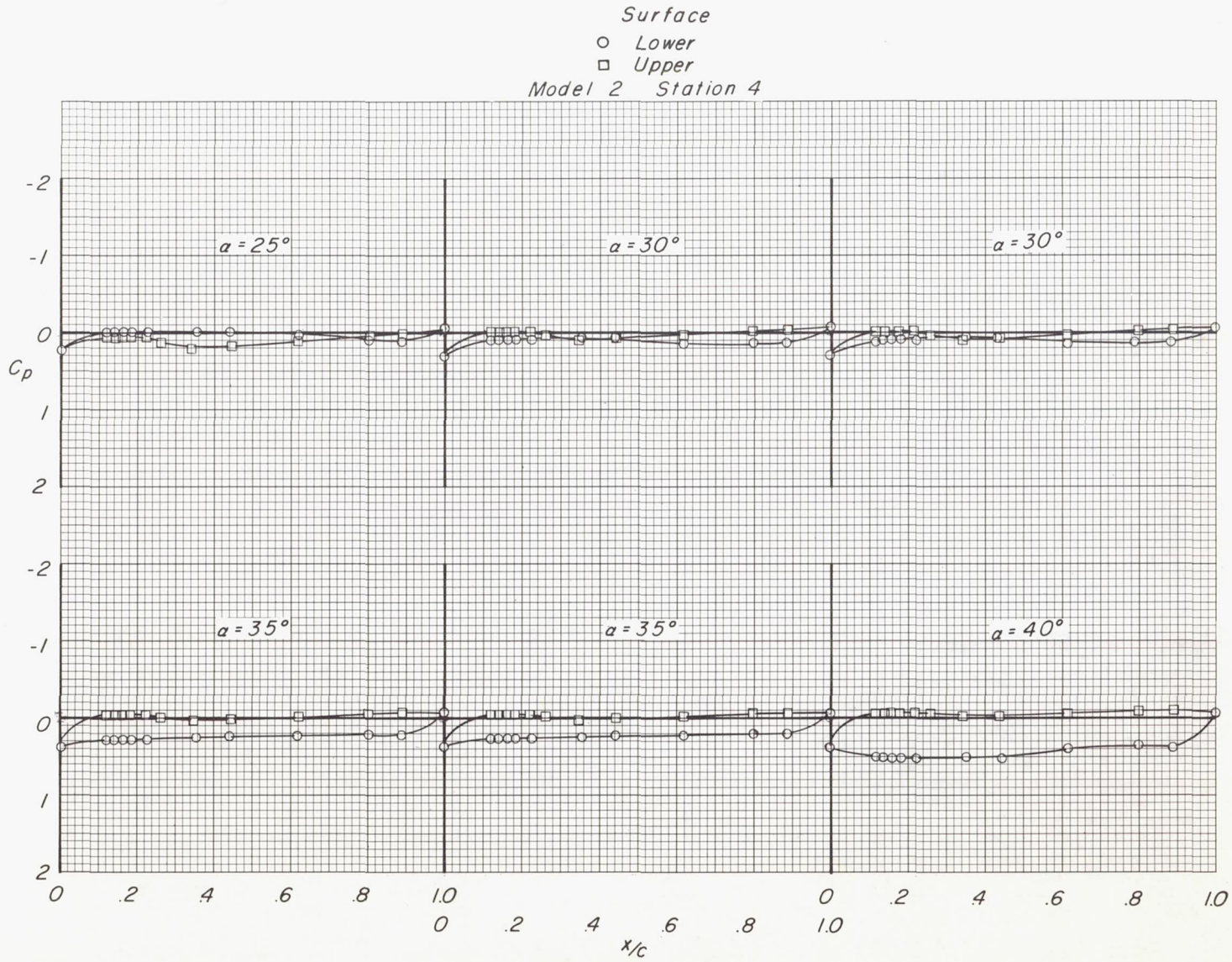

(b) M = 2.96. Continued.

Figure 7.- Continued.

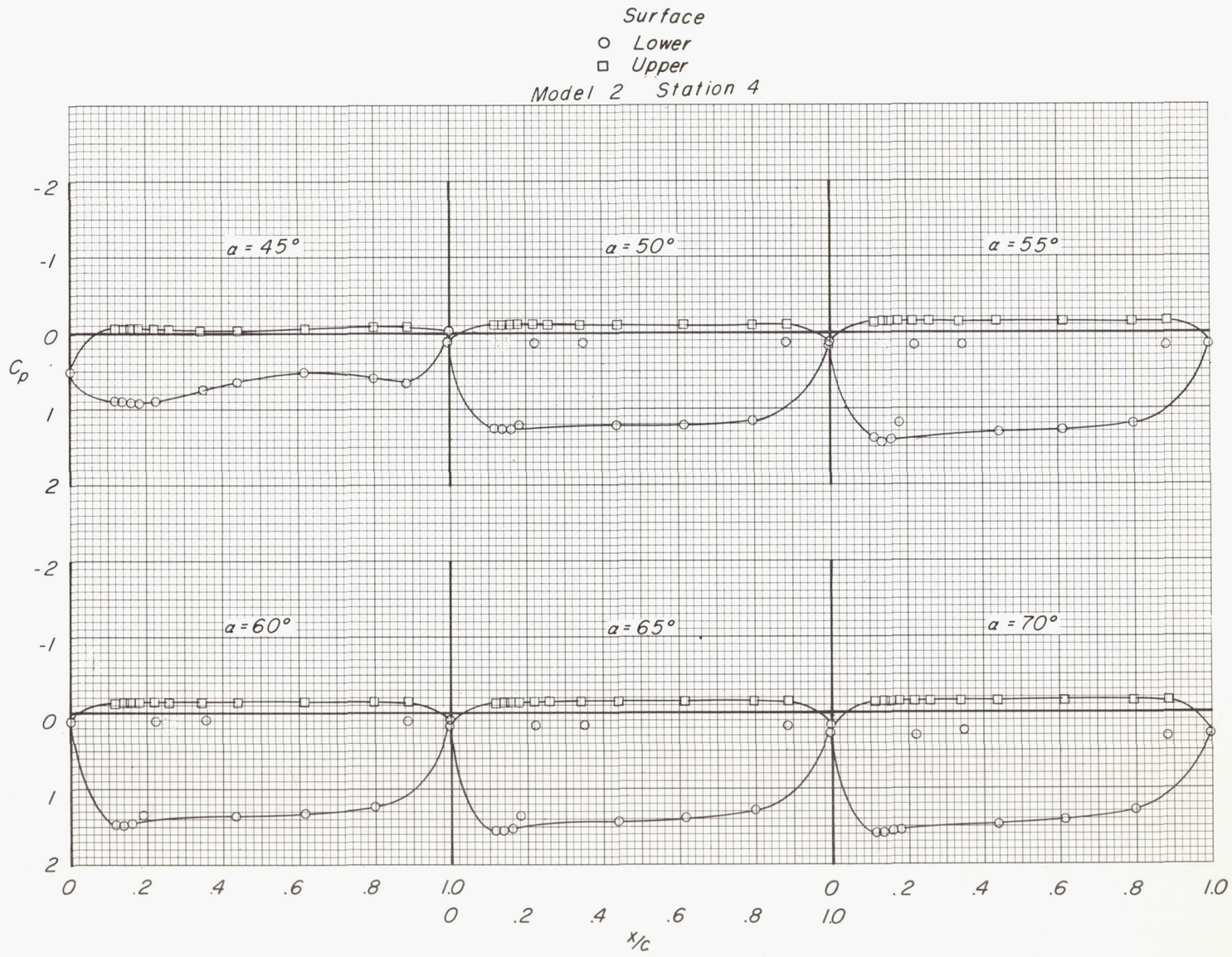

(b) M = 2.96. Concluded.

Figure 7.- Continued.

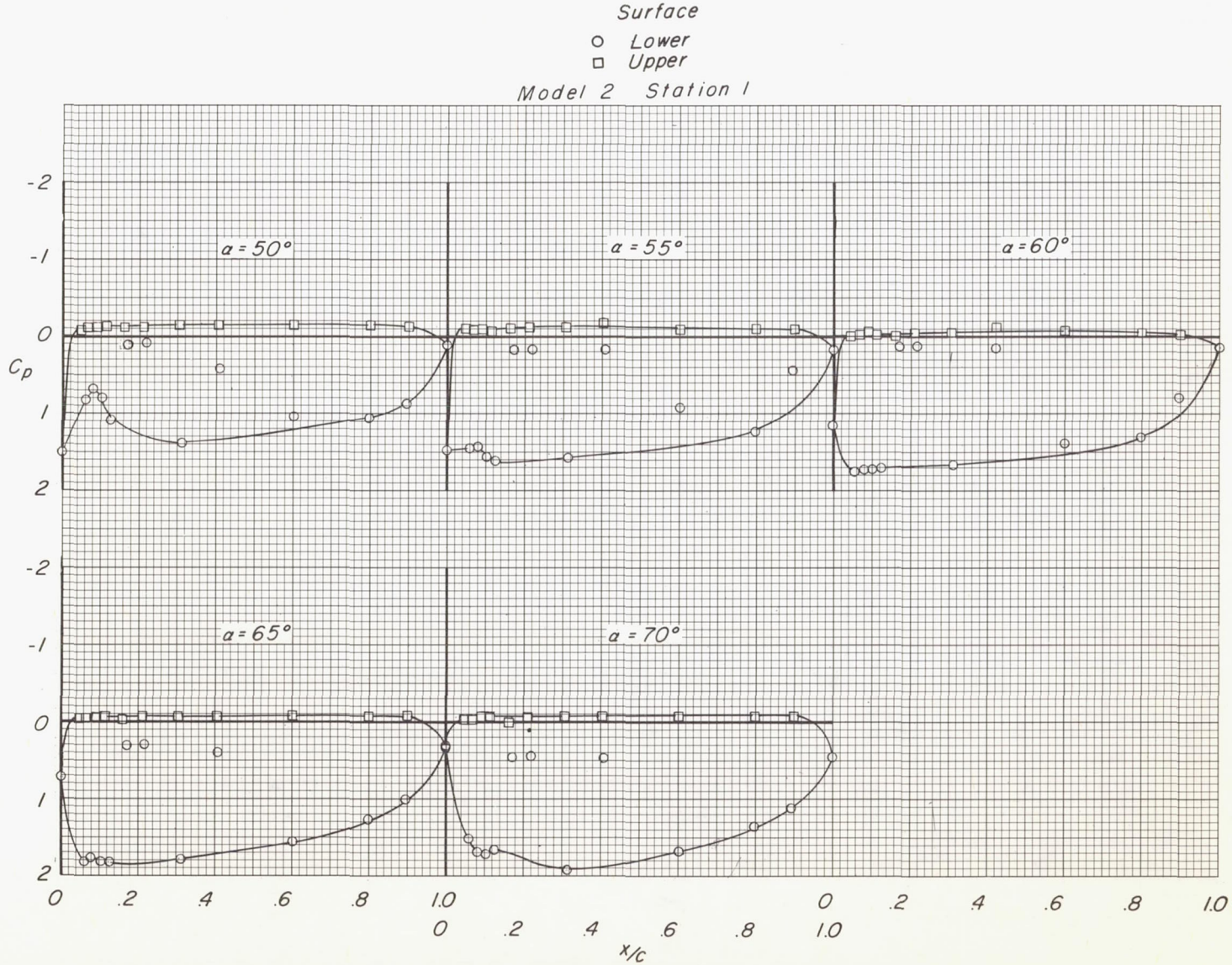

(c) M = 3.95.

Figure 7.- Continued.

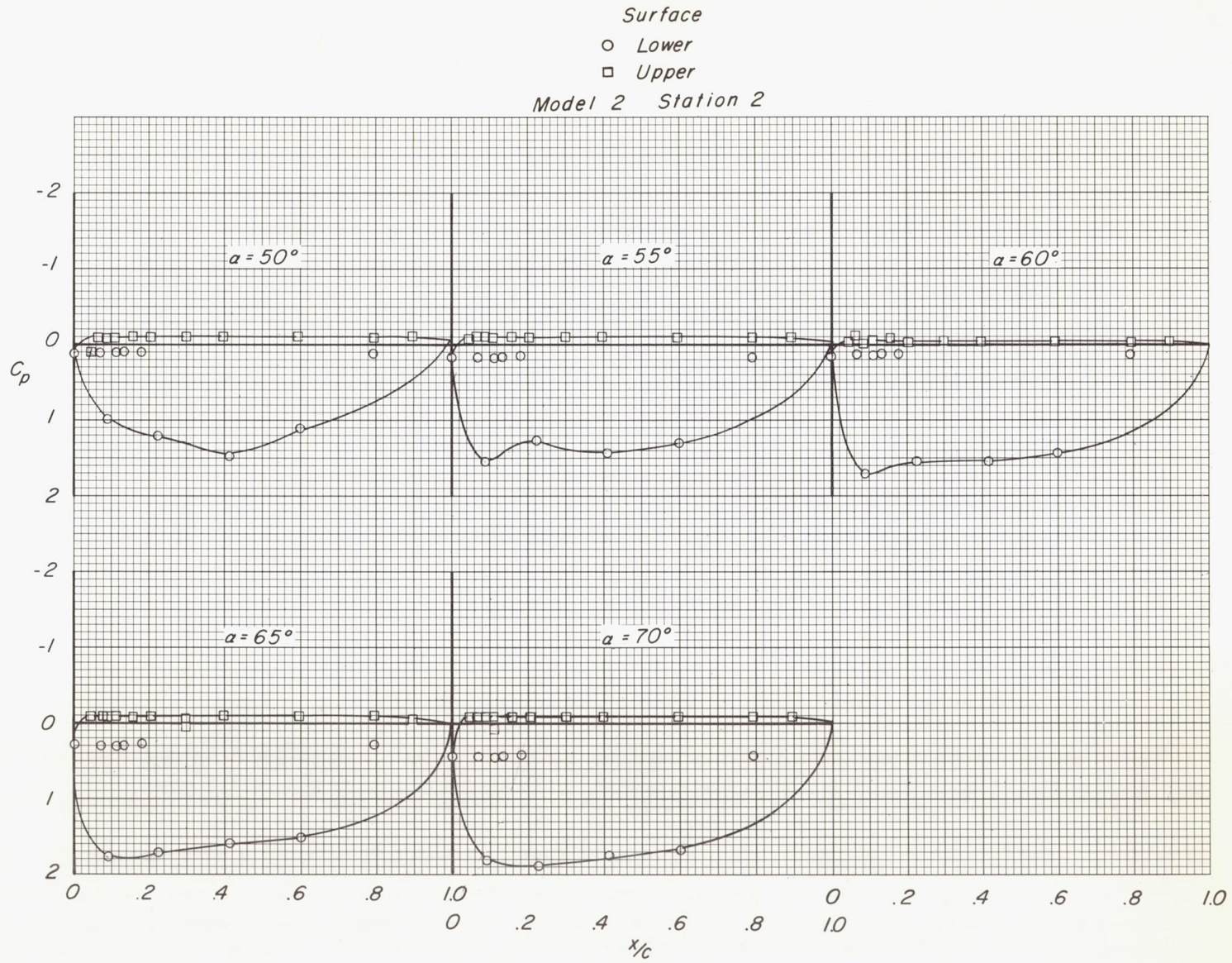

(c) M = 3.95. Continued.

Figure 7.- Continued.

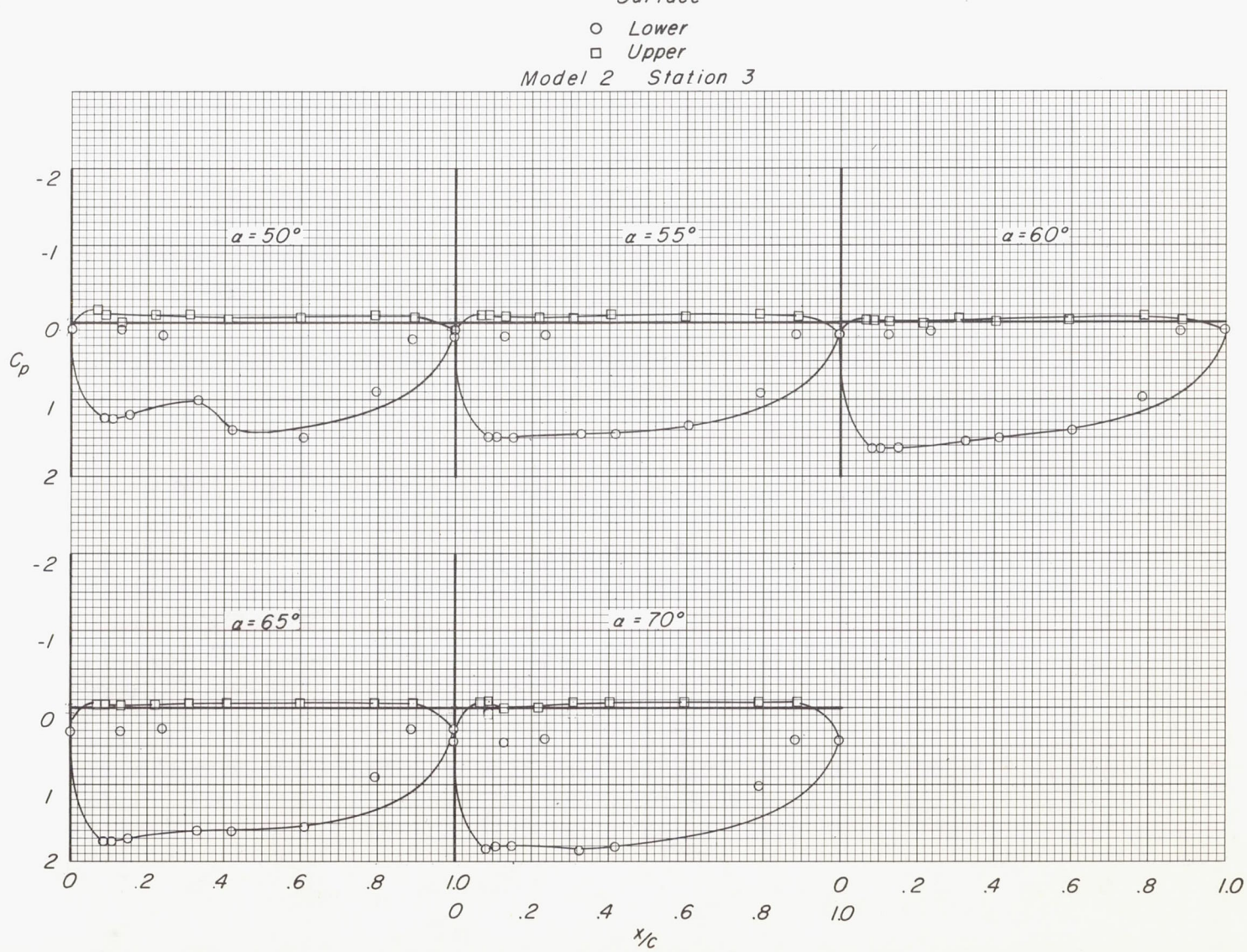

(c) M = 3.95. Continued.

Figure 7.- Continued.

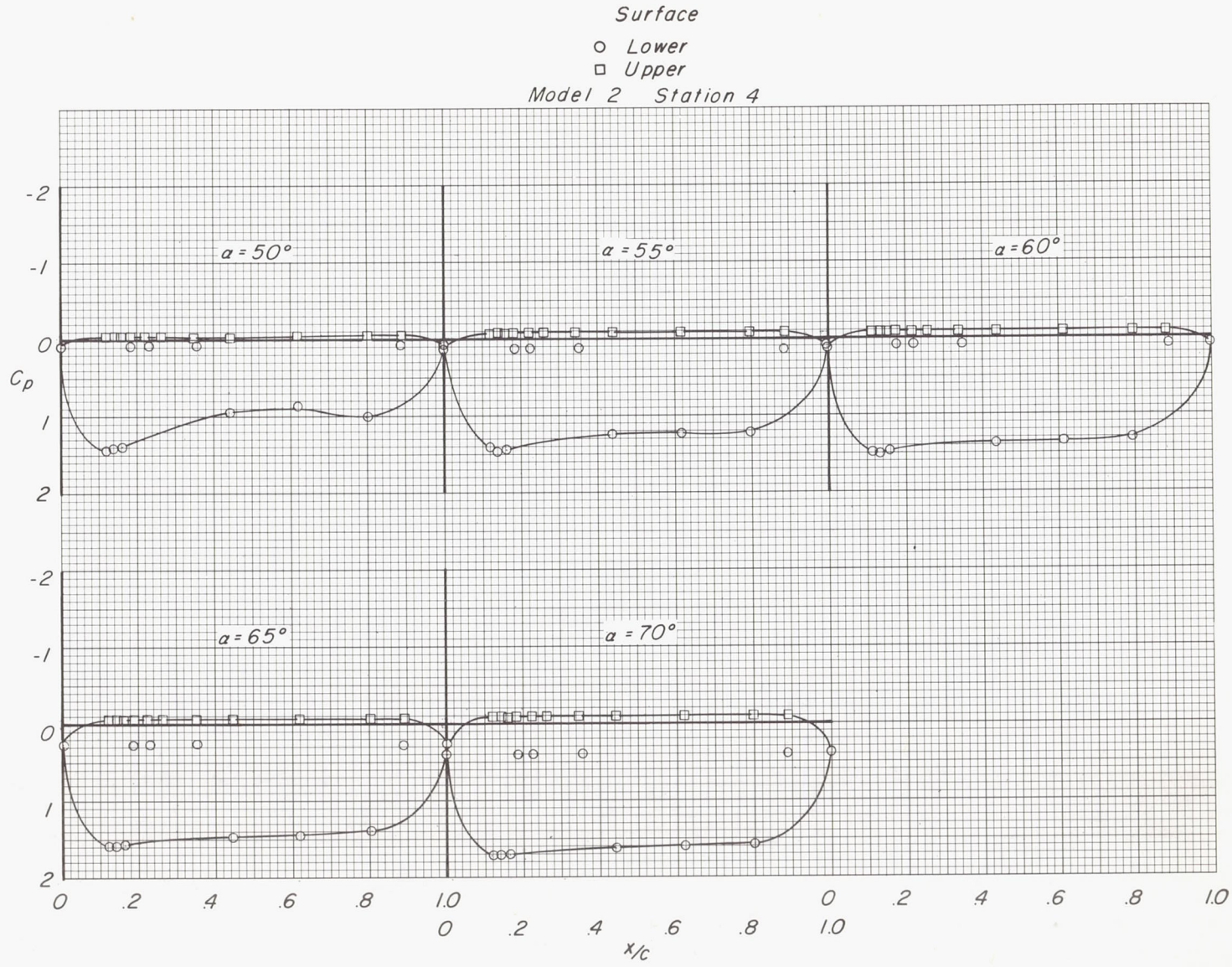

(c) M = 3.95. Concluded.

Figure 7.- Continued.

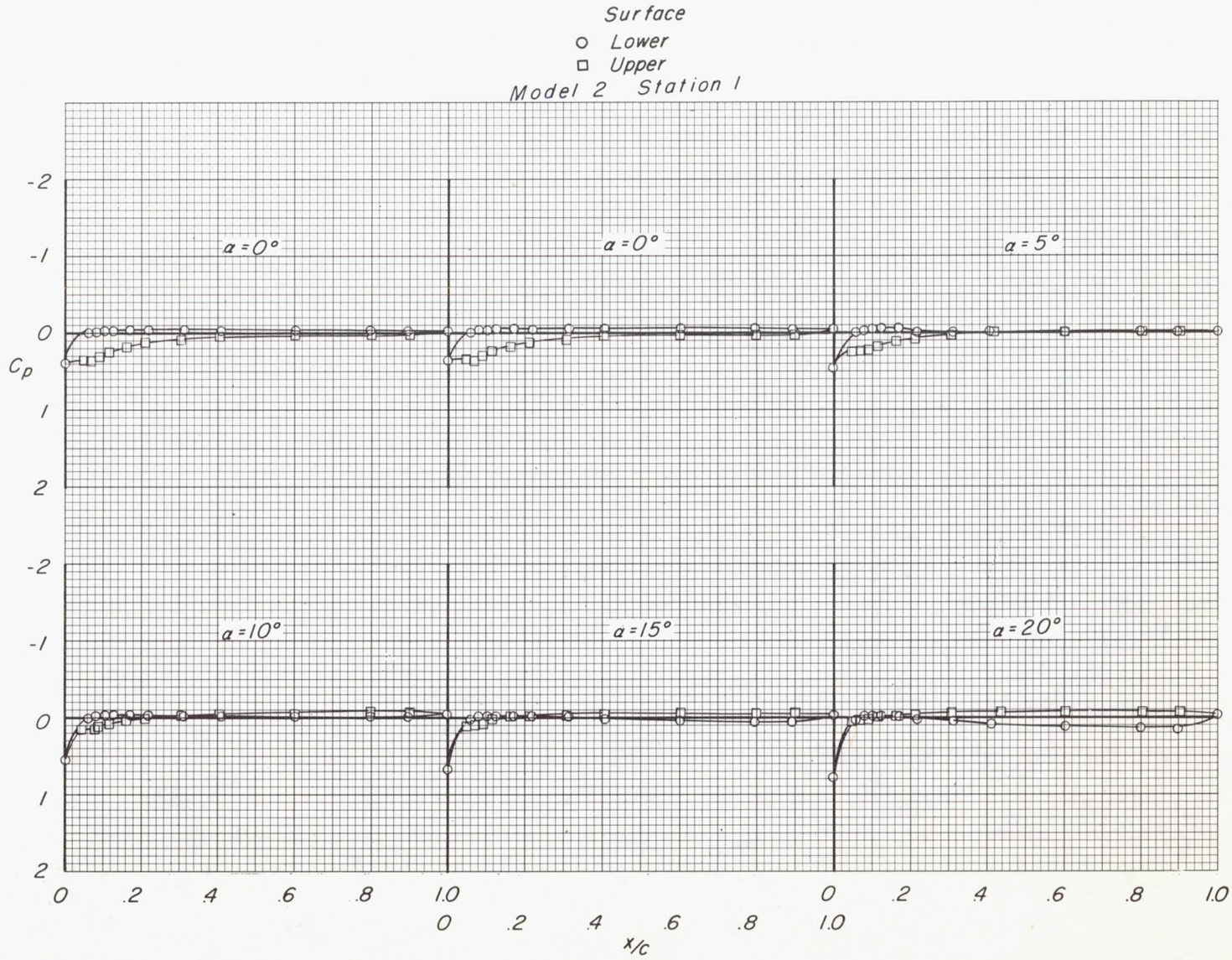

(d) M = 4.65.

Figure 7.- Continued.

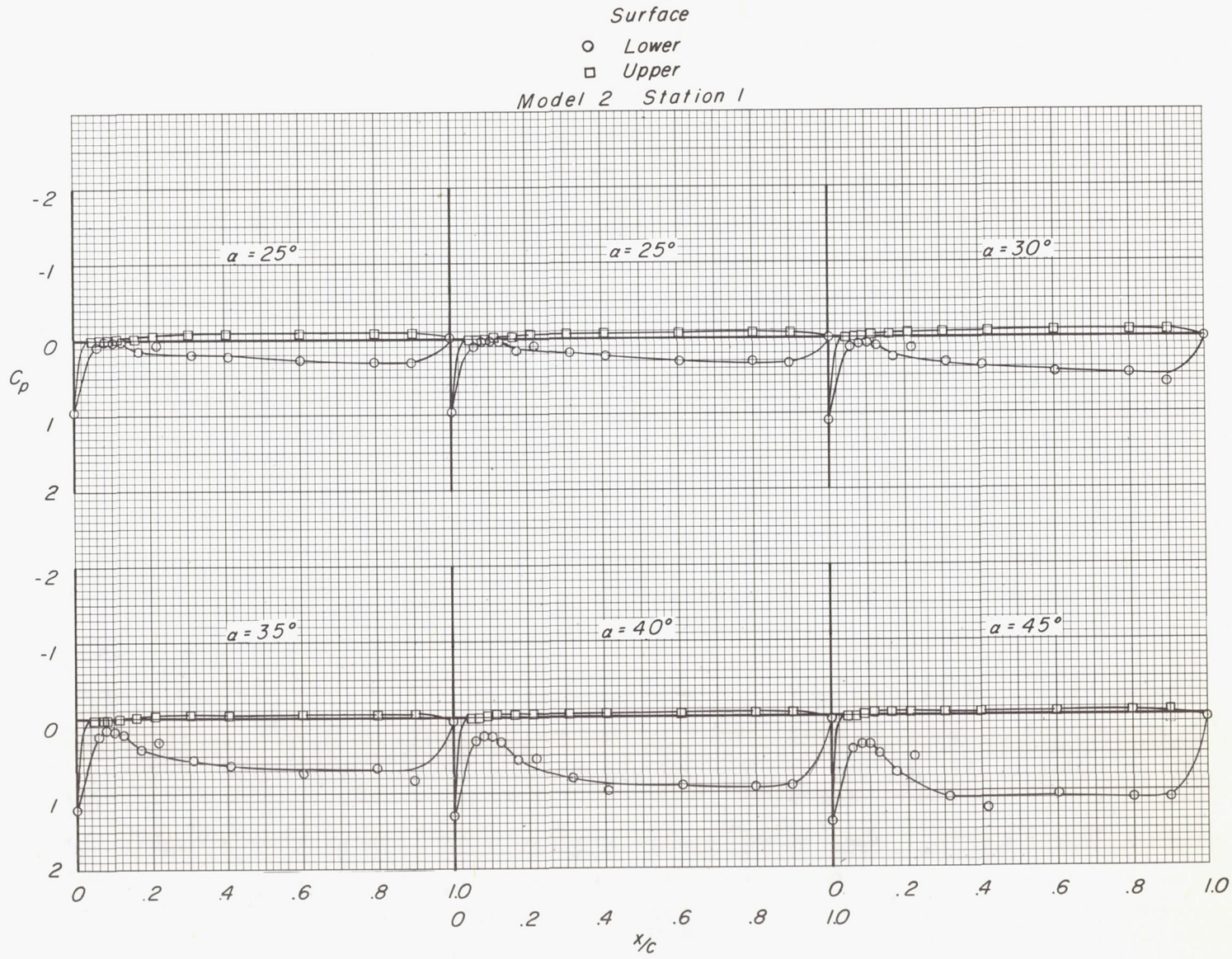

(d) M = 4.65. Continued.

Figure 7.- Continued.

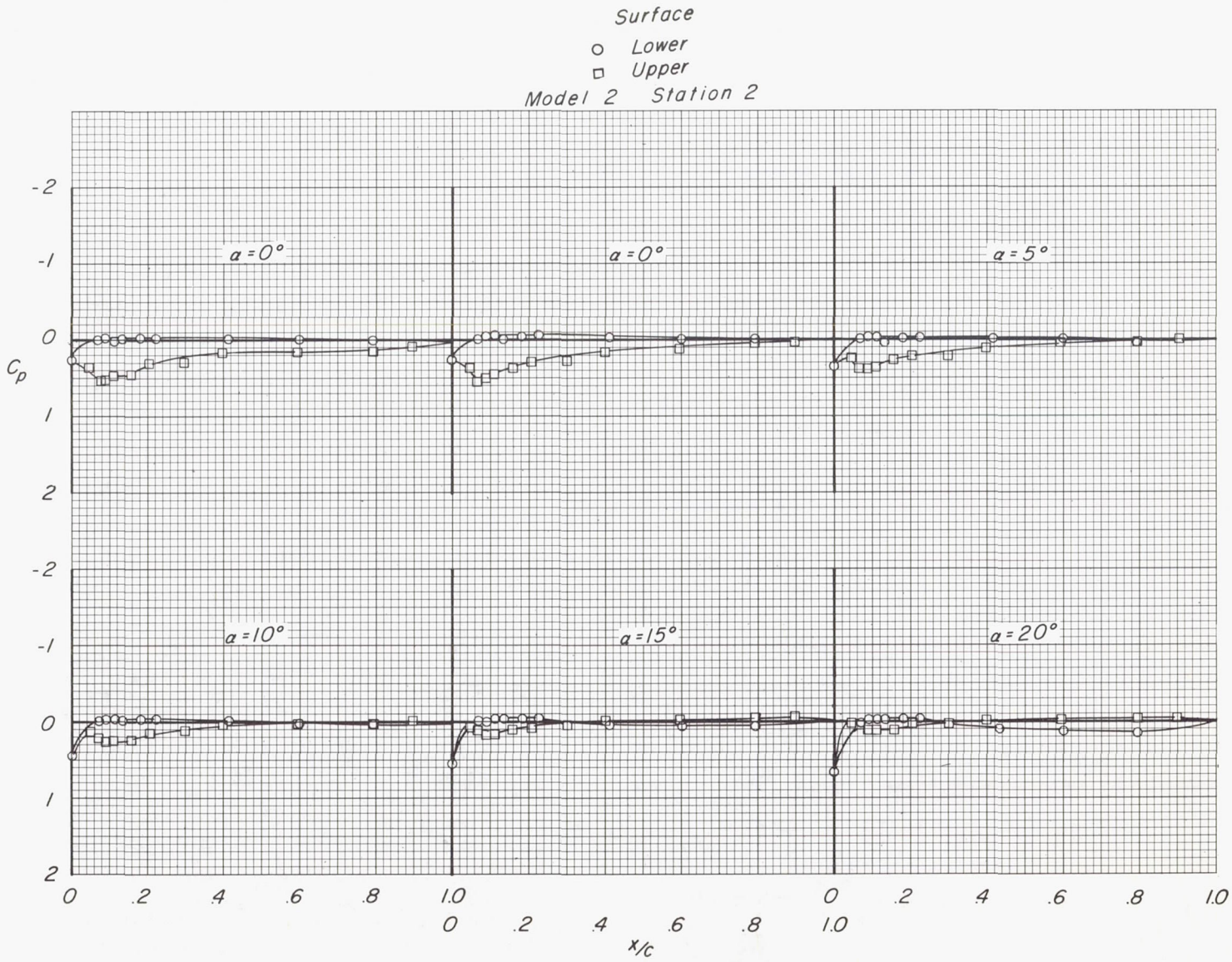

(d) M = 4.65. Continued.

Figure 7.- Continued.

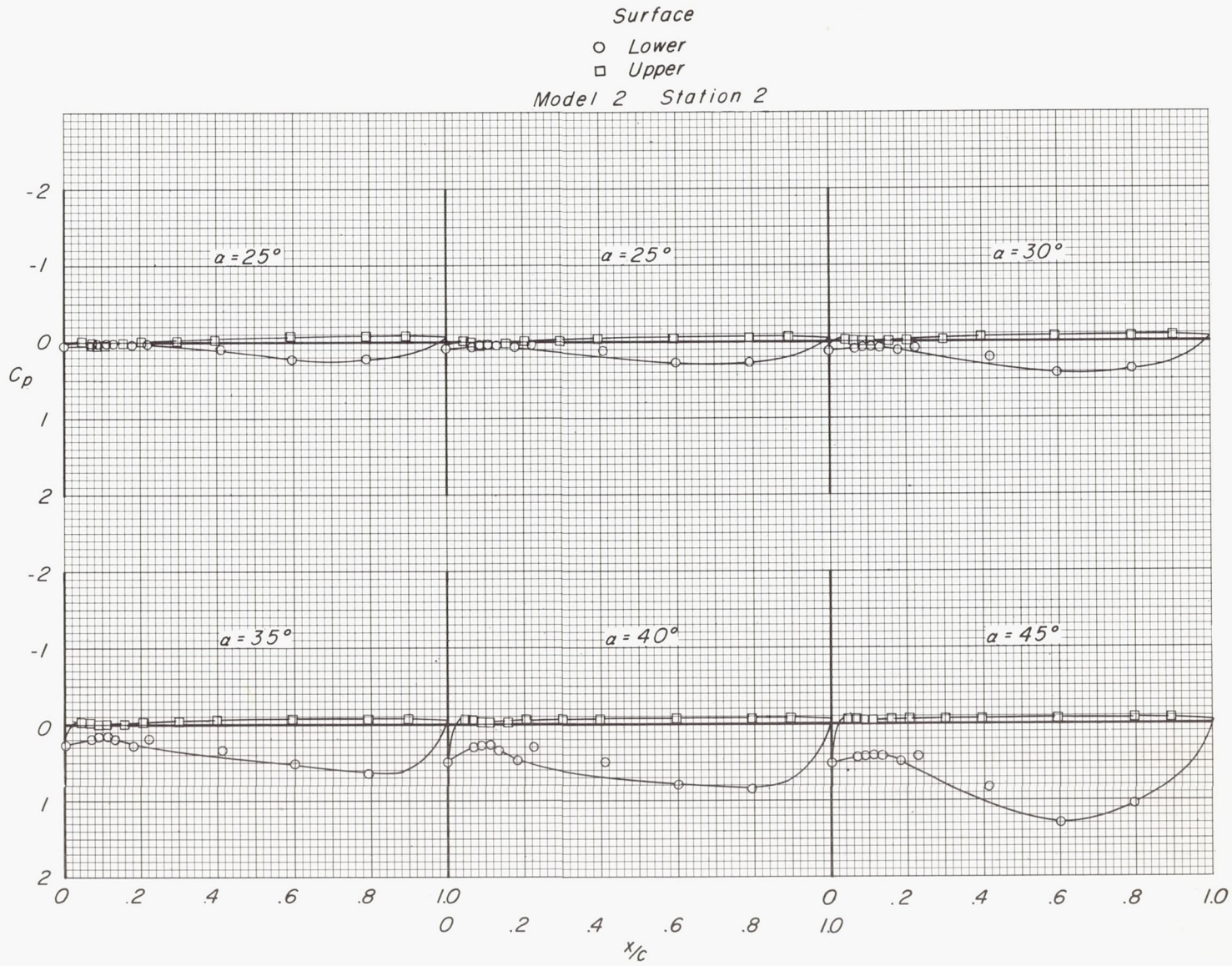

(d) M = 4.65. Continued.

Figure 7.- Continued.

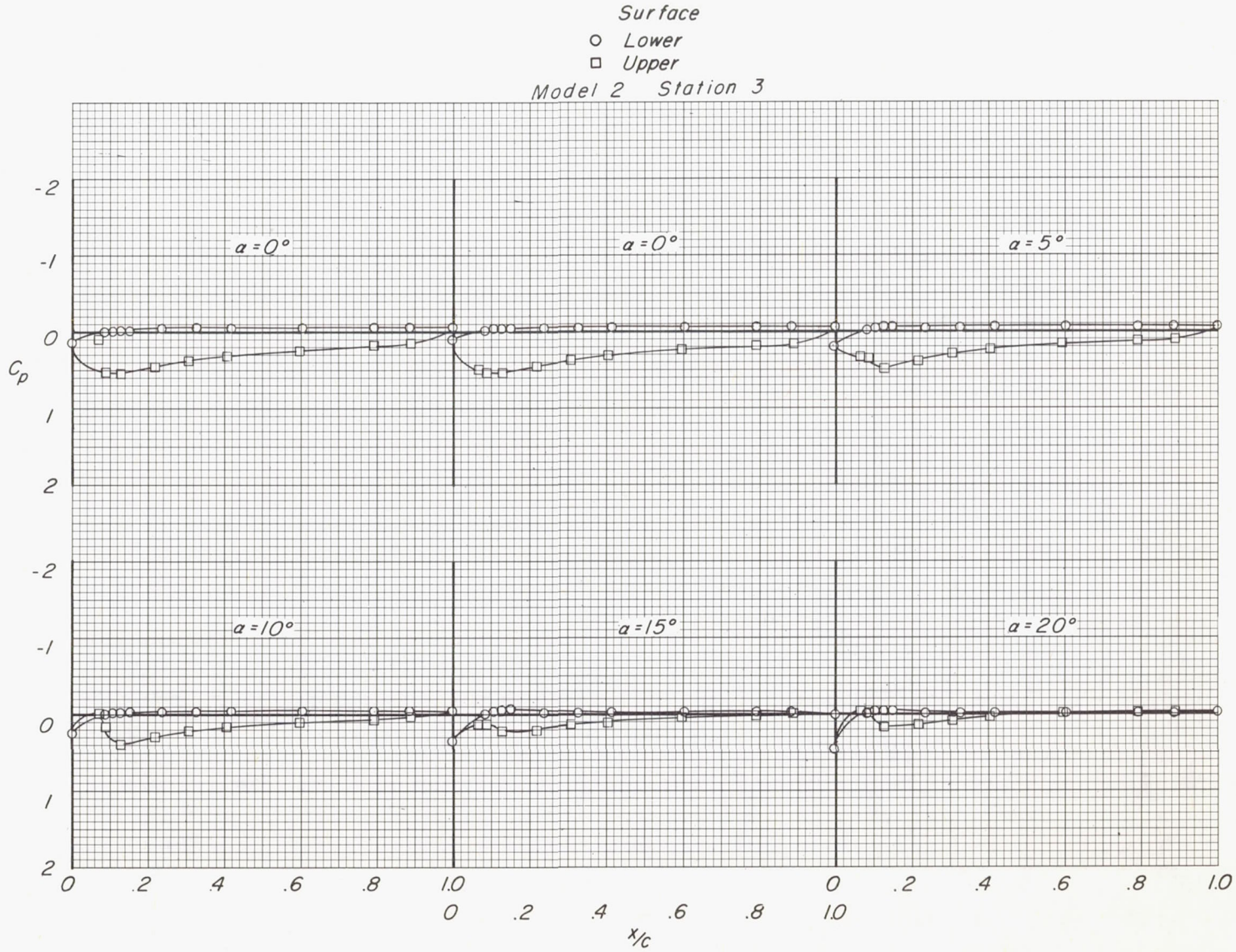

(d) M = 4.65. Continued.

Figure 7.- Continued.

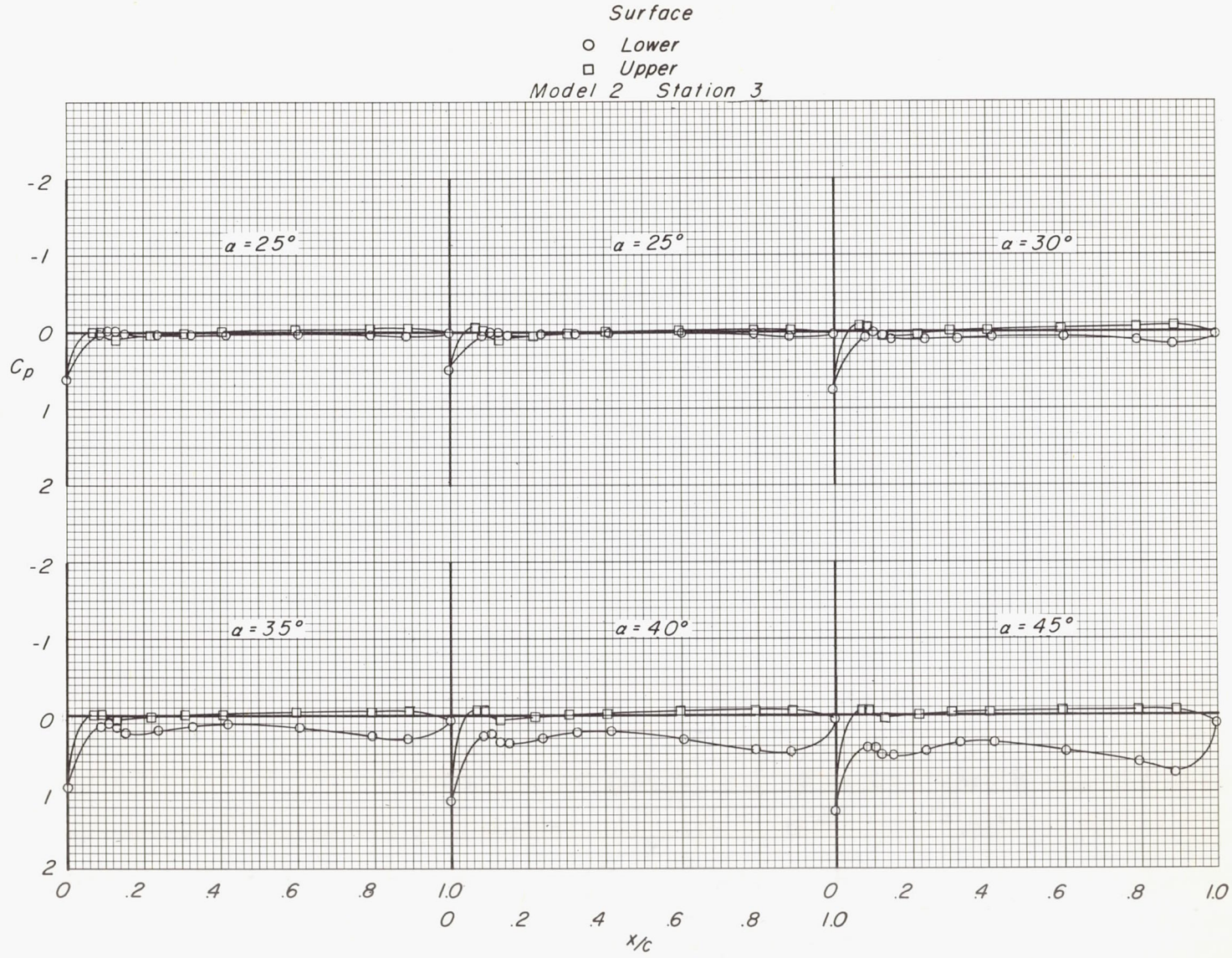

(d) M = 4.65. Continued.

Figure 7.- Continued.

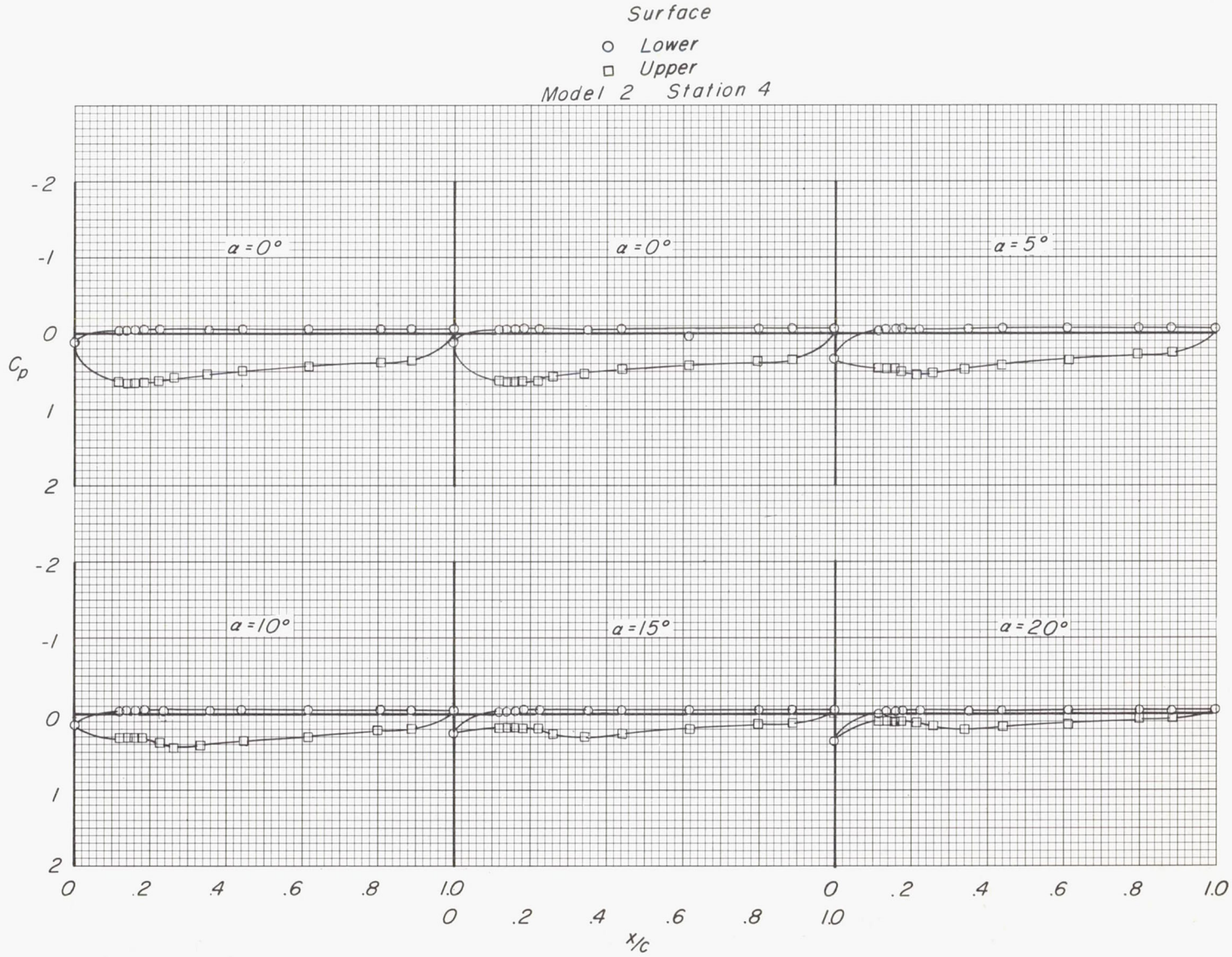

(d) M = 4.65. Continued.

Figure 7.- Continued.

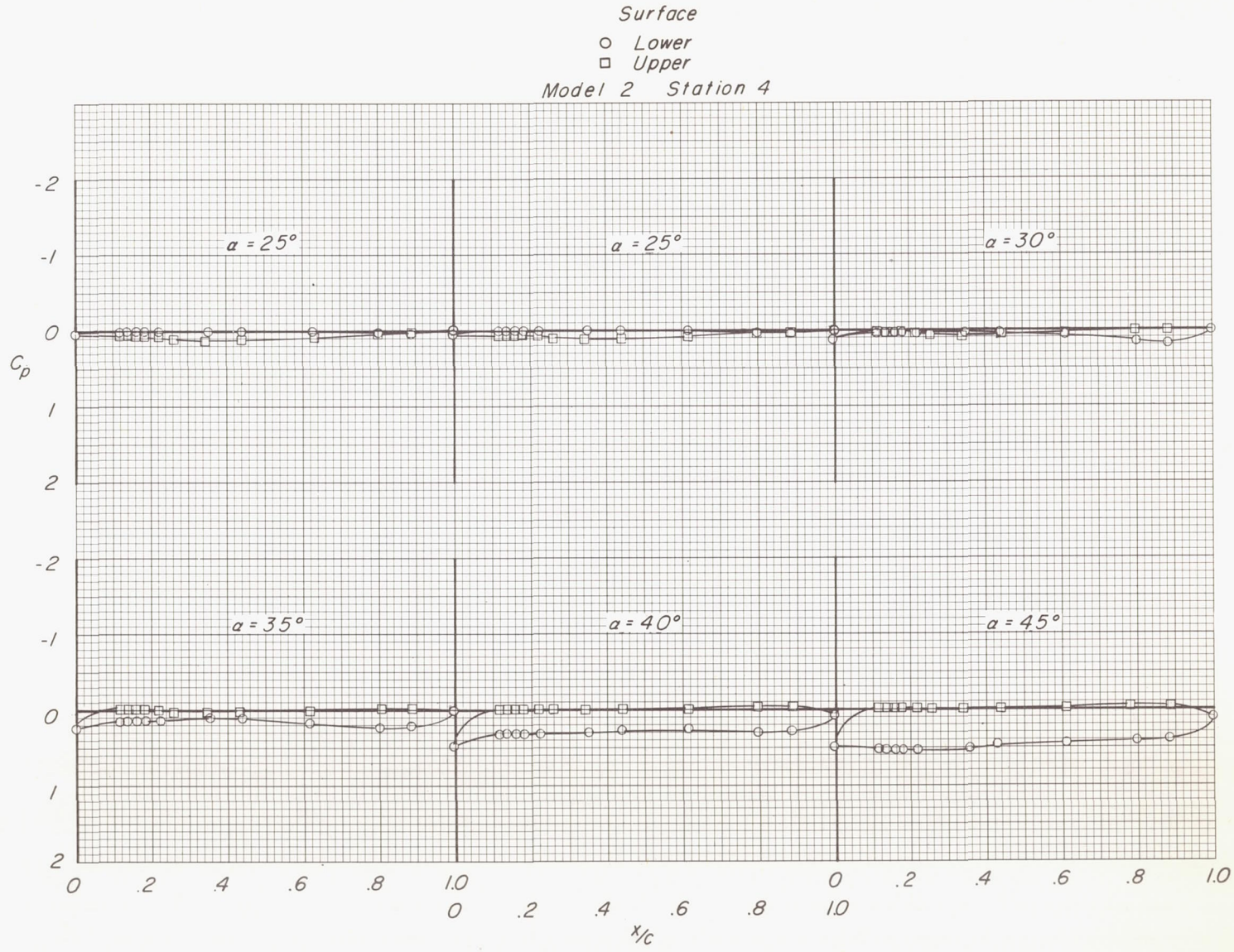

(d) M = 4.65. Concluded.

Figure 7.- Concluded.

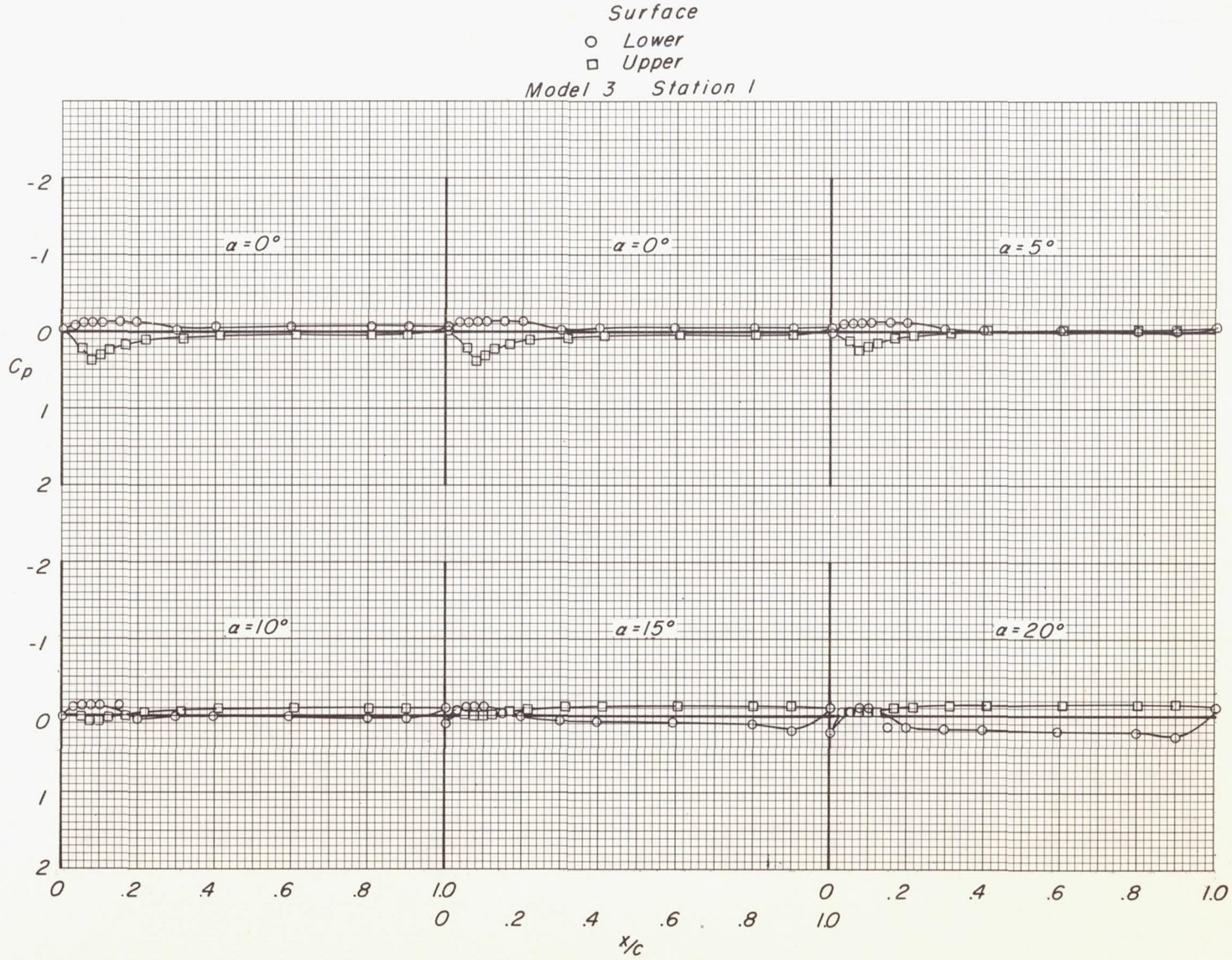

(a) M = 2.96.

Figure 8.- Pressure distributions on model 3 at various angles of attack and Mach numbers.

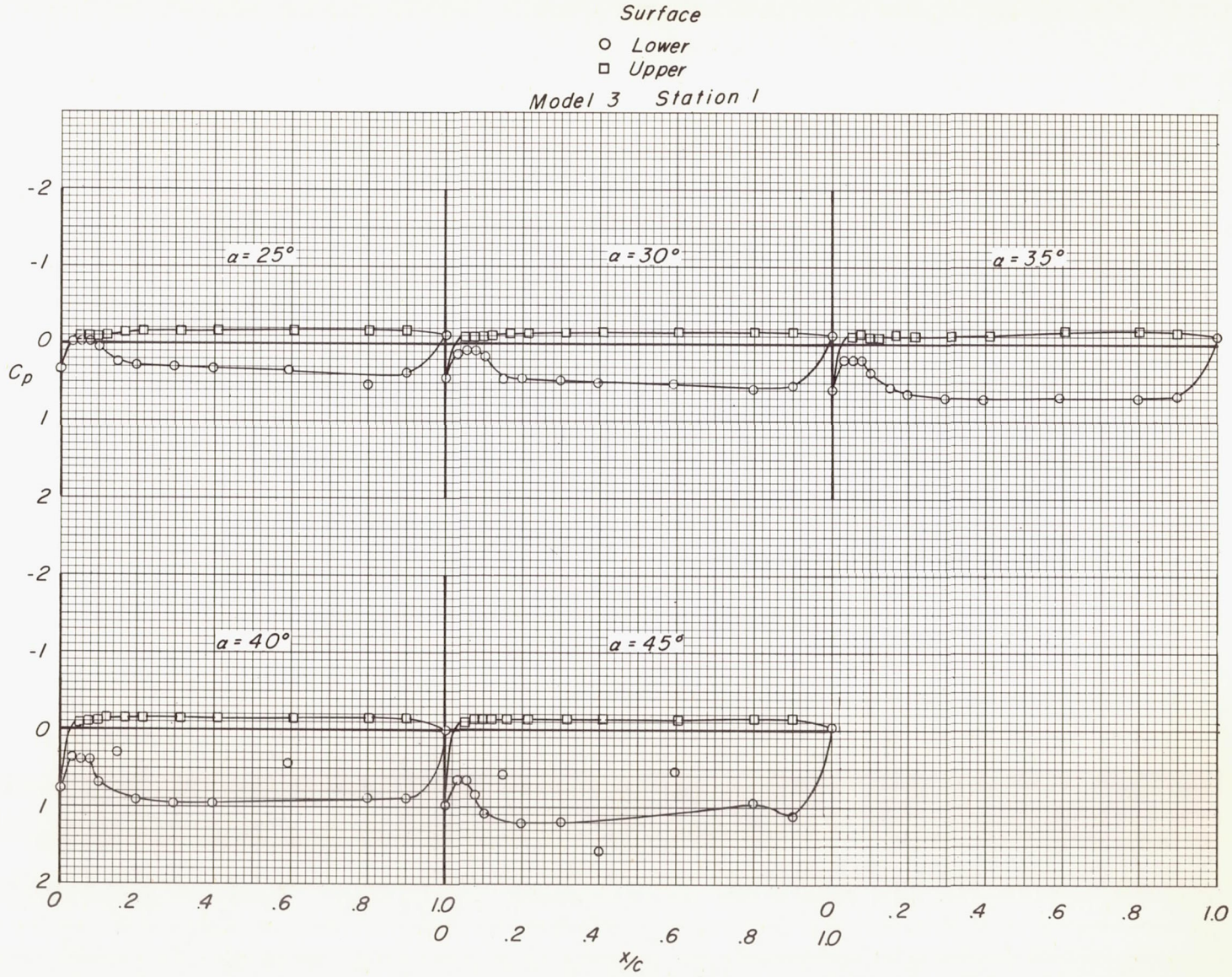

(a) M = 2.96. Continued.

Figure 8.- Continued.

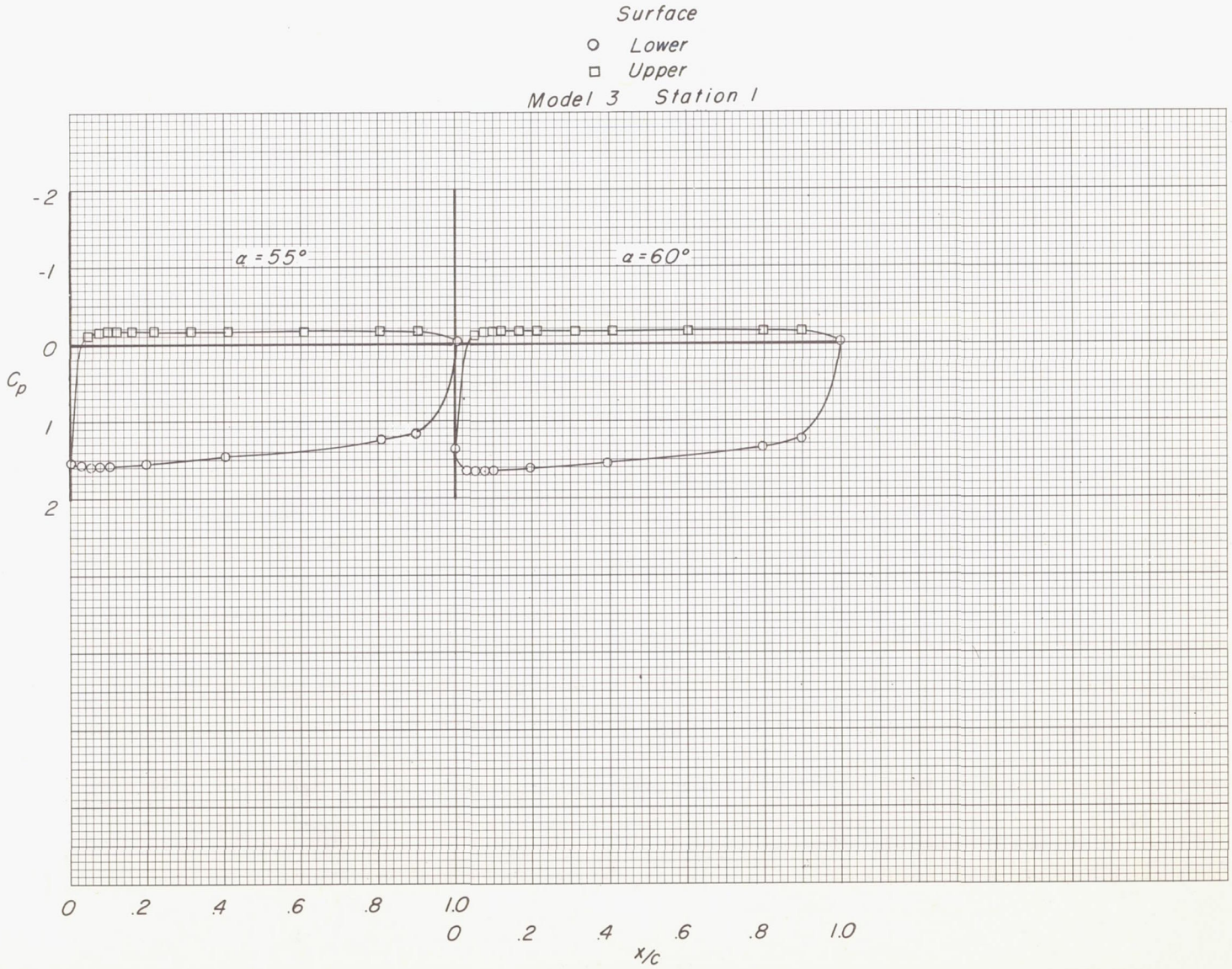

(a) M = 2.96. Continued.

Figure 8.- Continued.

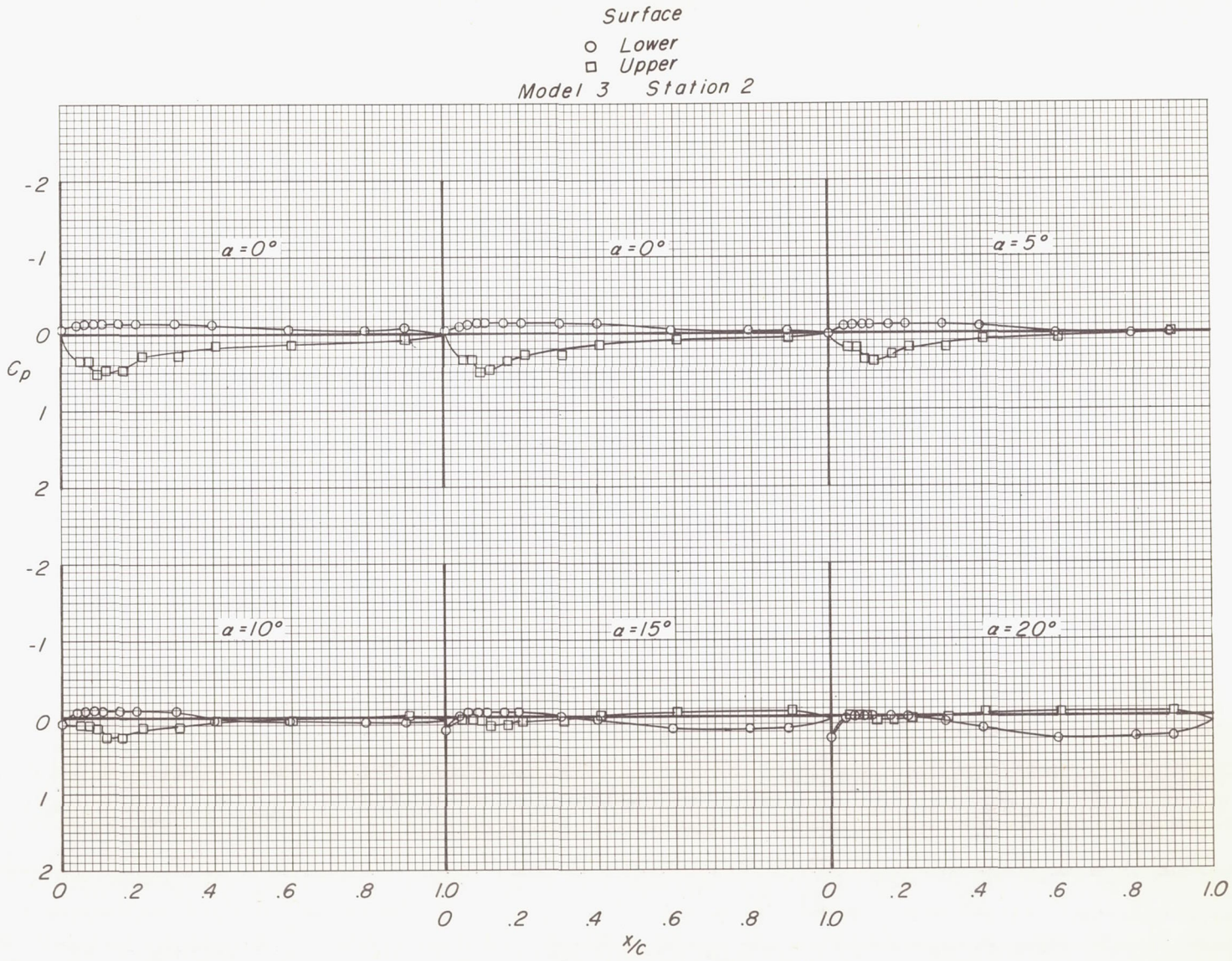

(a) M = 2.96. Continued.

Figure 8.- Continued.

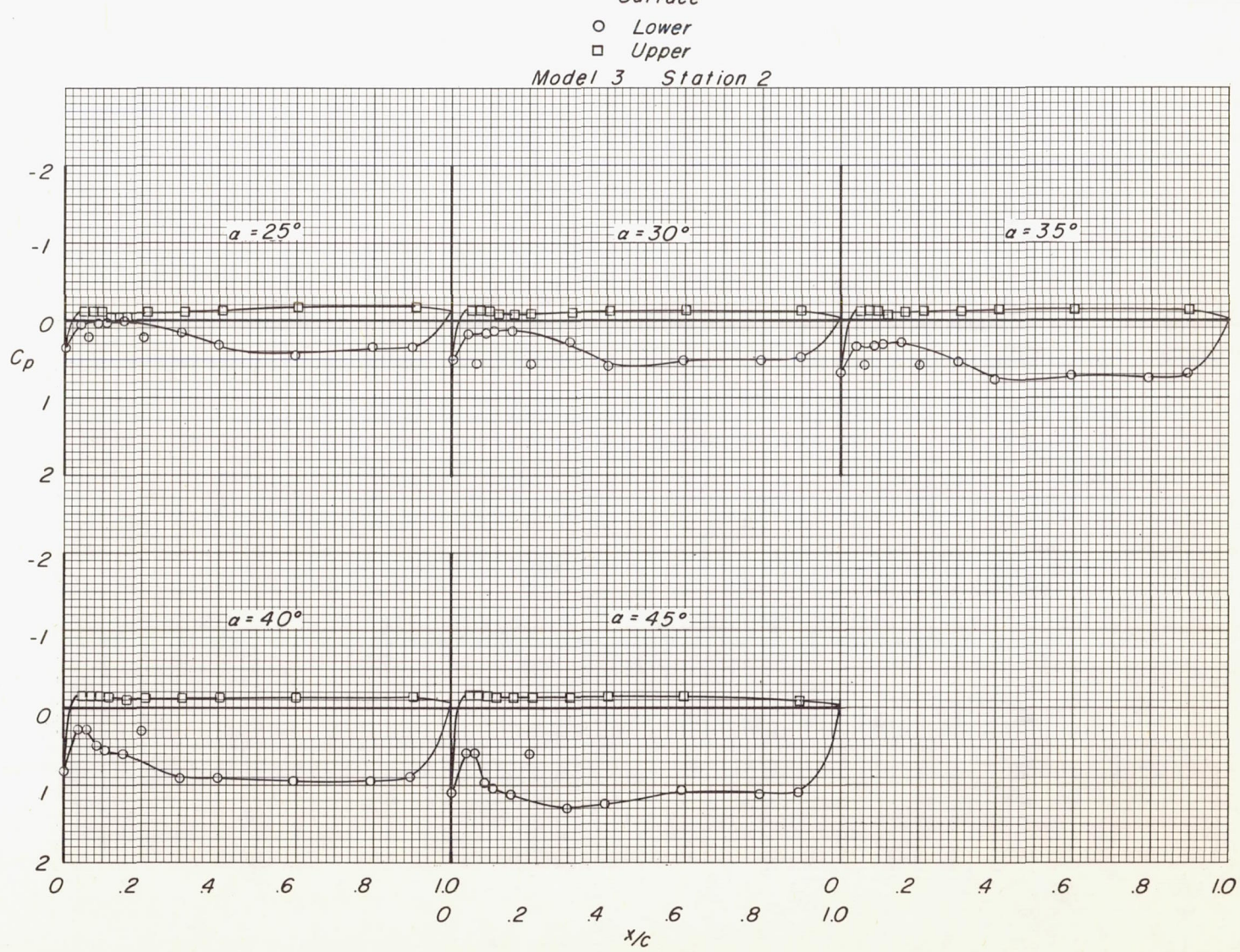

(a) M = 2.96. Continued.

Figure 8.- Continued.

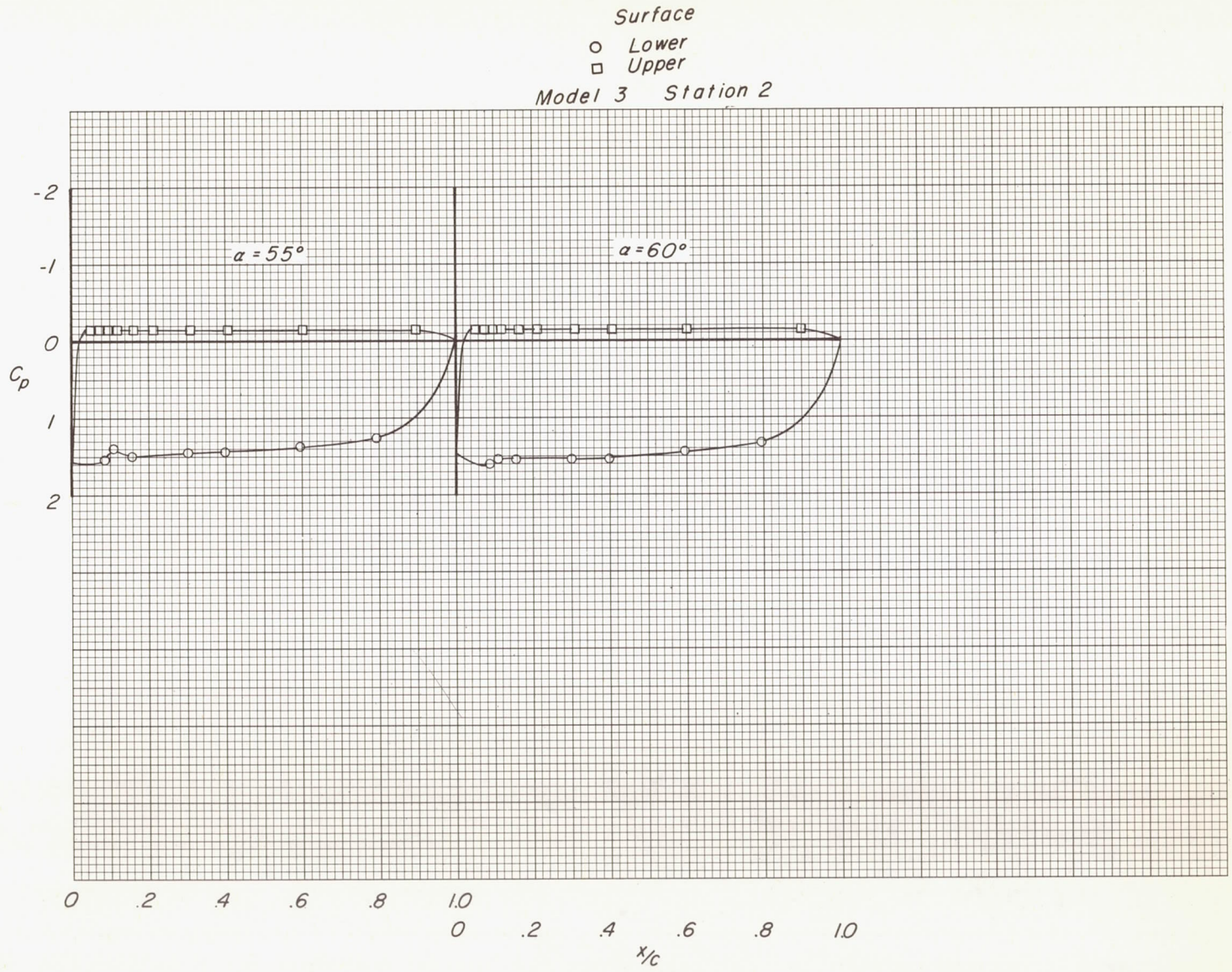

(a) M = 2.96. Continued.

Figure 8.- Continued.

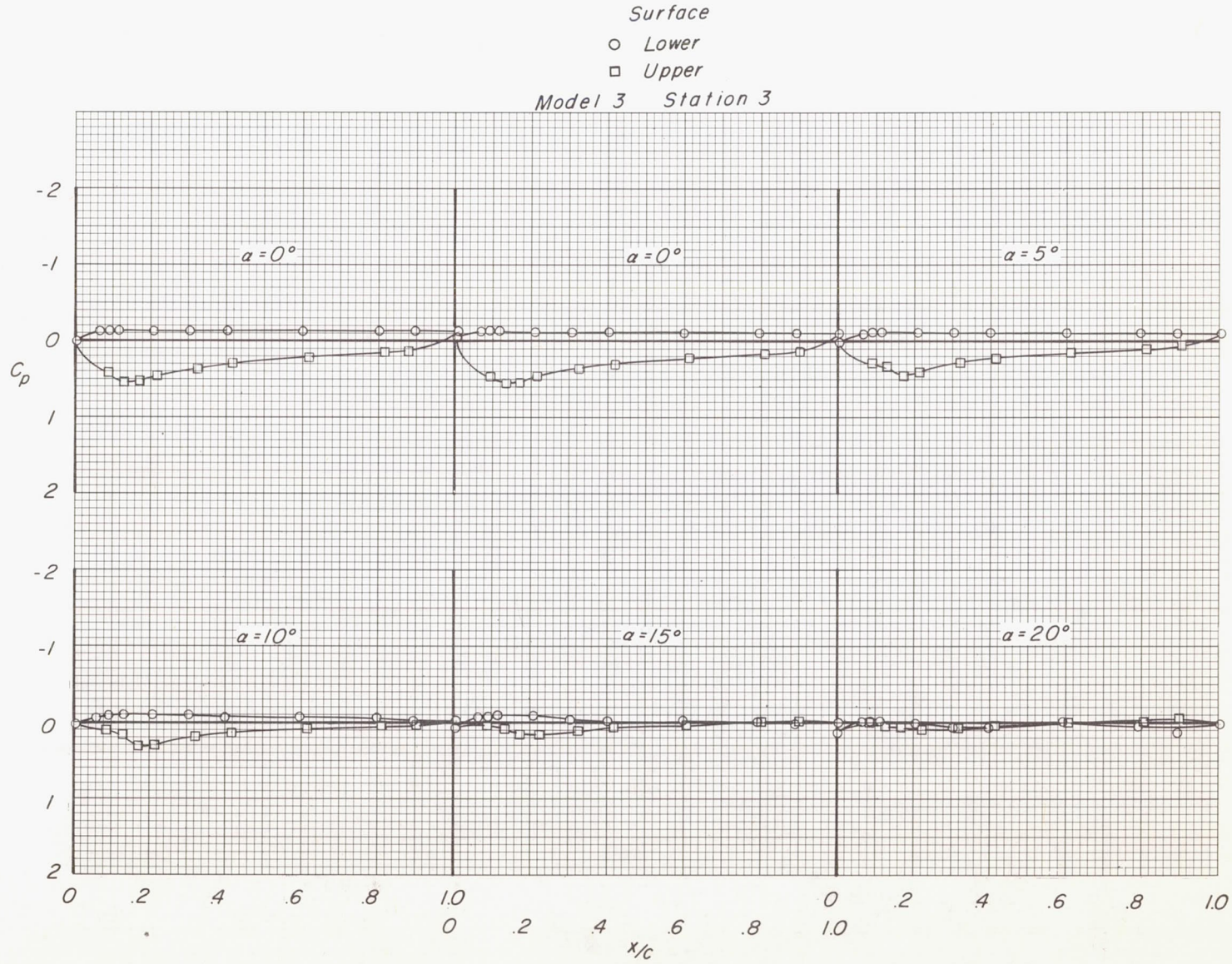

(a) M = 2.96. Continued.

Figure 8.- Continued.

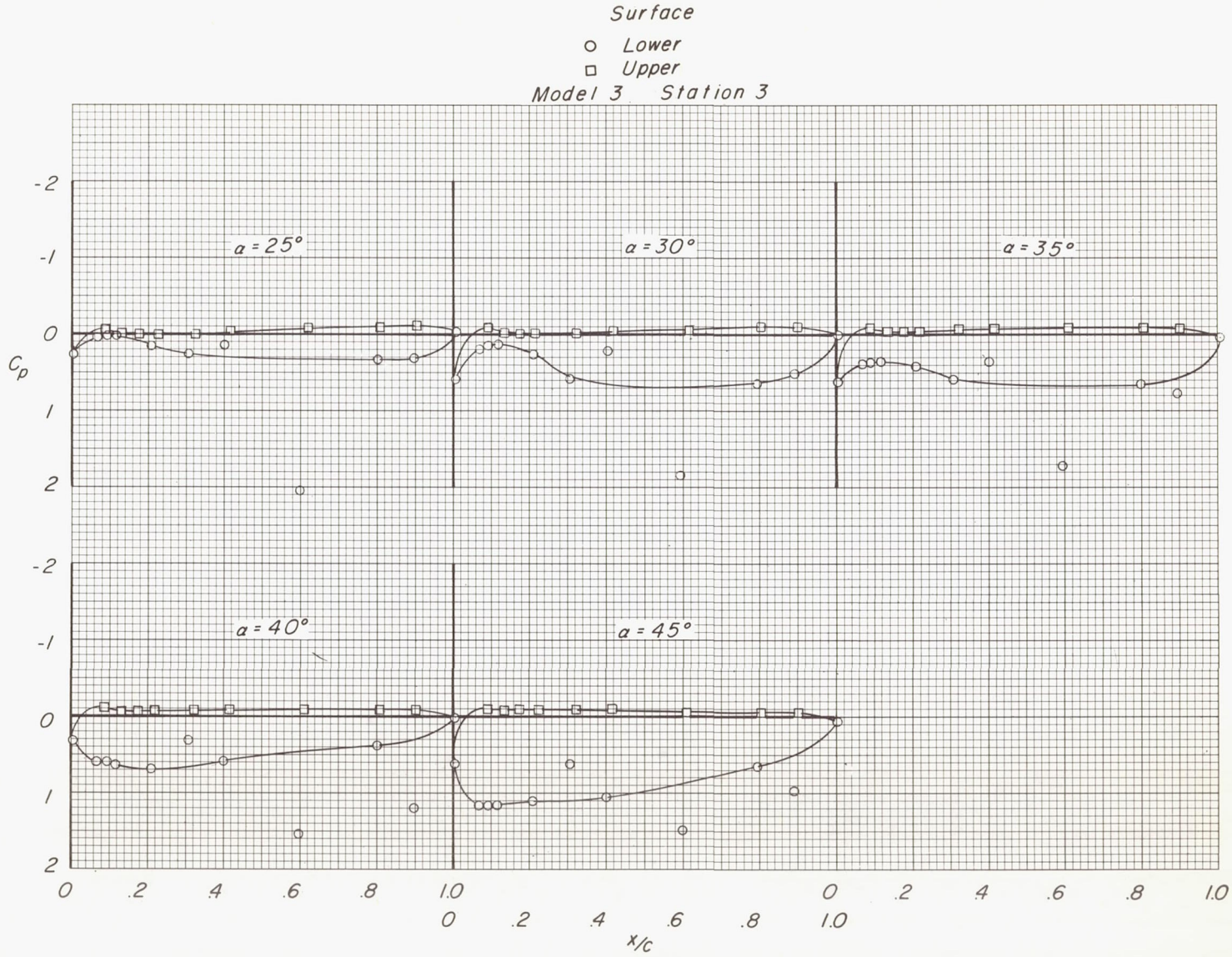

(a) M = 2.96. Continued.

Figure 8.- Continued.

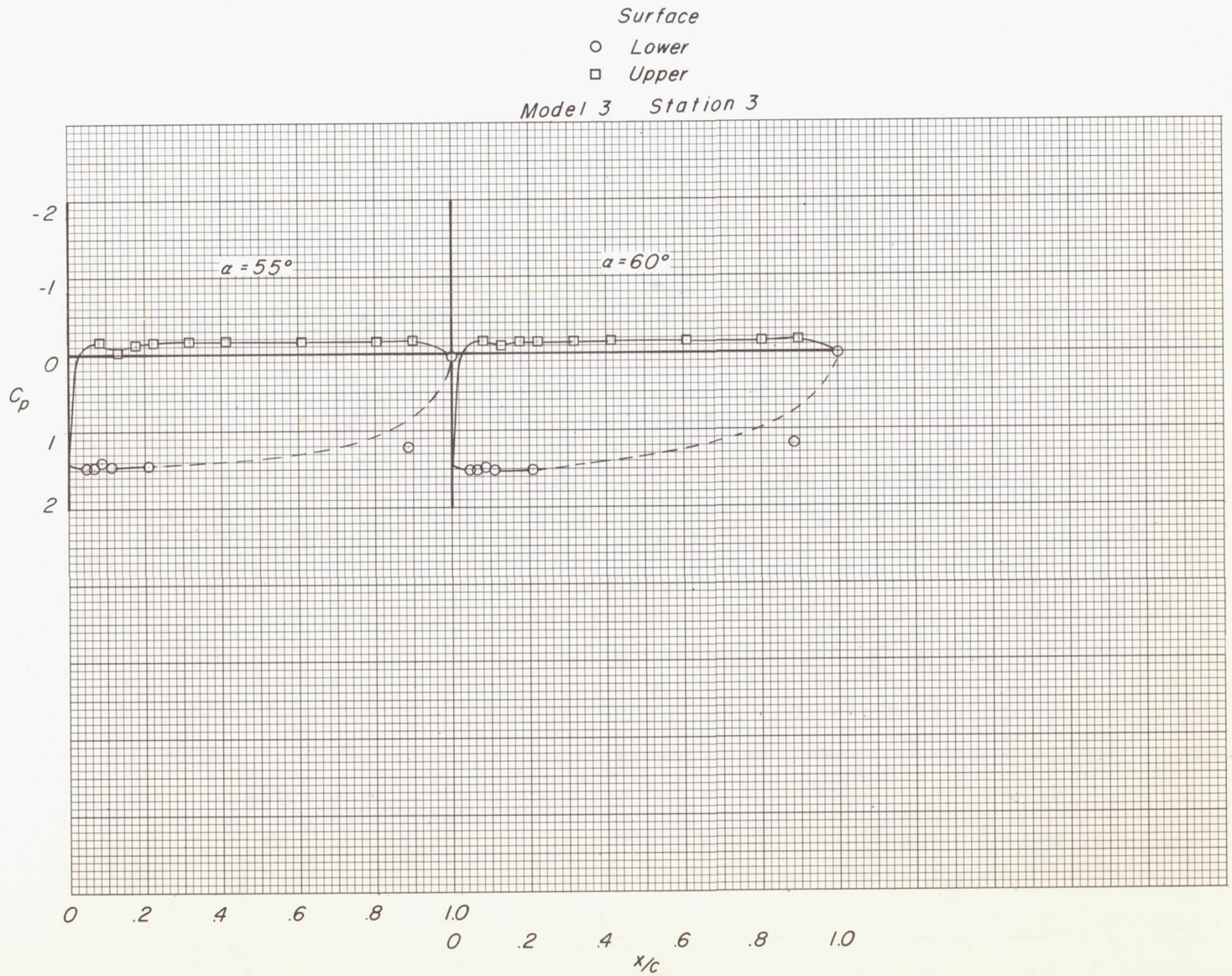

(a) M = 2.96. Continued.

Figure 8.- Continued.

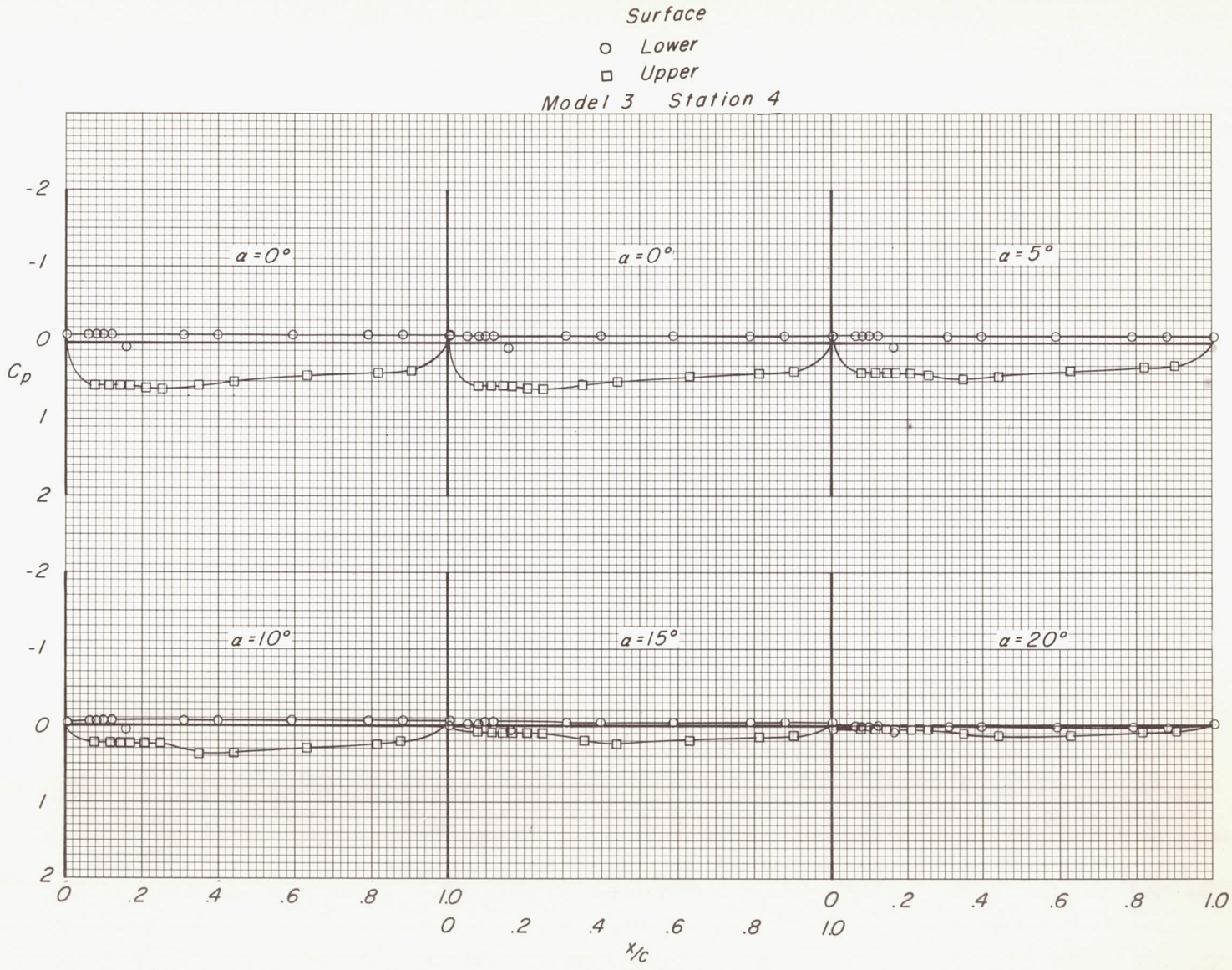

(a) M = 2.96. Continued.

Figure 8.- Continued.

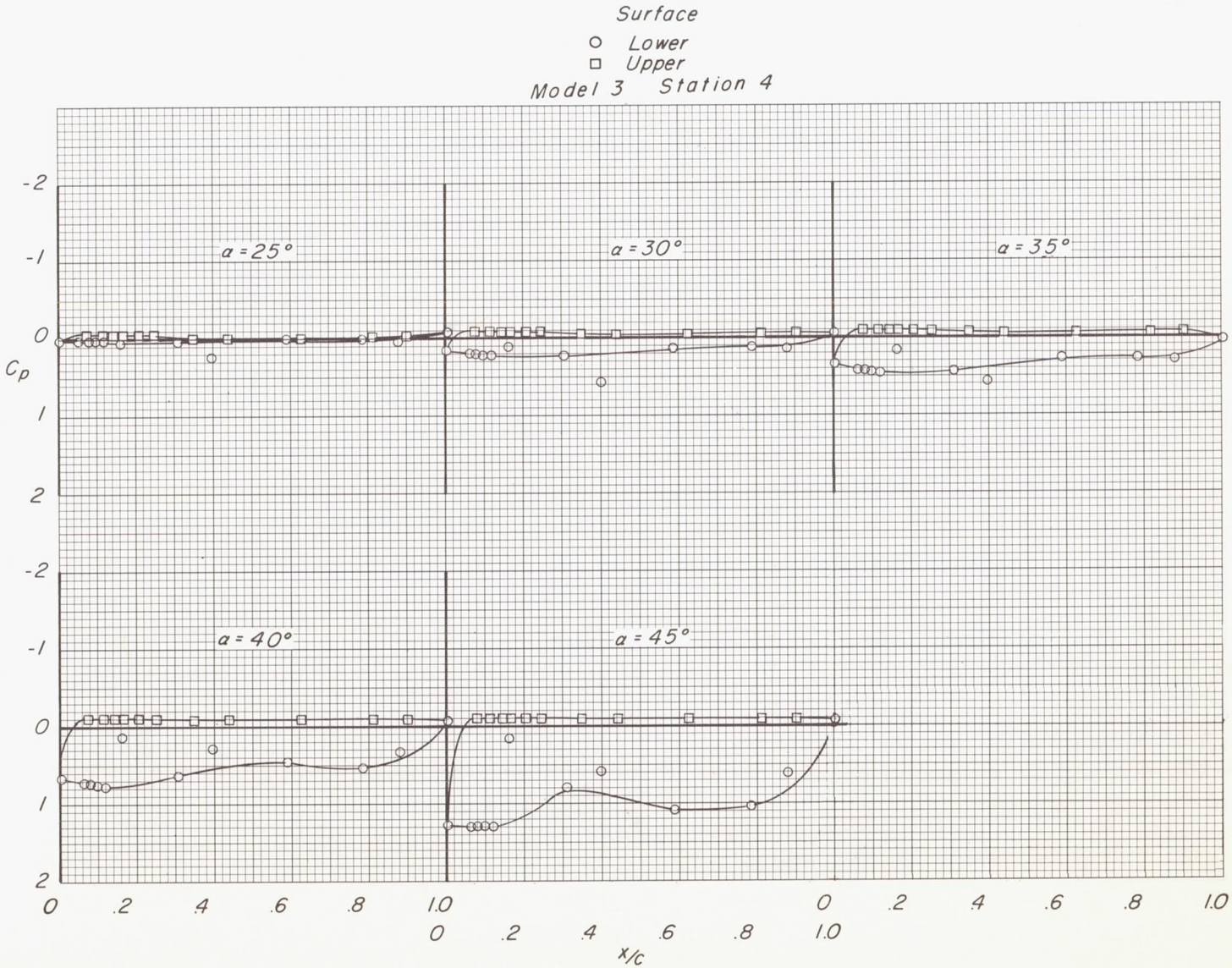

(a) M = 2.96. Continued.

Figure 8.- Continued.

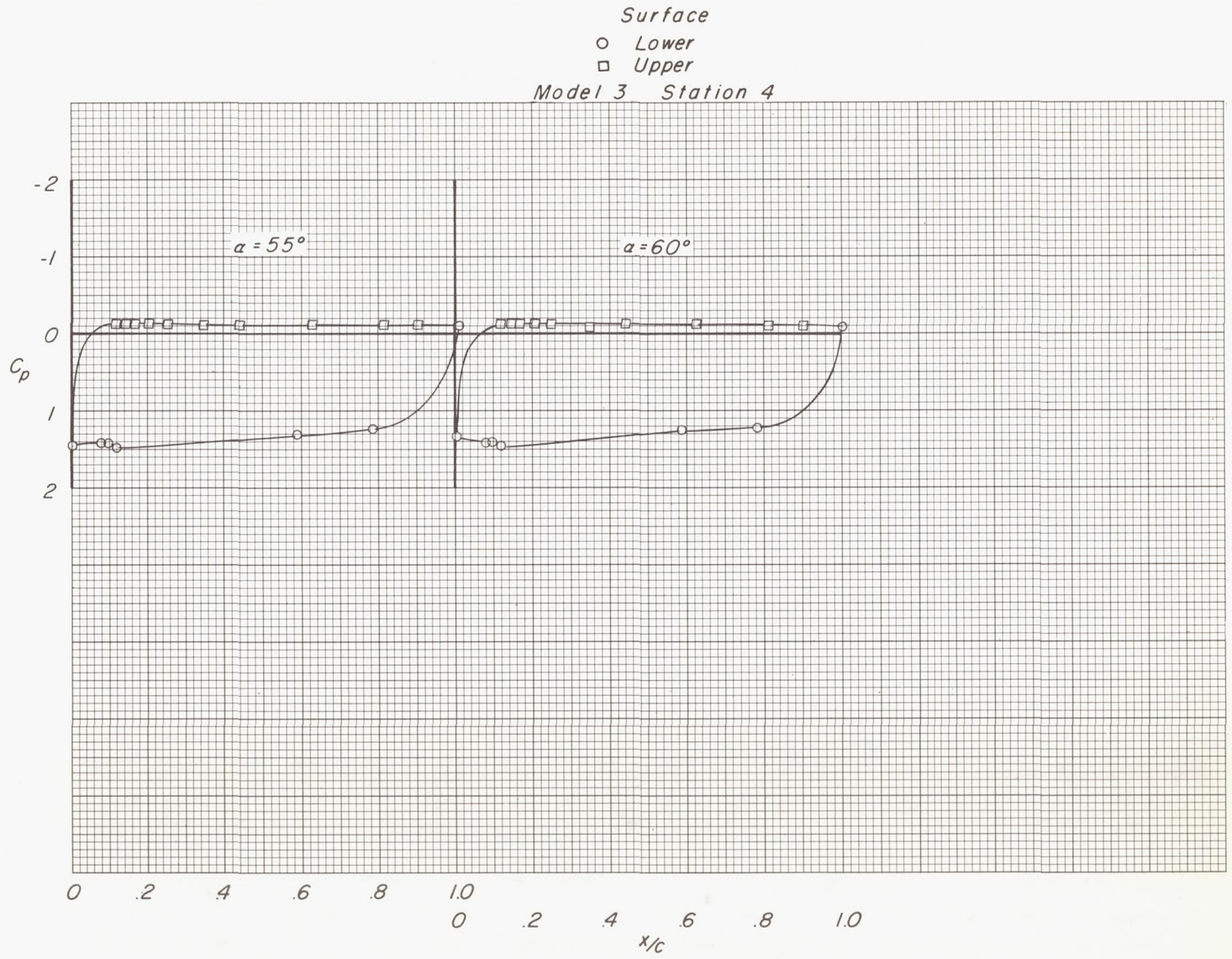

(a) M = 2.96. Concluded.

Figure 8.- Continued.

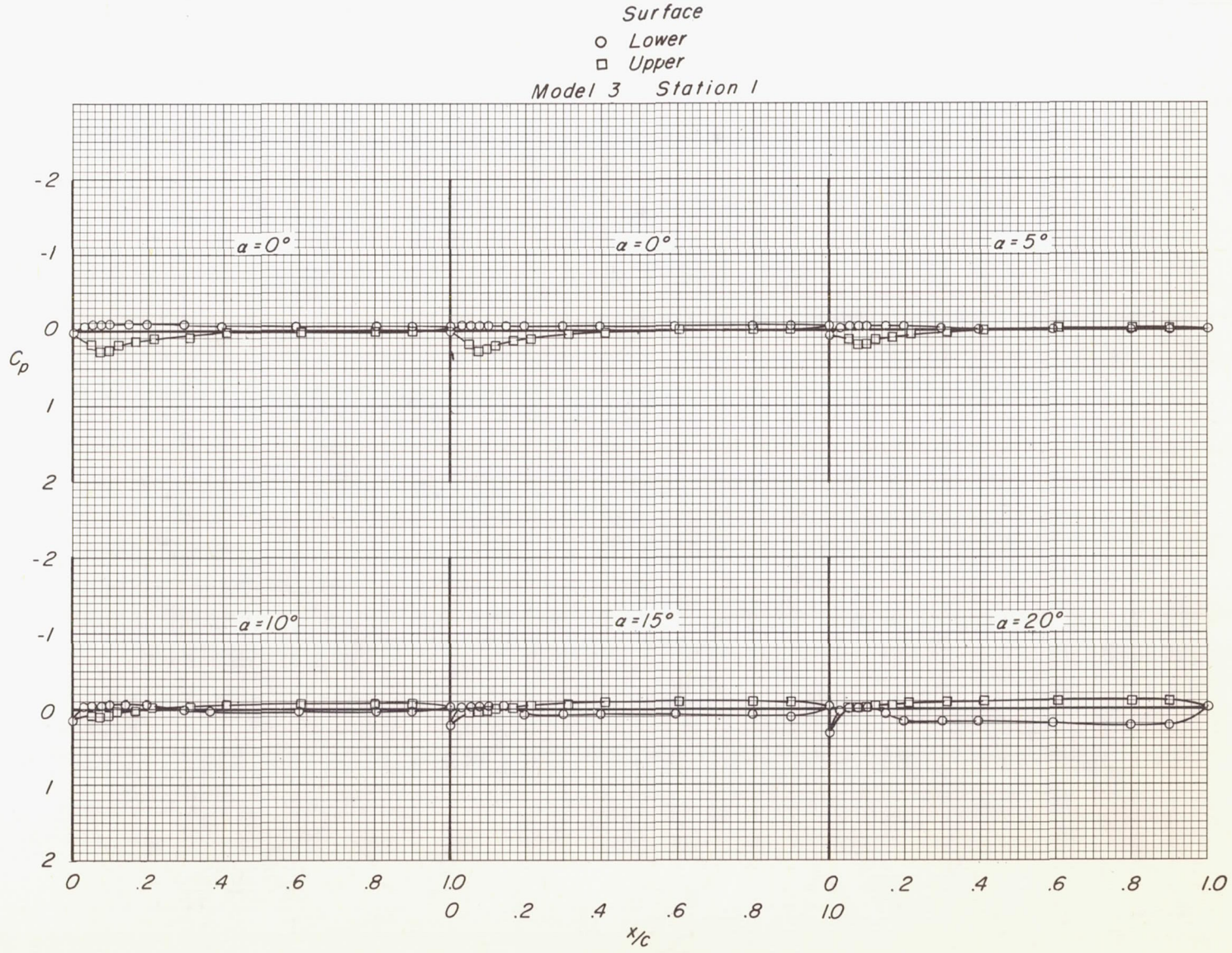

(b) M = 3.95.

Figure 8.- Continued.

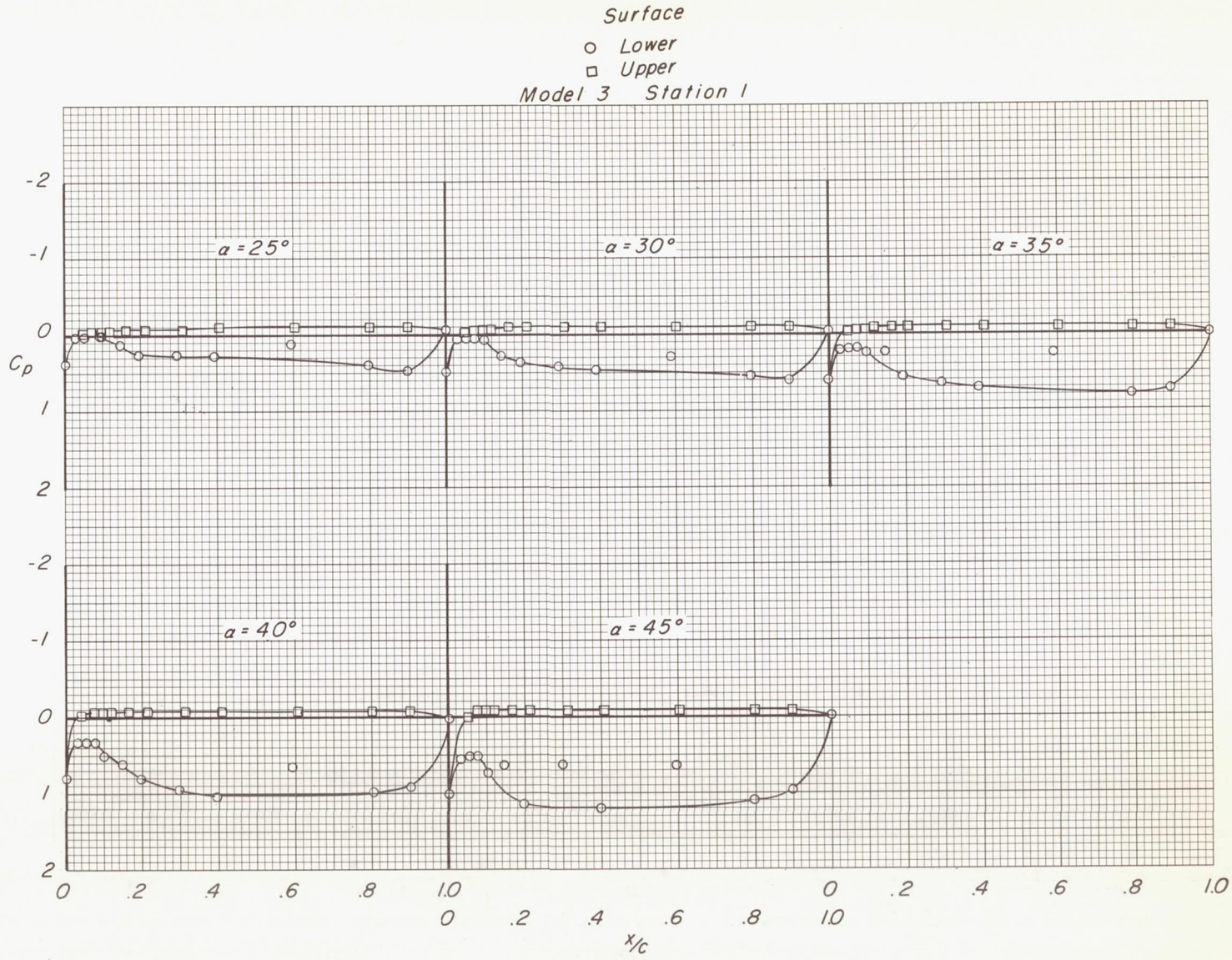

(b) M = 3.95. Continued.

Figure 8.- Continued.

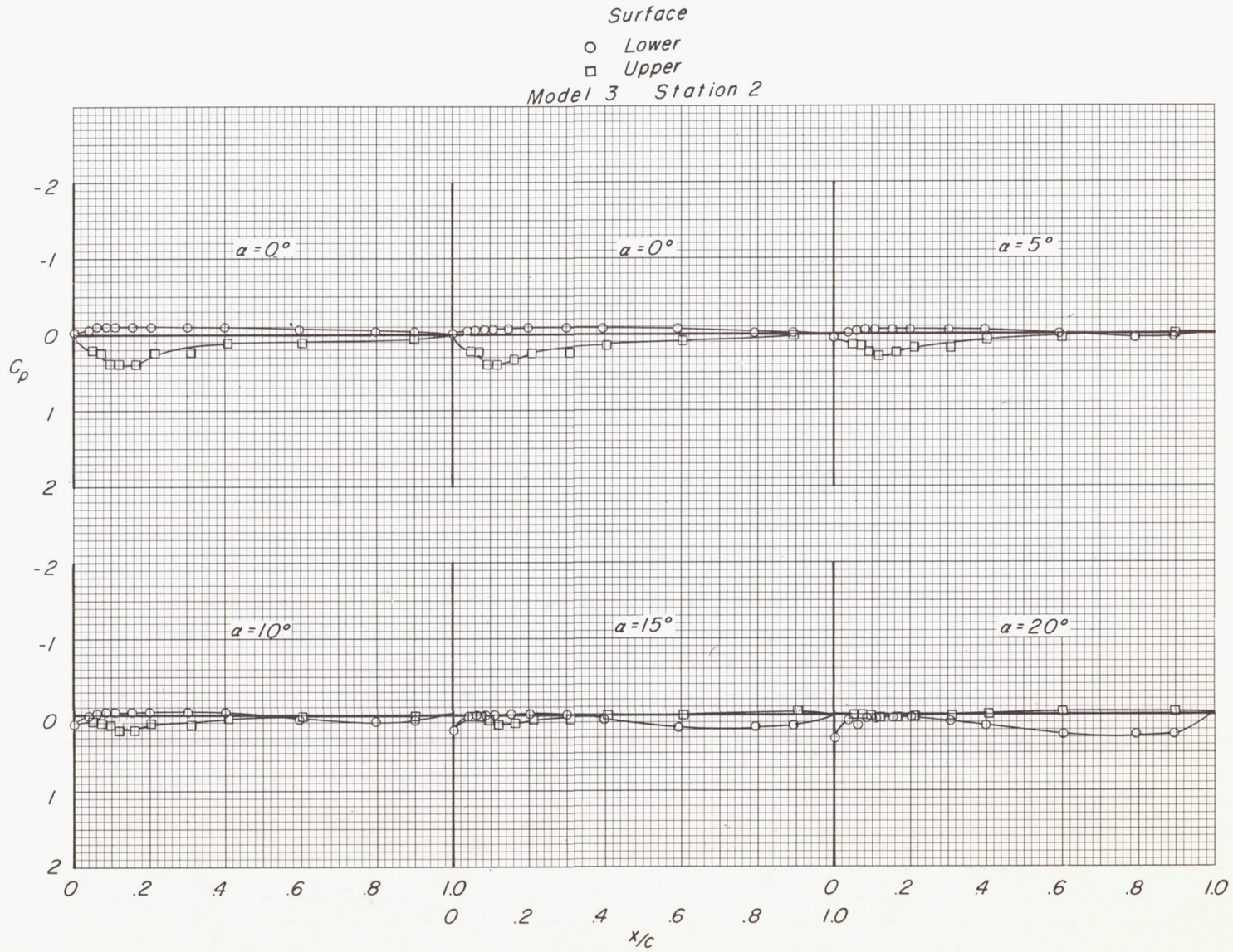

(b) M = 3.95. Continued.

Figure 8.- Continued.

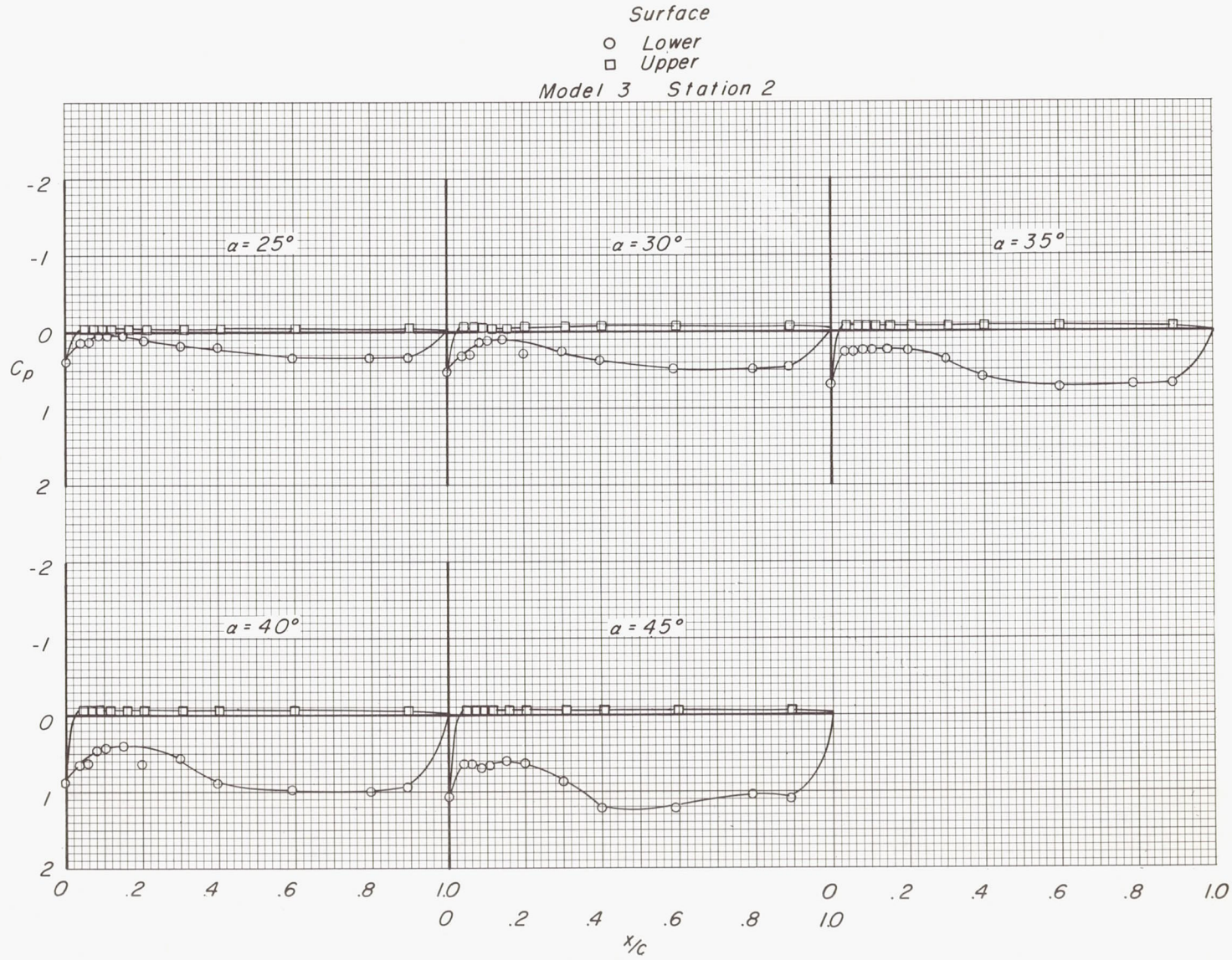

(b) M = 3.95. Continued.

Figure 8.- Continued.

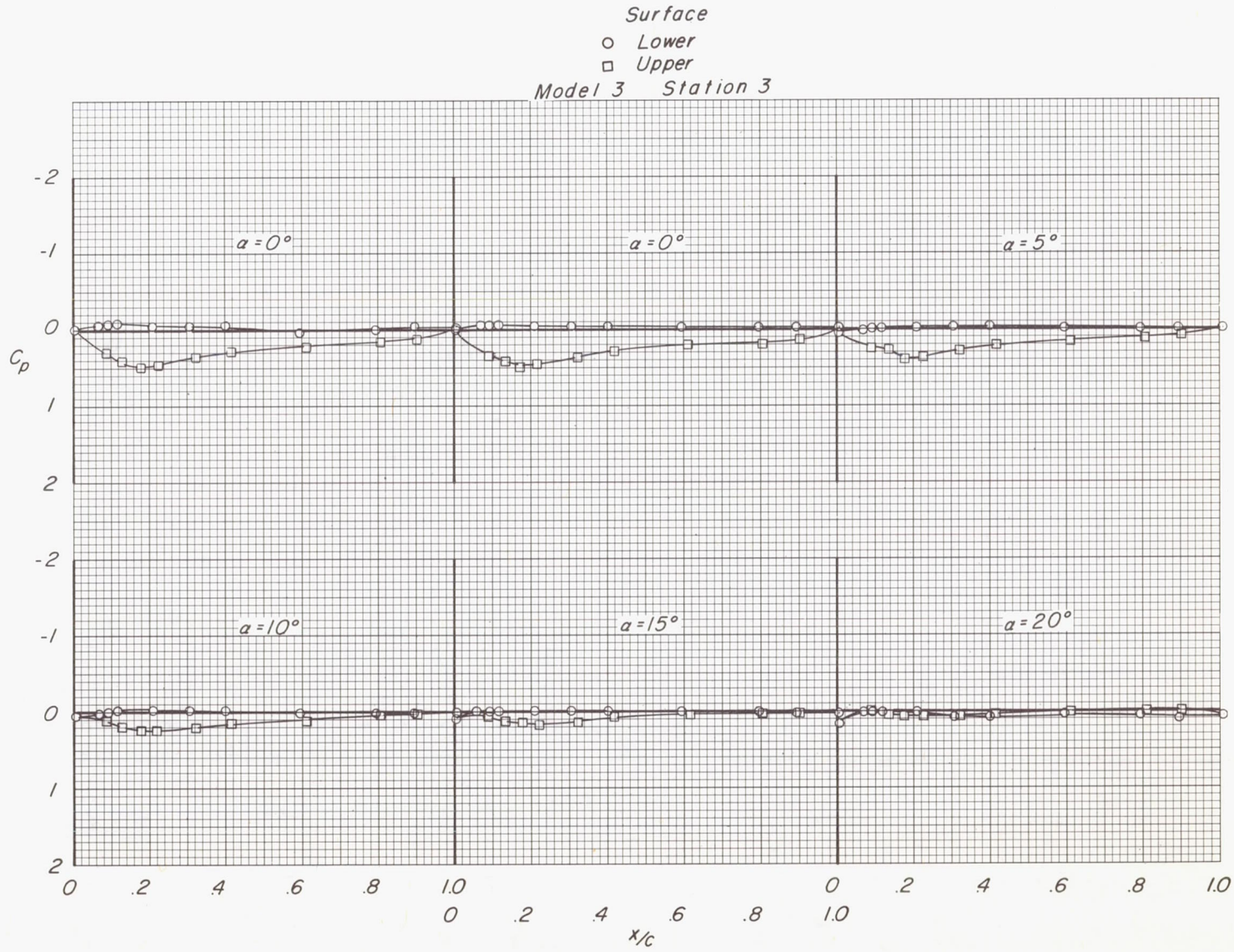

(b) M = 3.95. Continued.

Figure 8.- Continued.

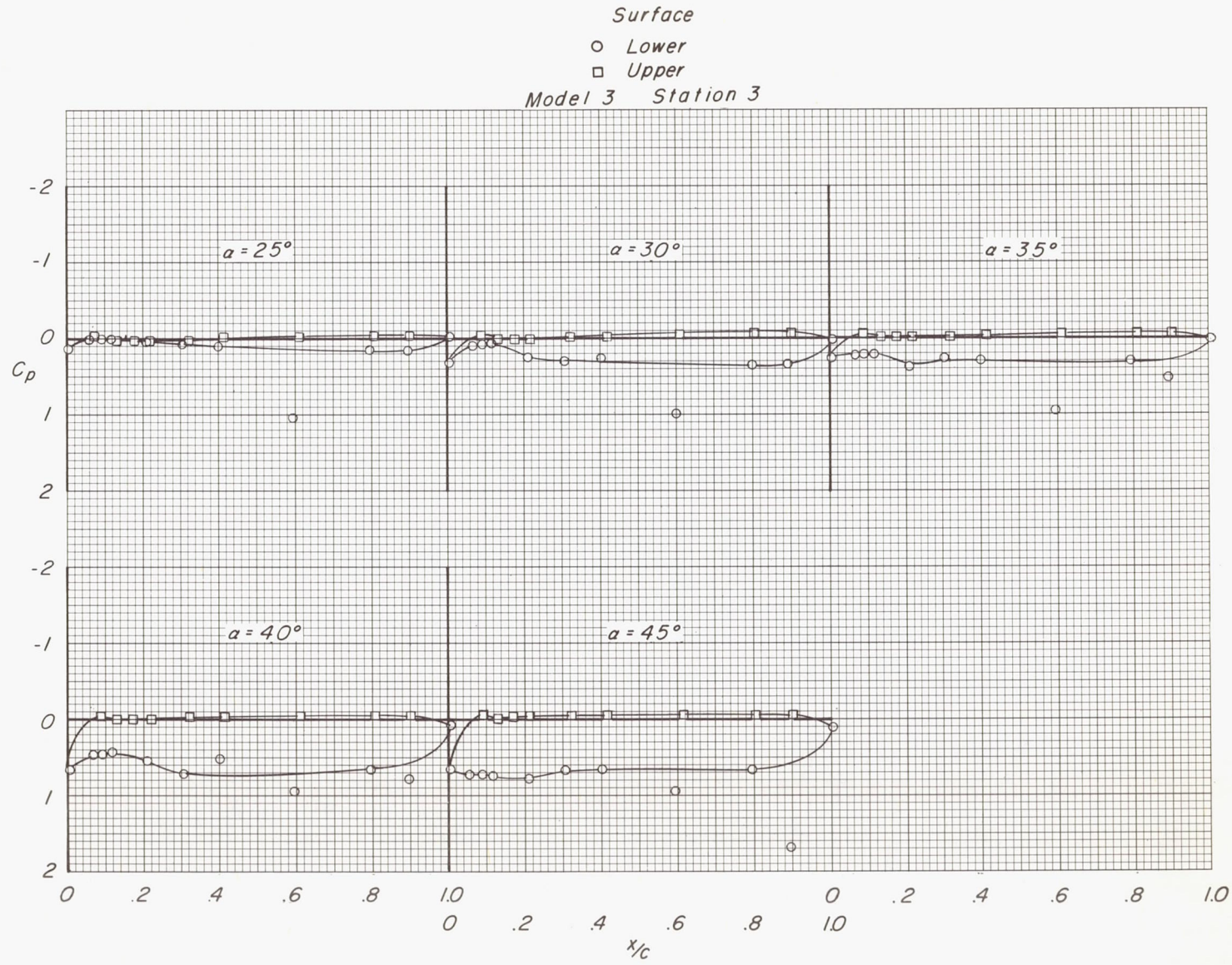

(b) M = 3.95. Continued.

Figure 8.- Continued.

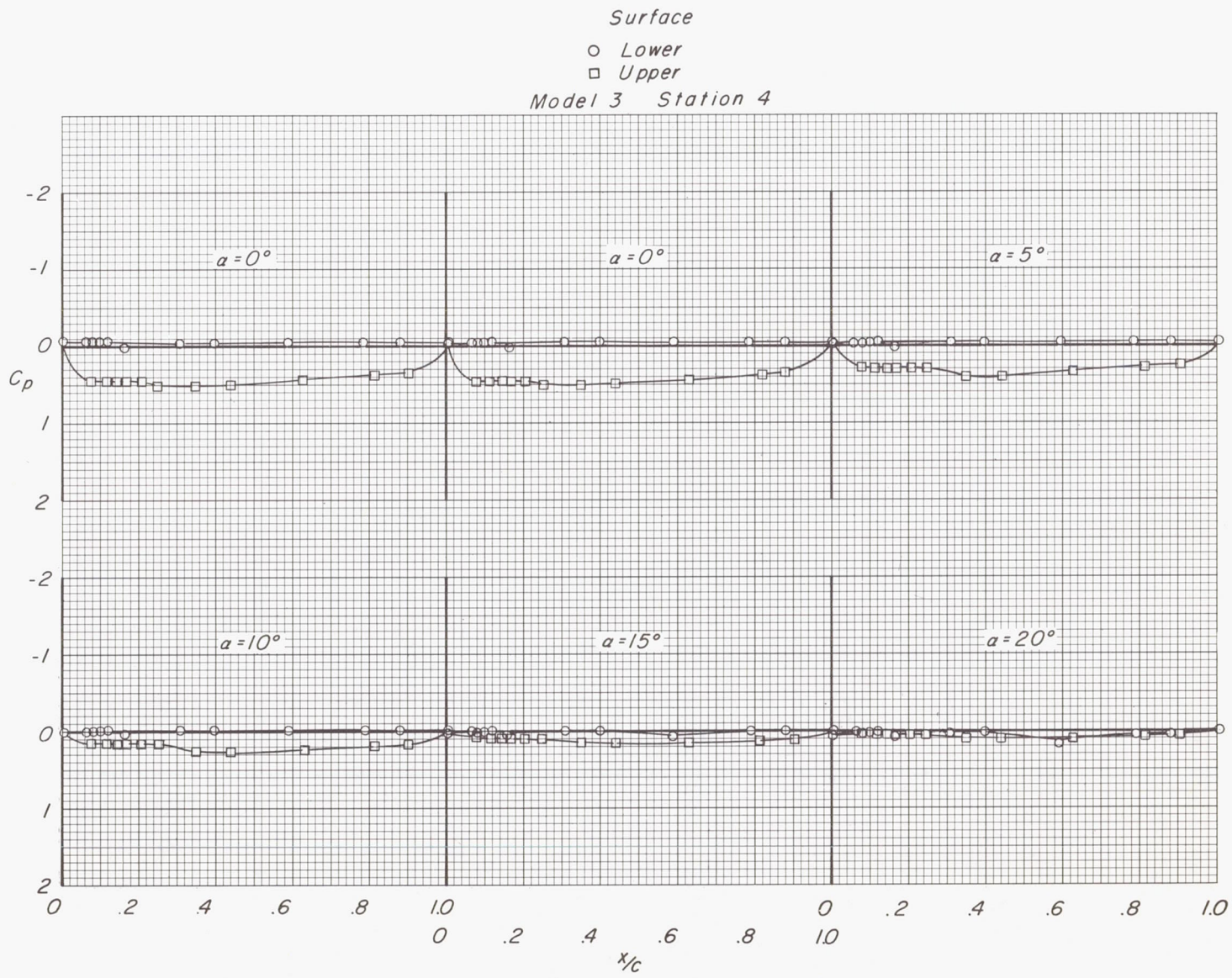

(b) M = 3.95. Continued.

Figure 8.- Continued.

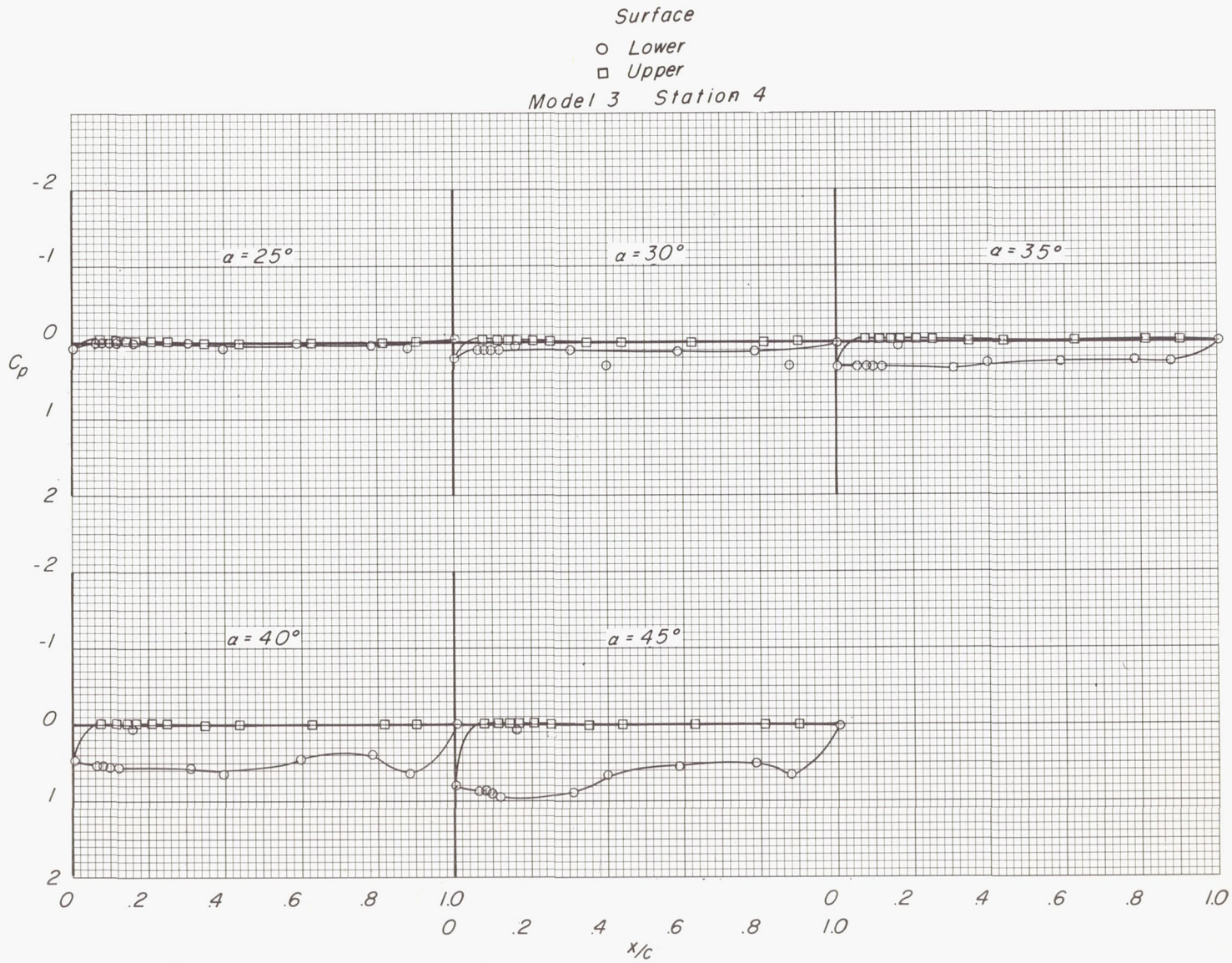

(b) M = 3.95. Concluded.

Figure 8.- Continued.

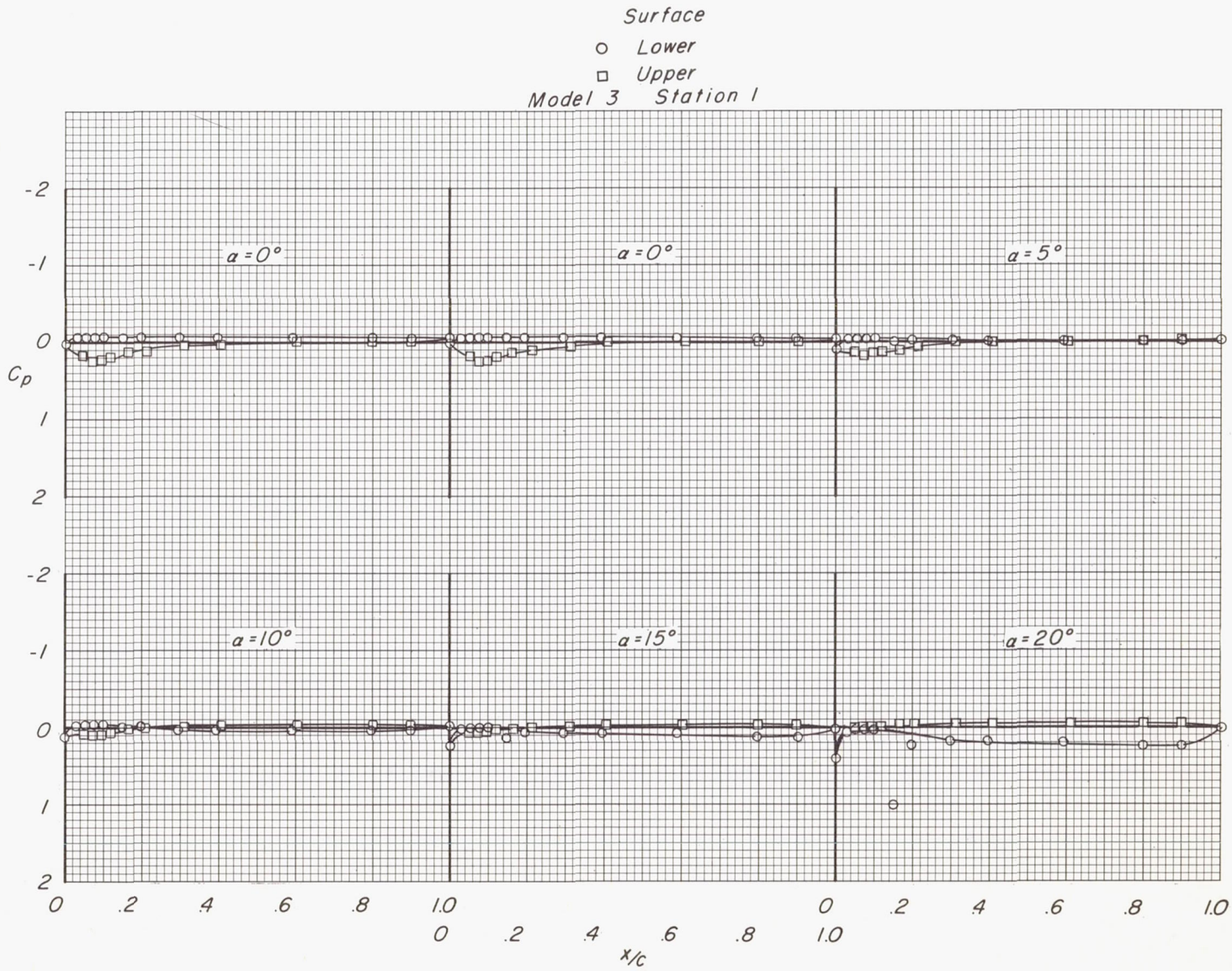

(c) M = 4.65.

Figure 8.- Continued.

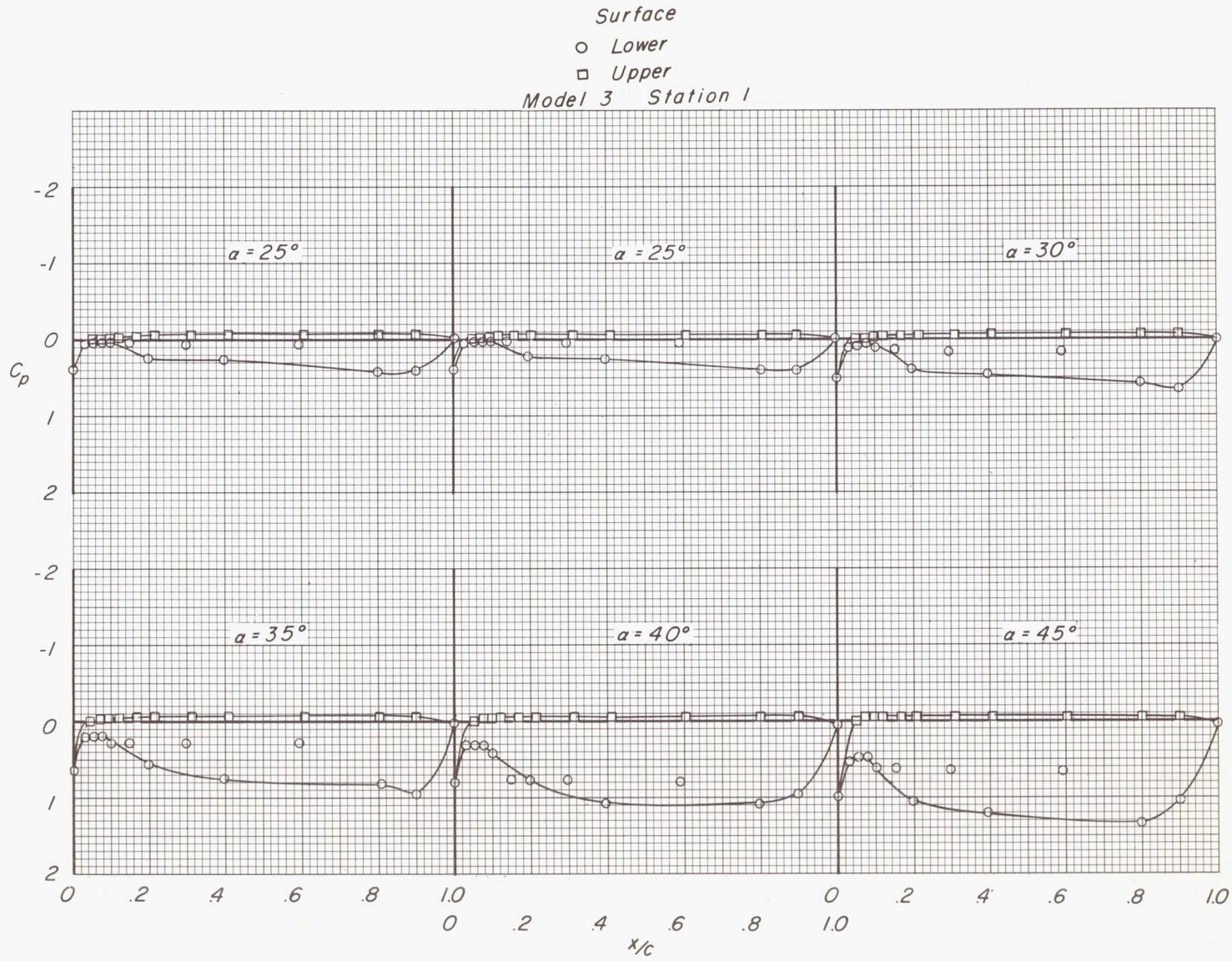

(c) M = 4.65. Continued.

Figure 8.- Continued.

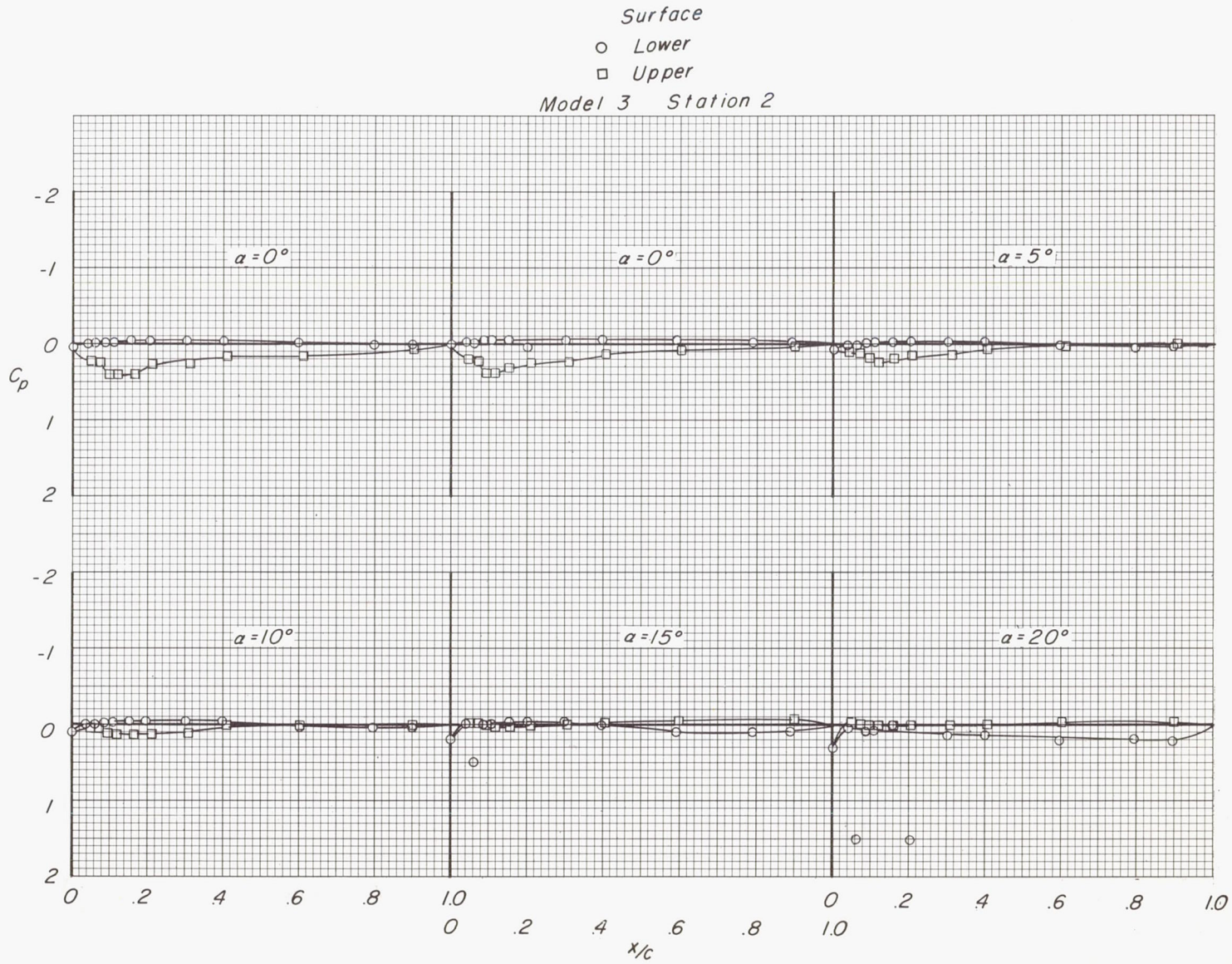

(c) M = 4.65. Continued.

Figure 8.- Continued.

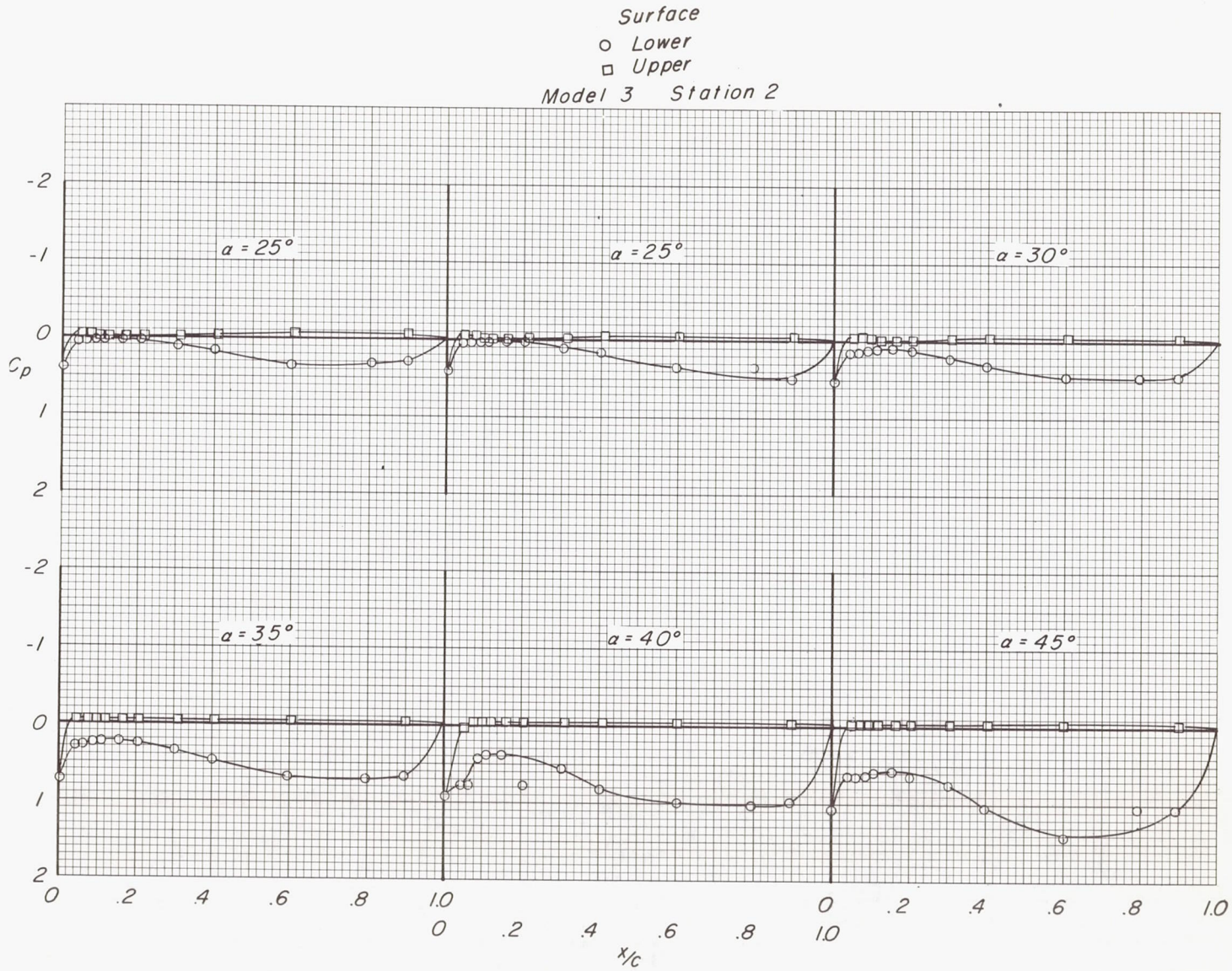

(c) M = 4.65. Continued.

Figure 8.- Continued.

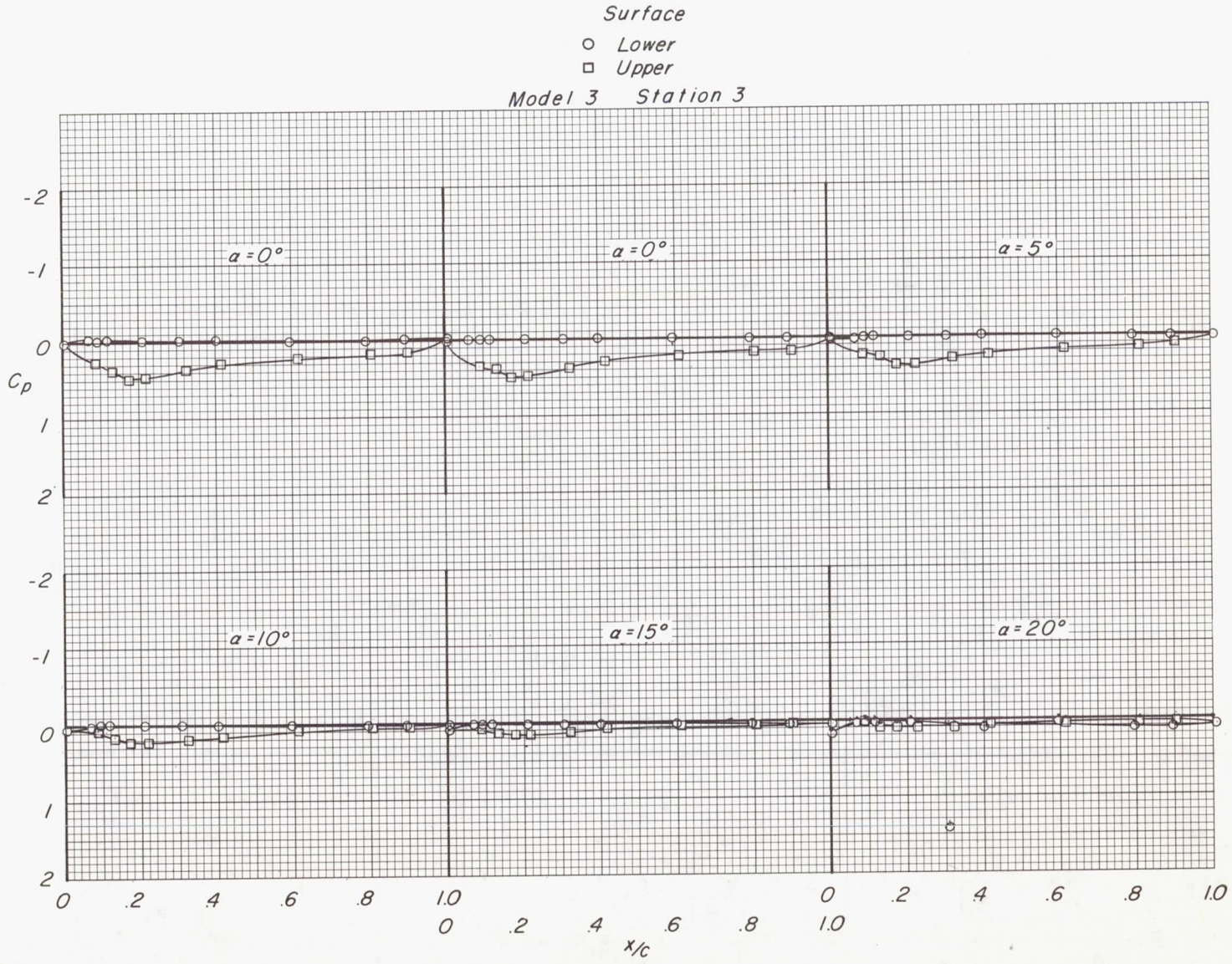

(c) M = 4.65. Continued.

Figure 8.- Continued.

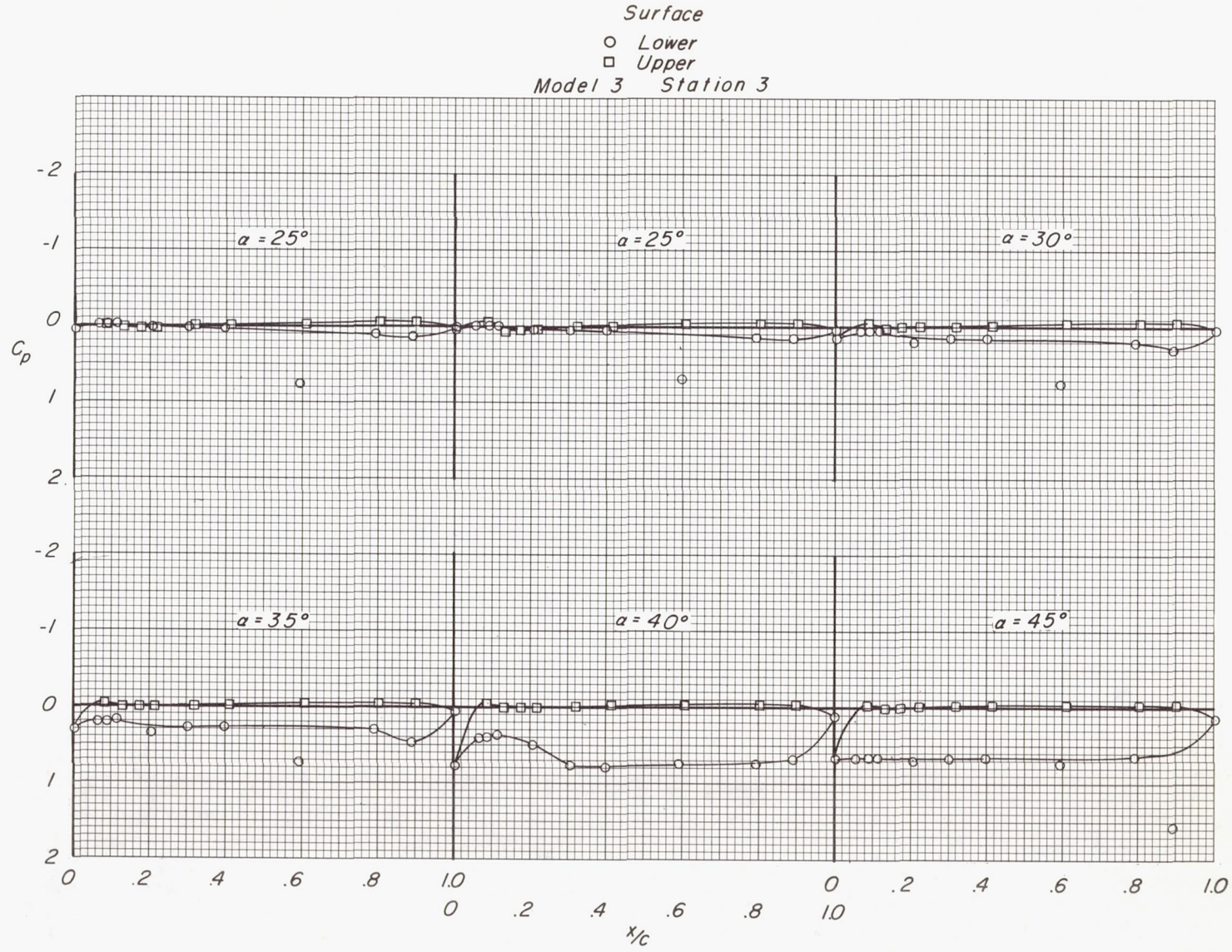

(c) M = 4.65. Continued.

Figure 8.- Continued.

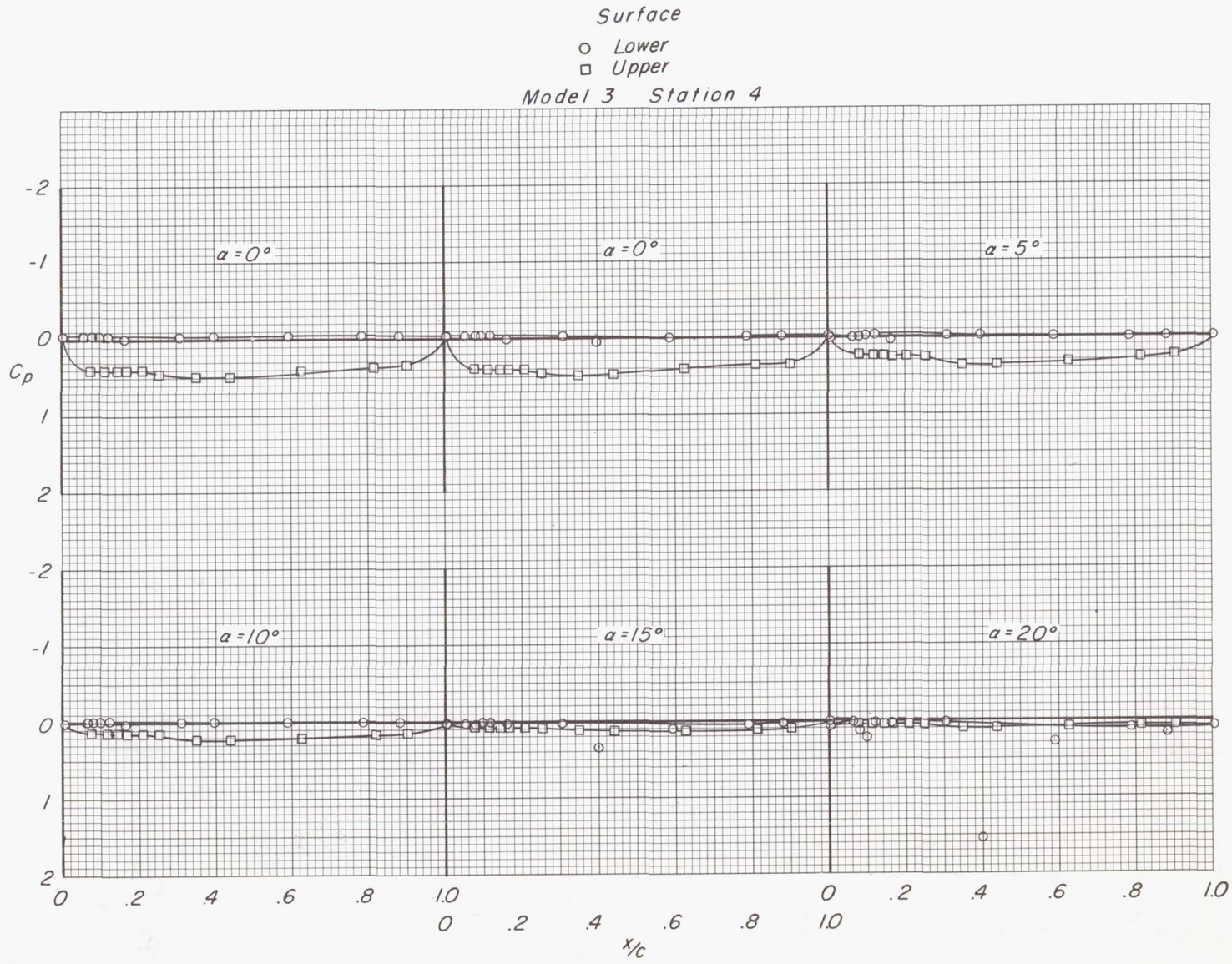

(c) M = 4.65. Continued.

Figure 8.- Continued.

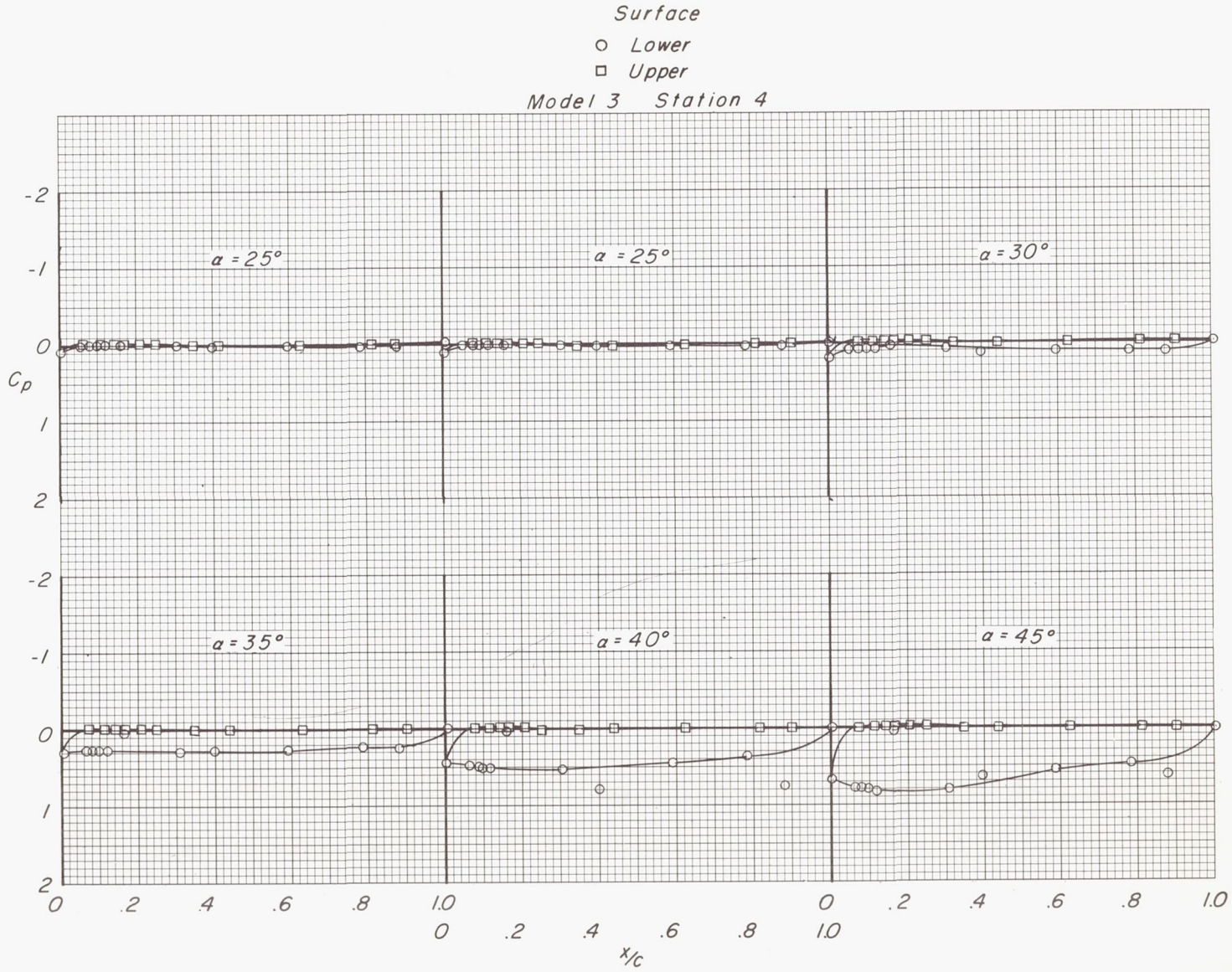

(c) M = 4.65. Concluded.

Figure 8.- Concluded.